

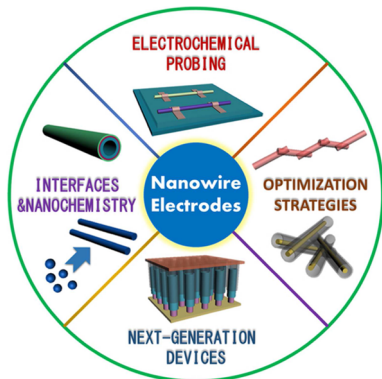
Nanowire Electrodes for Electrochemical Energy Storage Devices

Liqiang Mai,^{*,†} Xiaocong Tian,[†] Xu Xu,[†] Liang Chang,[‡] and Lin Xu^{†,§}

[†]State Key Laboratory of Advanced Technology for Materials Synthesis and Processing, WUT-Harvard Joint Nano Key Laboratory, Wuhan University of Technology, Wuhan 430070, China

[‡]Department of Materials Science and Engineering, Michigan Technological University, Houghton, Michigan 49931-1295, United States

[§]Department of Chemistry and Chemical Biology, Harvard University, Cambridge, Massachusetts 02138, United States



CONTENTS

1. Introduction	11828
2. Nanowire Devices for Electrochemical Probing	11830
2.1. Single Nanowire for ex-Situ Diagnosis	11830
2.2. Single Nanowire for in-Situ Diagnosis	11831
2.2.1. In-Situ TEM Diagnosis	11832
2.2.2. Other Methods for in-Situ Diagnosis	11833
3. Challenges and Optimization Strategies of Nanowire Electrodes	11834
3.1. Restraintment of Conductivity Decrease during Cycling	11834
3.2. Suppression of Structure Degradation	11835
3.3. Reduction of Self-Aggregation	11836
4. Interfaces of Nanowire Electrodes	11837
4.1. Interfaces between Electrodes and Electrolytes	11837
4.2. Interfaces Inside the Heterostructured Composite Nanowires	11839
5. Nanochemistry for Controlled Synthesis of Nanowire Electrodes	11840
5.1. Solution-Phase Route	11841
5.1.1. Hydro(sollo)thermal Strategy	11841
5.1.2. Microemulsion Strategy	11842
5.2. Hard Template Methods	11843
5.2.1. Template Filling Strategy	11843
5.2.2. Electrochemical Deposition	11843
5.2.3. Electrophoretic Deposition	11844
5.2.4. Electrospinning Strategy	11844
5.3. Oriented-Attachment Method	11845
6. Nanowire Electrodes for Advanced and Next-Generation Energy Storage Devices	11845
6.1. Nanowire Electrodes for Advanced Lithium-Ion Batteries	11845

6.1.1. Nanowire Electrodes for Ultrafast Lithium-Ion Batteries	11845
6.1.2. Nanowire Electrodes for Flexible Lithium-Ion Batteries	11847
6.2. Nanowire Electrodes for Advanced Sodium-Ion Batteries	11848
6.3. Nanowire Electrodes for Li–Air Batteries	11850
6.4. Nanowire Electrodes for Li–S Batteries	11851
6.5. Nanowire Electrodes for Supercapacitors	11853
6.6. Nanowire Electrodes for Micro/Nanoscale Energy Storage Devices	11853
7. Concluding Remarks	11854
Author Information	11855
Corresponding Author	11855
Notes	11855
Biographies	11855
Acknowledgments	11856
References	11856

1. INTRODUCTION

With the constantly increasing demands for the market of smaller and lighter portable electronics, establishment of efficient energy storage systems with high power, high energy, and long life span is becoming increasingly important in our daily life, which is also playing a vital role in the energy sustainable development.^{1–4}

There are numerous electric energy storage techniques. Among them, electrochemical devices possess a lot of advantages, including low cost, long life span, high energy-power density, good reversibility, and pollution-free operation. Lithium-ion batteries (LIBs) produced by Sony since 1991 are the most widely used electrochemical energy storage devices for personal electronics such as mobile phones, personal computers, and so forth. The LIBs operate following a “rock chair” concept, in which Li^+ ions are drawn from the electrodes, diffuse through the electrolyte, and insert into the opposite electrodes. The discharging process is on the contrary.⁵ Thus, the reversible capacity of LIBs is limited to the number of the exchanged electrons and the materials structure stability during intercalation/deintercalation.⁶ Recently, the higher energy-density lithium batteries such as lithium–sulfur (Li–S) and lithium–air (Li–air) batteries have aroused worldwide

Special Issue: 2014 Batteries

Received: March 29, 2014

Published: October 7, 2014

attention.^{7–10} The rechargeable Li–S batteries operate by reducing elemental sulfur at the cathodes on discharging to react with Li to ultimately produce Li₂S with a theoretical capacity of 1675 mAh g⁻¹. The Li–air batteries consist of a Li anode, a porous cathode, and nonaqueous/aqueous electrolyte. At the cathode, O₂ moves into the porous cathode and is dissolved in the electrolyte. The dissolved O₂ is then reduced to O₂²⁻ at the surface of the electrode, and Li₂O₂ is formed on discharging. Li₂O₂ is decomposed on charging.

On the basis of the larger abundance resources and lower cost of sodium, sodium-based batteries possess the promising potential to meet the demands of large-scale energy storage. Since sodium-ion batteries are newly developed compared with LIBs, they require exploration of new materials and discovery of redox couples. Fortunately, the general technology of LIBs can be utilized to realize the high performance of sodium batteries. Thus, sodium-ion batteries have been considered as a future prospective candidate for reversible energy storage and conversion.

Batteries can deliver a high energy density, but electrochemical capacitors, including electrical double-layer capacitors (EDLCs) and pseudocapacitors, are well known for their high power density. The EDLCs store charge by absorption of electrolyte ions on the surface of the electrode without a redox reaction, providing fast response to changes in potential. The pseudocapacitors undertake a redox reaction, reaching a close energy density to the batteries.^{11–15}

Whatever batteries or capacitors, higher specific capacities, less charge time, higher rate performance, and longer working life are necessary to meet the increased demands on electrical energy storage devices. The nanoscale science and technology, as research hot spots, bring revolutionary opportunities to meet the needs for the above requirements.^{16–18} Largely different from the bulk materials, nanomaterials have exhibited unique chemical and physical characteristics in the past few decades.^{18–21} Among the various nanostructures, one-dimensional (1D) nanostructures, including nanowires, nanobelts, nanofibers, nanoribbons, nanorods, nanotubes, and nanoscrolls, have attracted extensive interest because of their unique functional properties.^{17,19–24} These various nanostructures are classified as the category of nanowires in this review. For energy storage applications, the nanowire electrodes provide lots of benefits as listed briefly below and will be discussed in detail later in this review.

- Nanowires offer direct current pathways, which facilitate electrical transport compared with particle electrodes.^{19,25–28}
- The ion diffusion length is greatly shortened, which has the potential to increase the rate performance, since the characteristic time for ions to diffuse through an electrode material (*t*) depends on the diffusion length (*l*) and diffusion coefficient (*D*) according to the relation $t \approx l^2/D$.^{19,22,29–31}
- Nanowires provide high surface area, enabling large electrolyte–electrode contact area and reducing the charge–discharge time.^{24,29,32}
- Nanowires can accommodate the volume expansion and restrain the mechanical degradation, enabling long-life cycling.^{25,33,34}
- Nanowires can directly grow on a metal or carbon surface as uniform arrays, realizing the additive-free and binder-free applications.^{35–39}

- Nanowires can act as the building block to construct complex and multifunctional architectures, combining the advantages of each subunit.^{40–43}
- Nanowires have the natural geometrical advantage for in-situ electrochemical probing; with a length of over tens of micrometers and diameter around tens of nanometers, a single-nanowire electrode can be built to in situ investigate the high-resolution structural and electrical evolution without the influence of nonactive materials during battery operation.^{44,45}

Extensive published reviews focused on the different aspects in the field of nanomaterials for energy conversion and storage, and they offered great insights to the researchers.^{7,28,46–50} As a very important kind of electrode material for energy storage devices, nanowires have been always included but usually just summarized as a part of some reviews. No reviews have specifically focused on and summarized the various nanowire electrodes for energy storage devices. It is timely to have a review on this topic to summarize the recent advances and more importantly give a systematic understanding of the nanowire electrodes.

This review summarizes recent progress of nanowire electrodes for electrochemical energy storage devices where emphasis lies in in-situ electrochemical probing, optimization strategies, and outlook in the field of energy storage devices. Figure 1 represents the main structure of this review. First, the

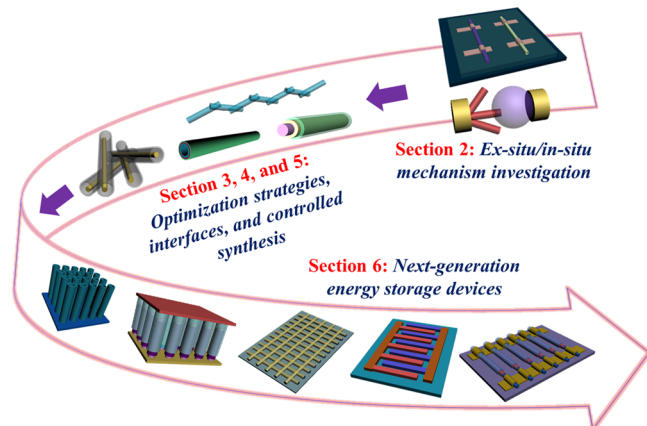


Figure 1. Schematic of the structure in this review.

fundamental concept, potential applications, and advantages of nanowire electrodes are introduced in section 1. The natural advantages of nanowires for ex-situ/in-situ electrochemical probing and recent progress are systematically illustrated in section 2. Then, based on the investigation of the reaction mechanism by in-situ diagnosis, the challenges, optimization strategies, and interfaces of nanowire electrodes will be systematically summarized and refined in sections 3 and 4. Meanwhile, section 5 summarizes the synthesis methods of high-quality 1D nanostructures with controllable diameter, length, composition, and phase. Moreover, we will further show that nanowires also play a vital role in advanced and next-generation energy storage devices in section 6, such as ultrafast charging and discharging batteries, flexible batteries, Na-ion batteries, Li–air and Li–S batteries, supercapacitors, micro/nanoscale energy storage devices, and so forth. In section 7, we finally summarize the present status and provide prospects for future evolution.

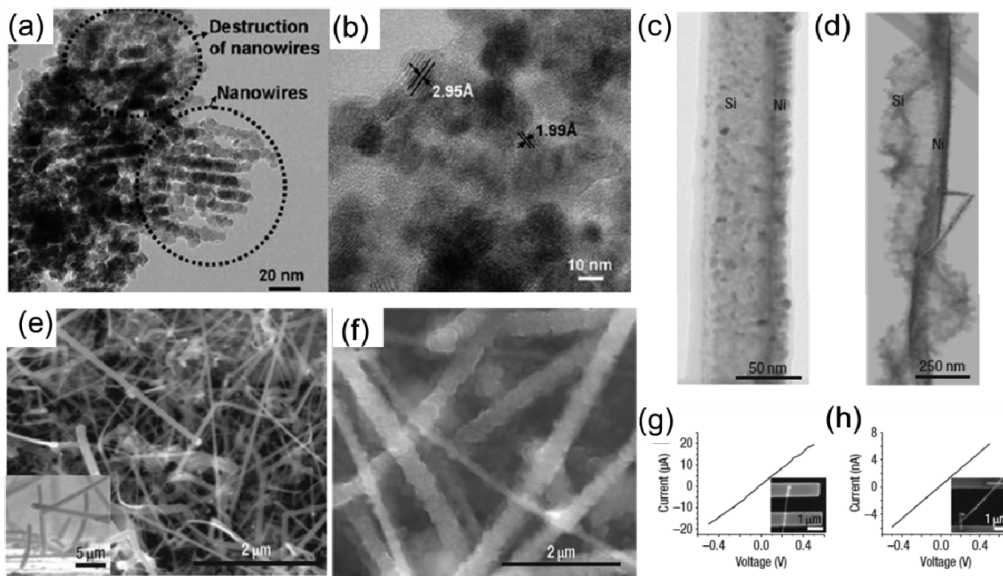


Figure 2. TEM image (a) and high-resolution TEM (HRTEM) image (b) of SnO_2 nanowire electrode after 50 cycles. TEM images of partial Ni-coated SiNW before (c) and after (d) cycling. SEM image of pristine SiNWs before (e) and after (f) cycling. (Inset in e) Cross-sectional image. $I\text{-}V$ curve for a single-nanowire device (SEM image, inset) constructed from a pristine SiNW before (g) and after (h) first cycling. (a and b) Reprinted with permission from ref 86. Copyright 2008 Royal Society of Chemistry. (c–h) Reprinted with permission from Macmillan Publishers Ltd.: *Nature Nanotechnology*, ref 25. Copyright 2008.

2. NANOWIRE DEVICES FOR ELECTROCHEMICAL PROBING

There exist several parameters, such as energy density, safety, and cycling stability, playing important roles in applications of energy storage devices. Among them, capacity fading has been considered as a critical problem which largely limits the development and optimization of high-performance electrode materials. Therefore, it has been considered extremely necessary to fully understand the intrinsic mechanism of the decrease in capacity as well as direct relations between electrode structure and their electrochemical properties.

Nanowires provide the capability as a platform to investigate the fundamental scientific issues in the field of nanoscience and nanotechnology.^{21,25,51–57} As for energy storage devices, first, a single nanowire can guarantee investigation of the high-resolution structural evolution of active materials without the influence of nonactive materials during battery operation. Second, the two ends of an individual nanowire with length on the micrometer or millimeter scale can be conveniently connected with two metal electrodes compared with other materials such as nanospheres. Before 2009, the design of a single-nanowire electrode was mainly focused on ex-situ electrochemical probing. With the development of technology and the progress of experiment design, increasing attention has been paid to a number of in-situ techniques, such as optical microscopy, transmission electron microscopy (TEM),^{44,45,58–80} X-ray diffraction (XRD),⁸¹ scanning electron microscopy (SEM),⁸² nuclear magnetic resonance (NMR) spectroscopy,⁸³ and Raman spectroscopy⁸⁴ for energy storage device studies. These in-situ single-nanowire electrode studies have provided deeper and more direct insight into the material degradation mechanisms and phase transformation during charge and discharge.

2.1. Single Nanowire for ex-Situ Diagnosis

Ex-situ study of a single-nanowire electrode applied in battery diagnosis is mainly focused on morphology characterization,

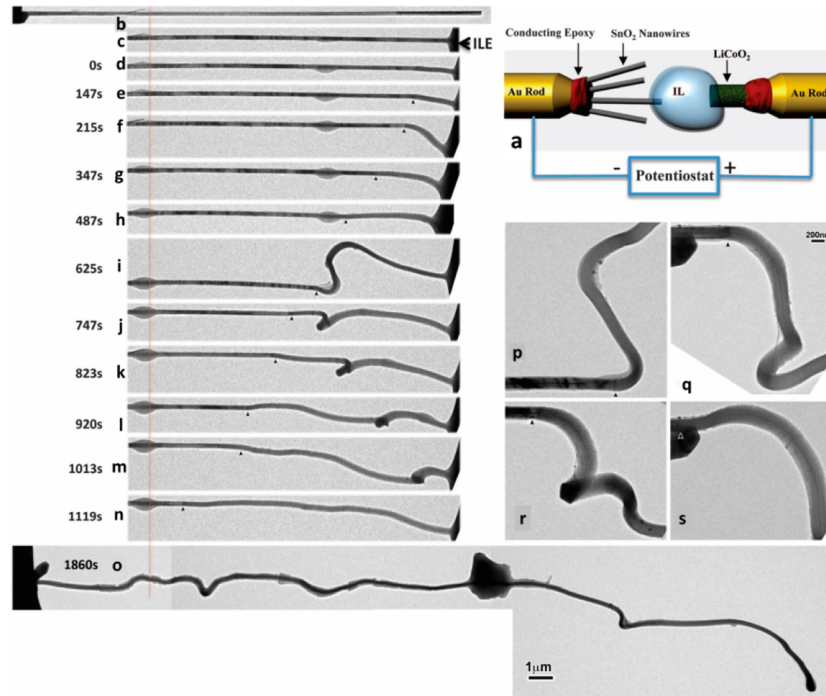
spectroscopy, and electrical transport. Among these ex-situ techniques, TEM and SEM offer the unique capabilities to analyze the electrodes' microstructural evolution. There exist various ongoing studies of ex-situ morphology measurement for the battery electrode materials, such as silicon nanotube/nanowires,⁸⁵ SnO_2 nanowires,⁸⁶ Co_3O_4 nanowires,⁸⁷ ZnMn_2O_4 nanowires,⁸⁸ and Ge nanowires.⁸⁹ The experiment of Ge et al. demonstrated the porous silicon nanowire maintained this structure after Li-ion intercalation through the ex-situ TEM test with low stress, which was beneficial for high capacity and long life span.⁹⁰ Such conclusion can also be obtained in SnO_2 . The mesoporous SnO_2 nanowire kept the mesoporous structure with the degraded crystal structure (Figure 2a and 2b).⁸⁶ Some ingenious experiments have been further designed by combining ex-situ TEM observation and single-nanowire $I\text{-}V$ test (Figure 2c–h). The inert Ni evaporated onto Si nanowires acted as a reference for measuring the length change of the silicon nanowires (SiNWs) (Figure 2e). After lithiation, the wrapped Si nanowires around the Ni backbone (Figure 2f) showed an expansion in the length of the nanowire. The $I\text{-}V$ curve of the pristine Si nanowire was linear, with a resistivity of $0.02 \Omega \text{ cm}^{-1}$ (Figure 2g). After the first charge and discharge, the $I\text{-}V$ curve of the amorphous nanowire was still linear, with a resistivity of $3 \Omega \text{ cm}^{-1}$ (Figure 2h).²⁵

In addition, Yang et al. also designed the single LiMn_2O_4 nanorod device and tracked the influence of the electrolyte on Al-doped LiMn_2O_4 electrode at the single-particle level.⁹¹ The results indicated that dissolution of manganese ions was reduced by Al dopants, and the Al-doped LiMn_2O_4 nanorod became more stable than pure LiMn_2O_4 at resisting electrolyte etching.

Compared with SEM and TEM ex-situ test, XPS^{92–94} and XRD^{25,95–99} can give more information about the crystal structure and valence state information on the electrode material during cycling. The ex-situ XPS experiment of Ma et al. showed the reduction processes of $\alpha\text{-CuV}_2\text{O}_6$ nanowires during discharging which was further confirmed through the

Table 1. Main Progress of in-Situ Nanowire Characterization for Electrochemical Energy Storage

characterization methods	materials	main phenomena and results	ref
in-situ TEM	SnO ₂ nanowires	the mobile dislocation cloud was formed	44
	carbon/Al/Cu-coated SnO ₂ nanowires	spherically shaped Li _x Sn alloy was dispersed in the amorphous Li _y O matrix	75
	ZnO nanowires	compared with uncoated ones, the charge rate of coated ones increased about 10 times, the radial expansion of coated nanowires was suppressed, and less dislocation cloud produced	76
	CuO nanowires	leapfrog cracks were generated before the reaction front, resulting in many glass–glass interfaces (GGI) in a single nanowire	77
	RuO ₂ nanowires	Cu ₂ O was detected, and the total volume expansion of CuO after lithiation was about 165%	78
	LiMn ₂ O ₄ nanowires	intermediate phase of Li _x RuO ₂ was detected	74
	SiNWs	local phase transformation occurred at the region of interface with electrolyte	79
	Ge nanowires	anisotropic expansion which was dependent on the crystallographic orientation was observed	70,73
	carbon-coated/phosphorus-doped SiNWs	sharp interface (~1 nm thick) between the crystalline silicon and the amorphous Li _x Si alloy was observed	72
	metal-coated SiNWs	phase transition process from amorphous Li _x Si to the crystal Li ₁₅ Si ₄ was spontaneous and congruent	71
	Al nanowires	physically contacted silicon nanowires were welded with the assistance of lithium ion	66
in-situ XRD	SiNWs	nano pores were formed during delithiation process, and isotropic volume expansion was observed	69
	SiNWs	charging rate of SiNWs was improved by 1–2 orders of magnitude by either phosphorus doping or carbon coating	68
in-situ SEM	SiNWs	metal coating suppressed volume expansion and improved conductance	67
in-situ NMR	SiNWs	pulverization occurred during delithiation	59
in-situ characterization for single-nanowire electrochemical devices	SiNWs and vanadium oxide nanowires	metastable Li ₁₅ Si ₄ phase was formed after deep lithiation	81
		tensile strength and Young's modulus of silicon nanowires decreased after one cycle	82
		overlithiated phase c-Li _{3.75+δ} Si was generated when the electrode underwent a slow cycling	83
		structure of SiNWs was destroyed during lithiation, and conductance of Si decreased for over 2 orders, and this change was permanent; conductance of vanadium oxides recovered to the previous level after lithium ions deintercalation	84

**Figure 3.** (a) Schematic of SnO₂ nanowire electrode in a nanoscale electrochemical device. (b–s) Structure evolution of SnO₂ nanowire in the lithiation process. Reprinted with permission from ref 44. Copyright 2010 AAAS.

XRD and charge–discharge curve.⁹³ In other work by Chan et al., they proved that the Li₁₅Si₄ did not form and the silicon nanowire remained amorphous after discharge through the ex-situ XRD test.⁹⁶

2.2. Single Nanowire for in-Situ Diagnosis

Although the ex-situ test can give a lot of information about the material in the charge/discharge state, test results are greatly influenced by the conductive additives and hydrolyzing of electrolyte. Accompanying development of the science and technology, some in-situ measurement techniques have been

developed. A single nanowire for in-situ probing can more accurately reflect the dynamic nature of battery operation under more realistic conditions than that of ex-situ probing. The main achievements of in-situ nanowire characterization are presented in Table 1, which are also discussed in detail in the following sections.

2.2.1. In-Situ TEM Diagnosis. Among the varieties of probing tools, in-situ TEM is widely used for detecting the microstructural evolution of single nanowires during different electrochemical processes because of its high resolution. We will introduce recent progress in three parts below.

2.2.1.1. Metal Oxide Nanowires. A nanoscale electrochemical device was creatively designed inside the TEM. In this device, a single SnO_2 nanowire anode was utilized where ionic liquid and a bulk LiCoO_2 cathode were used as the electrolyte and cathode, respectively (Figure 3a). On the basis of in-situ TEM observation of the dynamic structure of the SnO_2 nanowire in the lithiation process, it was shown that the reaction propagated along the nanowire, resulting in swelling, elongating, and spiraling of the nanowire (Figure 3b–s).⁴⁴ This study not only presents a vivid image of nanowire battery operation but also strongly proves that nanowire geometry can provide mechanical robustness and elasticity boundary condition which is very different from that of bulk materials. Compared with the sequential lithiation of SnO_2 nanowires from one end to the other, Wang et al. designed a modified model: the nanowires were soaked into the ionic liquid.⁷⁵ Except for the results similar to the previous work, the surface of SnO_2 nanowires became rough, lithiated Li_xSn and Li_yO were generated, and spherically shaped Li_xSn alloy was dispersed in the amorphous Li_yO matrix. Two of them made up the rough surface. Zhang et al. investigated the lithiation processes of SnO_2 nanowires with different coating materials; they found that the charged rate of SnO_2 nanowires coated with copper, carbon, and aluminum increased about 10 times more than uncoated ones.⁷⁶ Notably, for the coated nanowires, the expansion in radial direction could be suppressed at the reaction front, resulting in reduced tensile stress. It is confirmed that the coating strategy is an effective method for building better lithium-ion batteries.

The lithiation process of ZnO nanowires was investigated by Kushima et al.,⁷⁷ and the phenomenon which was different from SnO_2 nanowires was found: The movement of the reaction front in ZnO nanowires was not continuous. The leapfrog cracking occurred before the reaction front. The signal ZnO nanowire was divided into many segments by these leapfrogs, which matched results in the poor cycling stability of ZnO nanowires. By comparing ZnO with SnO_2 nanowires through ab initio tensile decohesion simulations, the strength of ZnO decreased from 29 (pure ZnO) to 17 and 8 GPa for 1Li/ $(\text{ZnO})_8$ and 2Li/ $(\text{ZnO})_8$, respectively, while SnO_2 decreased less than 20% with the two lithium ions inserting.^{77,80}

The other groups also explored other metal oxides through in-situ TEM. Gregorczyk et al. studied the lithiation process of RuO_2 . The dislocation cloud, significant surface roughening, and lithium embrittlement were presented.⁷⁴ The intermediate phase of Li_xRuO_2 and the phase transitions between RuO_2 and the nanostructure network of Ru/LiO₂ during charging and discharging were observed. Wang et al. investigated the lithiation/delithiation mechanism of CuO nanowires and found that the entire volume expansion of the first delithiated nanowires was 165% compared with that of pure CuO nanowires, and Cu_2O (theoretical capacity is 375 mAh g⁻¹,

much lower than that of CuO) was detected, corresponding to the fast capacity fading of the CuO electrode.⁷⁸ Lee et al. observed the local phase transformation during lithiation of LiMn_2O_4 and predicted that the cubic phase LiMn_2O_4 might be a candidate material of long-life lithium-ion batteries.⁷⁹ Developments of in-situ TEM diagnosis above give the fundamental understanding of the conversion and insertion reaction mechanism through real-time observation.

2.2.1.2. Silicon/Germanium Nanowires. As a traditional semiconductor material silicon has a high theoretical capacity,¹⁰⁰ the details of the alloying reaction process are not clear. The lithiation process of silicon is usually divided into two steps: (1) crystal silicon is converted to amorphous Li_xM alloys (Li_xM , $0 < x < 3.75$); (2) the crystallization process from $a\text{-Li}_x\text{M}$ to crystalline Li_{15}M_4 ($c\text{-Li}_{15}\text{M}_4$).⁸⁰ Huang's group found that the volume expansion of silicon nanowires was anisotropic, and the largest volumetric change occurred along the $\langle 110 \rangle$ direction during the lithiation process by the in-situ TEM test.⁷³ Then high resolution, even to atomic scale, was achieved by Liu et al. A sharp interface was generated between the crystalline silicon ($c\text{-Si}$) and the amorphous Li–Si alloy, the lateral movement of ledges on the $\{111\}$ atomic planes made the interface migrate, and peeling of the ledge which consists of the $\{111\}$ atomic facets produces the amorphous Li_xSi .⁷² Existing evidence on the orientation-dependent mobility of the interfaces was found. Wang et al. investigated the $a\text{-Si}/\text{carbon}$ nanofiber core–shell structure by in-situ TEM; they found that the crystallization process from Li_xSi to $\text{Li}_{15}\text{Si}_4$ was spontaneous and congruent. In this phase transition process there were no phase separations or large-scale motions.⁷¹ They also proved that the capacity fading after long-term charge/discharge derived from the damage accumulated on the surface of the silicon layer. Recently, Gu et al. designed a liquid electrolyte cell which was more similar to conventional batteries in TEM, instead of the previous solid lithium oxide or ionic liquid cell. Compared with the results from open-cell studies, some behaviors of SiNWs lithiation/delithiation are accordant. However, some unique properties of the liquid electrolyte, such as compact contact with electrode material, bring this design a possibility to quantitatively investigate formation of solid electrolyte interphase (SEI) layer and evolution of structures.⁷⁰ For the other semiconductor material, such as Ge nanowires, the volume expansion was isotropic. The porous structures formed in the Ge nanowires after Li⁺ ions extraction.⁶⁹ They concluded that the main cause of this difference between Si and Ge is the orientation dependence of interfacial mobility.⁸⁰ The porous structure generated on the surface of Ge nanowires improved the rate performance and cycling stability of electrode materials.⁶⁹

Then some optimization strategies are implemented. Liu et al. found that the phosphorus doping and carbon coating could improve the charging rates of silicon nanowires from 2.3 to 117 nm s⁻¹.⁶⁸ This strategy provides an effective way to increase the power density of silicon-based batteries. A copper coating was introduced into a single sidewall or the entire surface of SiNW by either thermal evaporation or sputtering. The copper coating could suppress volume expansion during lithiation, improve the rate behavior, and optimize the silicon anode framework.⁶⁷ Another interesting phenomenon was observed through in-situ TEM, and two physical contact SiNWs were welded after electrochemical lithiation and delithiation with the assistance of Li⁺ ions.⁶⁶ After delithiation, the shear strength in the welded region was measured to about 200 MPa. These features and

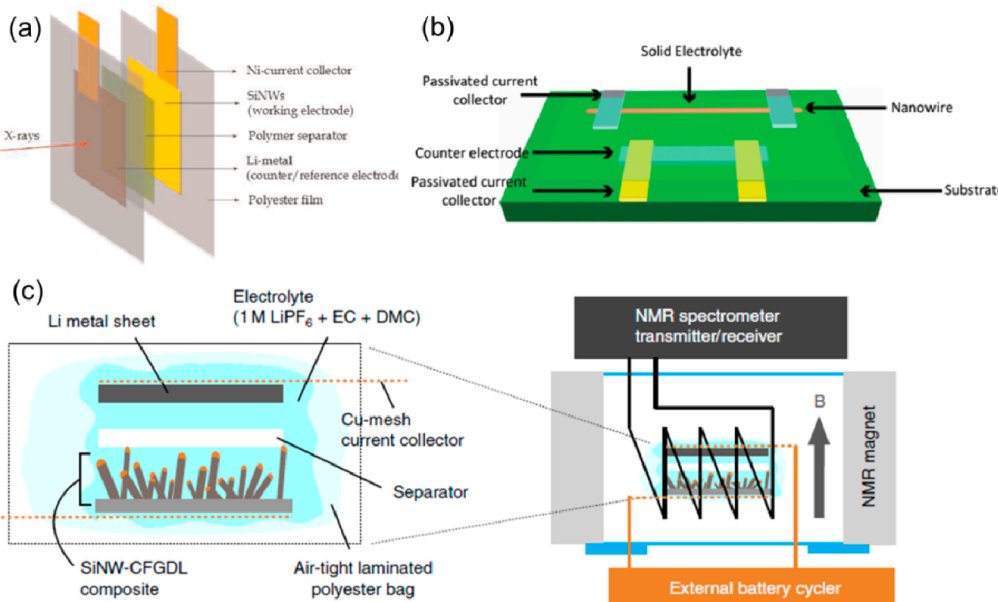


Figure 4. (a) Schematic of a cell model in the in-situ XRD. (b) Schematic of a single-nanowire electrode device design. (c) Schematic of the SiNWs-composite-based cell, and setup for in-situ ⁷Li NMR measurements. (a) Reprinted with permission from ref 81. Copyright 2012 American Chemical Society. (b) Reprinted with permission from ref 84. Copyright 2010 American Chemical Society. (c) Reprinted with permission from ref 83. Copyright 2014 Rights Managed by Nature Publishing Group.

detachment of SiNWs might take part in lithium storage when they were still parts of the robust contacted networks. This discovery offers a new strategy for improving the cycling stability of SiNWs.

The SiNW was the first nanostructure which was investigated by in-situ TEM. The silicon nanowires also offered a powerful platform for observing the lithiation processes of the other nanostructures, such as silicon nanoparticles,^{60,64} nanospheres,⁶² and yolk–shell structure. The silicon nanowire was even used for constructing a Li–O₂ cell model in in-situ TEM. Li₂O₂, which was supported on the multiwalled carbon nanotube (MWCNT), was contacted with a silicon nanowire, and the electrochemical oxidation process of Li₂O₂ was observed.⁶³

2.2.1.3. Metal Nanowires. Pulverization of the electrode is a great challenge in the charging and discharging of lithium-ion batteries, resulting in decreased electrical contact and capacity fading after charging and discharging. The in-situ TEM technology was employed by Liu et al. to investigate the pulverization process. The Al nanowire with oxidized Al₂O₃ surface layers was used as a model. They found that the surface Al₂O₃ layer was lithiated first, and then lithiation of the inner Al core began. The volume expansion of Al nanowires is almost 100%. After the forth delithiation process, the voids were connected with each other, which results in pulverization of the Al nanowires into isolated nanoparticles, corresponding to fast capacity fading in the ex-situ test. However, the nanoparticles were confined in the Li–Al–O, which was formed during lithiation of the Al₂O₃ surface layer. These discoveries provide the basis for the strategy which could enhance the performance of electrode materials by atomic layer deposition.⁵⁹

2.2.2. Other Methods for in-Situ Diagnosis. In addition to in-situ TEM,^{51,52,58–80} XRD,⁸¹ SEM,⁸² NMR,⁸³ and Raman⁸⁴ are also common measuring and testing technologies for phase and morphology detection.

Misra et al. used an X-ray transparent battery cell (Figure 4a) to study the silicon nanowire which was grown on the stainless steel mesh in real time during electrochemical cycling. They found that the metastable Li₁₅Si₄ phase is formed after deep lithiation. This phase, which is disadvantageous for the cyclability of the silicon electrodes, was avoided through increasing growth temperature of SiNWs from 485 to 500 °C, which resulted in the obviously enhanced cycling performance of SiNWs.⁸¹ Boles et al. studied the tensile performance of the dealloyed silicon by SEM, which was composed of a microelectromechanical force sensor and a piezo-driven actuator. The tensile strength and Young's modulus of silicon nanowires decreased after one cycle.⁸² Similar results were acquired by Kushima et al. through in-situ TEM observation.⁶⁵ Ogata et al. studied the kinetics and thermodynamics of a model half battery system which was composed of silicon nanowires grown on the carbon-fiber support by in-situ NMR. Combined with the density-functional theory calculations, the complete component diagram of SiNWs with the different cutoff potential and the different discharge rate was obtained. They found the overlithiated phase, which consists of *c*-Li_{3.75+δ}Si generated when the electrode was undergoing a slow cycling (Figure 4c).⁸³

Mai et al. designed and assembled the first all-solid-state single-nanowire electrochemical devices in 2010.⁸⁴ This device contained a single nanowire as either the cathode or the anode where the conventional electrode materials and all-solid-state PEO-LiClO₄-PC-EC polymer were utilized as the counter electrodes and electrolyte, respectively (Figure 4b). The conductance of vanadium oxides could recover to the previous level after lithium-ion deintercalation, indicating a reversible structure change after a shallow lithiation process, but for the SiNW anode, the conductance of the electrode decreased over two orders and this change was permanent. This observation implied permanent structure change, which was further

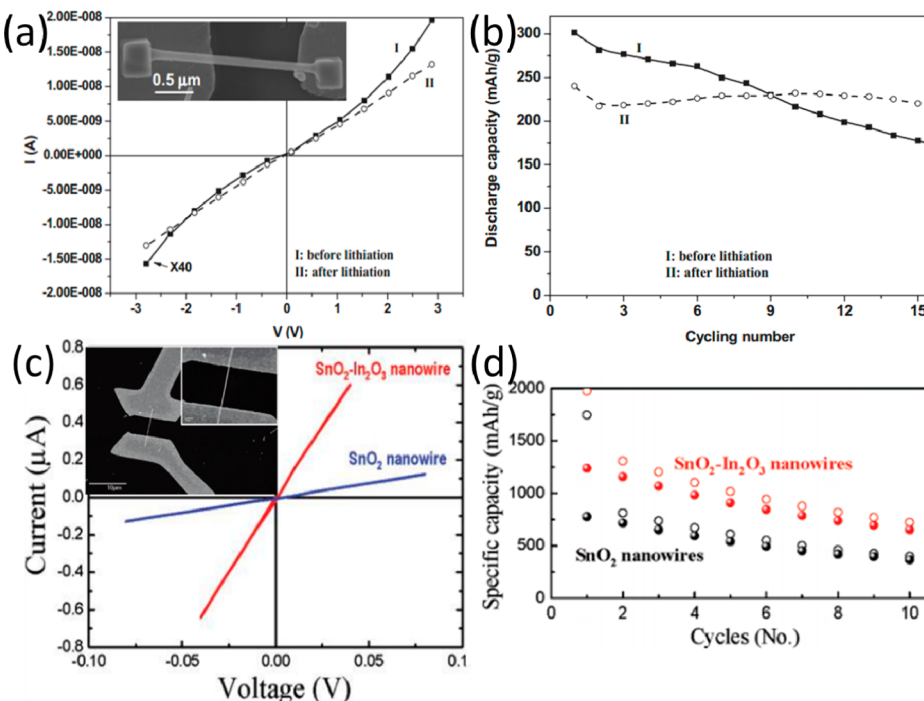


Figure 5. (a) I – V curves of α -MoO₃ nanobelts before and after lithiation. (Inset) SEM image of a single nanobelt contacted by two metal electrodes. (b) Cycling performance of α -MoO₃ nanobelts before and after lithiation. (c) I – V curves of single SnO₂–In₂O₃ and SnO₂ nanowires. (Inset) SEM image of single SnO₂–In₂O₃ nanowire contacted by two metal electrodes. (d) Cycling performance of the SnO₂–In₂O₃ and SnO₂ nanowires. (a and b) Reprinted with permission from ref 105. Copyright 2007 WILEY-VCH Verlag GmbH&Co. KGaA, Weinheim. (c and d) Reprinted with permission from ref 110. Copyright 2007 American Chemical Society.

confirmed by Raman mapping together with the Raman spectra.

Overall, the in-situ observation methods have been explored by some researchers, and the reaction mechanism of lithium-ion batteries was gradually understood. However, some complex processes are still unclear. To solve this problem, the real-time dynamic lithiation/delithiation processes need to be fully investigated. Nanowire devices will provide an excellent platform to investigate the intrinsic lithiation/delithiation mechanism during these in-situ observation.

3. CHALLENGES AND OPTIMIZATION STRATEGIES OF NANOWIRE ELECTRODES

Nanowire electrodes have some unique advantages for electrochemical energy storage. However, they are still facing some challenges which significantly affect the performance of electrochemical energy storage devices. This section mainly focuses on the conductivity decrease, structure degradation during charge/discharge, and self-aggregation, which are considered as vital elements for nanowire electrodes. To overcome these challenges, the corresponding optimization strategies have been put forward, which are summarized in this section.

3.1. Restraint of Conductivity Decrease during Cycling

One of the most significant advantages of the nanowire electrode is the continuous, fast electron transport pathway along the nanowire. However, the conductivity decrease during the charge/discharge process severely limits this advantage. Basically, capacity fading results from the transformation from active materials into inactive phases, which increases the impedance and lowers the operating voltage.¹⁰¹ To some degree, capacity fading is directly related to impedance increase.

Chan et al. studied the chemical, structural, and electrical transformations of V₂O₅ nanowires at the single-nanostructure level.¹⁰² They measured the conductivity change of a single V₂O₅ nanowire before and after lithiation by butyllithium and found that the electrical conductivity of V₂O₅ nanoribbons was 3 orders of magnitude lower after lithiation.

To solve the issue of an obvious conductivity decrease of electrode materials during cycling, several possible strategies have been proposed, such as conductive polymers and carbon coating,^{103,104} prelithiation treatment,^{105,106} and so forth. Prelithiation treatment has been discussed in this part for its efficiency to restrain the conductivity decrease. García-Alvarado et al. prepared Li_xV₂O₅ phase by chemical lithiation of V₂O₅ using *N*-butyllithium.¹⁰⁷ After being aged for 48 days, the capacity of Li_{1.16}V₂O₅ reached 300 mAh g⁻¹ after 20 cycles when cycled between 1.8 and 3.8 V, indicating an obvious improvement compared with V₂O₅. Mai's group developed a secondary hydrothermal lithiation method to synthesize α -MoO₃ nanobelts, and their structure and morphology were well retained.¹⁰⁵ Electrochemical tests showed that the 15th capacity of the nonlithiated nanobelts was 180 mAh g⁻¹, indicating a capacity retention of 60%, while for lithiated nanobelts the high capacity of 220 mAh g⁻¹ and capacity retention of 92% were achieved after 15 cycles, demonstrating the enhanced cycling stability (Figure 5b). Moreover, electrical conductivities of a single nanobelt before and after lithiation were also measured (Figure 5a), and the results showed that the conductivity of prelithiated nanobelts was improved to 10⁻² S cm⁻¹, much higher than that of a nonlithiated nanobelt (10⁻⁴ S cm⁻¹). It was inferred that the prelithiated Li⁺ ions remained in the lattice of α -MoO₃ nanobelts; thus, electrical transport was enhanced. Due to the existence of preinserted Li⁺ ions in the crystal structures, further insertion and extraction of ions

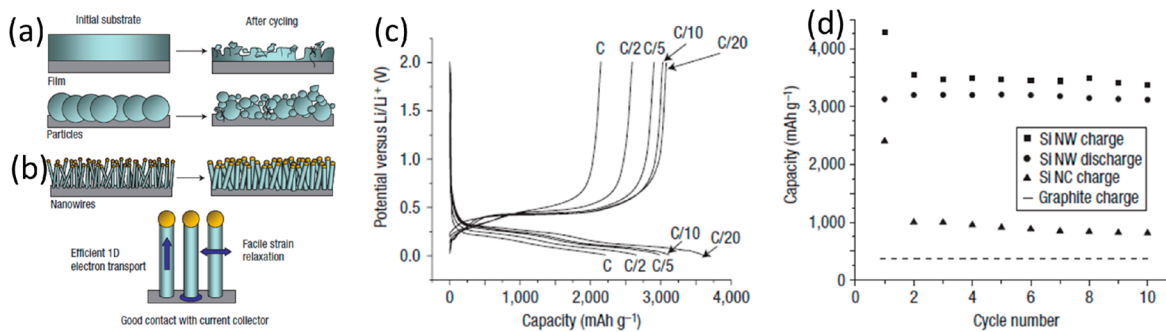


Figure 6. (a, b) Schematic of electrochemical cycles of nanowire arrays. (c) First voltage profiles for the SiNWs cycled at different rates. (d) Cycling performance of the SiNWs at the C/20 rate. Reprinted with permission from Macmillan Publishers Ltd.: *Nature Nanotechnology*, ref 25. Copyright 2008.

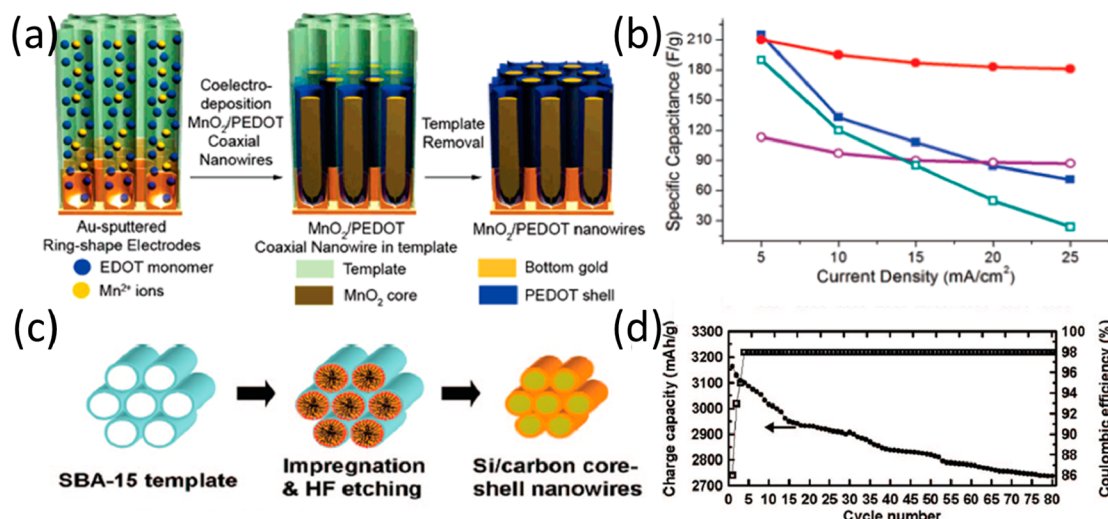


Figure 7. (a) Schematic of the fabrication process of MnO₂/PEDOT coaxial nanowires. (b) Specific capacitances of MnO₂ nanowires (closed blue square), PEDOT nanowires (open purple dots), MnO₂ thin film (open green square), and MnO₂/PEDOT coaxial nanowires (closed red dots) at different current densities. (c) Schematic of the fabrication process of Si@carbon core–shell nanowires. (d) Cycling performance and Coulombic efficiencies of the Si@carbon core–shell nanowires. (a and b) Reprinted with permission from ref 117. Copyright 2008 American Chemical Society. (c and d) Reprinted with permission from ref 124. Copyright 2008 American Chemical Society.

became more accessible, resulting in enhanced cycling performance in charge/discharge processes. The prelithiation technique has also been extended to other materials, and improved electrochemical performance was obtained compared with their parent structures, such as FeSe₂¹⁰⁸ and CoP_x¹⁰⁹.

Coaxial and heterostructure architecture could also restrain the conductivity decrease during cycling. Kim et al. reported SnO₂–In₂O₃ heterostructured nanowires.¹¹⁰ As revealed by the electron transport measurement, the electronic conductivity of the single SnO₂–In₂O₃ nanowire was improved by 2 orders of magnitude compared with the pure SnO₂ nanowire, which was attributed to ITO shell formation (Figure 5c). Similarly, the enhanced electrical transport improved the electrochemical performance, primarily in the specific capacity, of SnO₂–In₂O₃ nanowires (Figure 5d). Another coaxial architecture, MnO₂-coated carbon nanotube arrays were reported by Reddy et al., which exhibited high capacity and cycling stability. The electronic transport and volume changes of the MnO₂ shell were enhanced and alleviated, respectively, due to the existence of the CNT core, leading to the excellent electrochemical performance.⁹²

Indeed, decreased charge-transfer resistance and hence improved electrochemical energy storage can be achieved by

effective surface modification, such as depositing metals and metal oxides.^{92,111} In addition, as mentioned above, the architecture with ordered nanowire aligned onto the conductive substrate helps to form continuous conducting pathways for electrons and will partly overcome the conductivity decrease issue during cycling.

3.2. Suppression of Structure Degradation

During the Li⁺-ion intercalation/deintercalation processes, large strain will be induced into the host materials.^{112–115} This problem is especially obvious in lithium metal alloy anode materials (Li_xM_y), which are able to accommodate large amounts of lithium and hence have specific capacities exceeding that of the conventional graphite anodes. However, storage of such a large amount of lithium induces large volume expansion–contraction that accompanies their electrochemical alloy formation. These changes lead rapidly to deterioration of the electrode, thus limiting its lifetime to only a few charge–discharge cycles. The lithiation/delithiation-induced structure degradation has been widely reported. Cui's group showed that silicon nanowire arrays circumvented the issue mentioned above.²⁵ During the charge/discharge processes, they could accommodate and alleviate the strain where the strain was divided into many small parts on every nanowire. In addition,

the 1D structure provided a short diffusion distance for Li⁺ ions. In this work, the theoretical capacity of silicon anodes was achieved with little fading in the charge/discharge processes (Figure 6). Lee et al. synthesized molybdenum oxides nanomaterials via hot-wire chemical vapor deposition (HWCVD) and used as-prepared molybdenum oxides nanomaterials as the electrode.¹¹⁵ Upon cycling, the nanomaterials became highly disordered together with a large volume expansion as evidenced by both XRD and in-situ Raman measurements.

Even though nanostructured materials exhibit more facile relaxation than bulk/microsized materials there still remains much space for further improvement due to limited lithium concentration gradient and efficient stress reduction in the vicinity of the surface. It is necessary to note that the conductivity decrease during cycling and lithiation/delithiation-induced structure degradation of electrode materials may be interrelated. The lower conductivity may be caused by the generated mixed phases which block efficient electronic transport. However, from different starting points, different optimization strategies have been adopted, which will be introduced in detail below.

Because coating can act as an elastic buffer to accommodate the strain during Li⁺-ion insertions and extractions, coating another kind of material on the surface of the host material is an efficient way to get protection and enhancement. Moreover, if conductive materials, such as conducting polymers and carbon, were used as coatings, the drawback of low conductivities of the electrodes could be solved to some extent as well.^{116–118} In addition, the flexibility and high conductivity of conducting polymers and carbon could facilitate the transport and diffusion of electrons and ions into the core materials, respectively.

Liu et al. reported the MnO₂/poly(3,4-ethylenedioxythiophene) coaxial nanowires through a one-step coelectrodeposition approach (Figure 7a).¹¹⁷ The internal MnO₂ nanowires enabled the high energy density. Meanwhile, the external PEDOT materials with high conductivity and porosity facilitated the electron transport and ion diffusion into the internal MnO₂ nanowires. Moreover, it provided an efficient way to protect the MnO₂ from structural collapse and cracks. Due to the combined properties, the specific capacities of these coaxial nanowires reached at a very high level at various current densities (Figure 7b). Mai et al. synthesized β -AgVO₃/Ag_xVO_(2.5+0.5x)/PANI ($x < 1$) triaxial nanowires through an in-situ polymerization approach based on β -AgVO₃ nanowires.¹¹⁹ The triaxial nanowires exhibited much lower charge transfer resistance than that of β -AgVO₃ nanowires, which indicated faster kinetics. Thus, the higher capacity is achieved. A similar strategy has been utilized for MoO₃ electrode materials in order to improve discharge/charge capacity and cycling stability.^{120–122} Murugan et al. reported the synthesis of LiFePO₄/C nanocomposites by in-situ carbon coating of high-crystalline LiFePO₄ nanorods.¹²³ After annealing, the rate capability and cycling stability were significantly improved because of a more ordered structure and increased conductivity due to the carbon coating. Kim et al. used SBA-15 as template to synthesize mesoporous Si/C core–shell nanowires¹²⁴ (Figure 7c). The nanowires exhibited an excellent initial charge capacity of 3163 mAh g⁻¹ at a rate of 0.2 C (600 mA g⁻¹) between 1.5 and 0 V and a capacity retention of 87% after 80 cycles. Moreover, carbon-coated Si nanotubes have been reported to achieve capacities as high as 3000 mAh g⁻¹ at

rates of 5 C (15 A g⁻¹) (Figure 7d).¹²⁵ Obviously, carbon coating^{123–126} can effectively increase conductivity, protect the electrode from direct contact with electrolyte, and provide buffer for the volume change during cycling. As is known, carbon is mostly placed as the shells to modify the host materials and improve electrochemical performance.

Other free-standing device structures have been developed as a variation of a traditional carbon coating. Cui et al. reported the core–shell nanostructure, amorphous silicon-coated carbon nanofibers, which showed excellent performance as an anode with a high charge capacity of ~2000 mAh g⁻¹ and long cycle life.⁴² Significantly, an areal capacity of ~4 mAh cm⁻² was also obtained with the high mass loading using these nanowires in a full cell with LiCoO₂ as cathode, whose values were comparable to that of commercialized batteries. Similar improvements were observed in MoS₂ overlayers supported on coaxial carbon nanotubes.¹²⁷ Thus, carbon coating is thought to be an effective method to improve the capacity and cycle life of electrodes. However, it is worth noting that even though cladding nanowires could efficiently suppress the material degradation and improve the resistance to fracture, these polymer additives would make the batteries more difficult to endure higher temperatures and carbon coating would lower the volumetric energy density.

Designing and fabricating hierarchical nanostructures are also novel approaches to address the issues of the large volume changes during Li⁺-ion intercalation and deintercalation. Cui et al. fabricated a silicon-based core–shell nanowire anode.¹²⁸ It was believed that the reduction potentials of Li varied in crystalline and amorphous silicon electrodes. They selected amorphous Si as the shell to realize high electrochemical activities and chose crystalline Si as the core to provide high mechanical supports and electrical transport along the entire parts of the nanowire. The fabricated core–shell nanowires exhibited a high specific capacity of ~1000 mAh g⁻¹ and high capacity retention of ~90% after 100 charge/discharge cycles, making them promising candidates for practical applications. The heterostructured or hierarchical nanowires mentioned above are all defined with a core–shell structure, while fabrication of 1D nanostructured electrodes with axially modulated composition is also an alternative, such as porous α -Fe₂O₃ branches on β -MnO₂ nanorods.¹²⁹ The β -MnO₂ nanorods grew along the 4-fold axis; the as-produced branches of FeOOH and α -Fe₂O₃ were aligned on their side in a nearly 4-fold symmetry. This structure exhibited a high reversible specific capacity of 1028 mAh g⁻¹ at a current density of 1000 mA g⁻¹.

3.3. Reduction of Self-Aggregation

1D nanomaterial electrodes offer superiority over the bulk counterpart due to their small size and shorter path lengths for lithium ions, leading to higher capacities especially at high rates. Meanwhile, during the Li⁺-ion intercalation and deintercalation, the small size in the radial direction can release the stresses easily along with the expansion/contraction. However, a plain 1D nanostructure is certainly not an elixir. Self-aggregation usually occurs for 1D nanostructures because of their high surface area and large surface energy, which results in fast capacity fading. In order to overcome the limits of plain 1D nanostructure electrode materials, many novel complex nanowires, such as hierarchical nanowires,^{130–132} mesoporous nanowires,^{87,133} and ordered nanowire architectures,^{134–136} are proposed to inhibit self-aggregation. The resulting materials

have shown the enhanced lithium-ion battery performance with longer cycle life.

To reduce the influence brought up by the self-aggregation of nanomaterials, constructing a mesoporous nanowire and keeping the high surface area at the same time is a wise choice and further confirmed by some remarkable works. Li et al. reported mesoporous Co_3O_4 nanowire arrays growing on Ti foil as anodes with high capacities and rate capabilities.⁸⁷ At 1 C, the mesoporous nanowires maintained a high capacity of 700 mAh g^{-1} after 20 cycles. This excellent performance is attributed to sufficient contact between electrolyte and the oxide surface, which was introduced by the high porosity of mesoporous nanowires. Another effective nanostructure configuration was reported by Kim et al.,¹³⁵ the SnO_2 nanorod-planted graphite particles (SNP-GPs), where rectangular-shaped SnO_2 nanorods were uniformly attached on the surface of microsized graphite particles (Figure 8). The SNP-

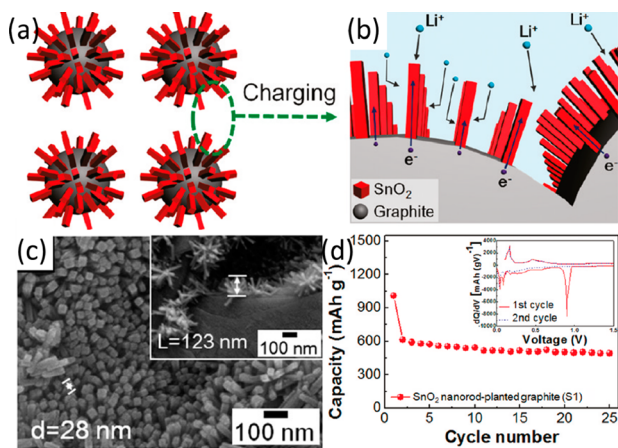


Figure 8. Schematic of SNP-GPs (a) and electrochemical reactions (b) during cycling. (c) SEM image of SNP-GPs (inset shows the cross-sectional image). (d) Cycling performance of SNP-GPs. (Inset) Differential capacity versus voltage plot. Reprinted with permission from ref 135. Copyright 2011 American Chemical Society.

GPs delivered a high specific capacity of 1010 mAh g^{-1} , which was attributed to the novel architecture that effectively prevented aggregation of the electroactive materials. Additionally, homogeneous electrical interconnections between SnO_2 and graphite greatly improved the electrical conductivity. This kind of nanorod-planted particles demonstrates a new class of structural complexity in nanomaterials.

Apart from the above strategies, another efficient approach to restrain self-aggregation is to develop ultralong nanowires with a length up to a few hundred micrometers or even at millimeter scale. Mai et al. assembled ultralong vanadium oxide nanowires with a hierarchical structure by electrospinning combined with annealing.¹³⁷ The fabricated nanowires' length reached up to the millimeter or even centimeter grades, which was realized through continuous self-attachment of nanorods. Notably, the attachments in the ultralong nanowires reduced the self-aggregation greatly, which enabled the electrode to sustain large contact with the electrolyte (Figure 9a). The initial discharge capacity of ultralong V_2O_5 nanowires was up to 275 mAh g^{-1} and retained at 187 mAh g^{-1} after 50 charge and discharge cycles, which were much better compared with self-aggregated short nanorods (Figure 9b). Xu et al. reported topotactically intercalated ultralong LiV_3O_8 nanowires (Figure 9c), which

exhibited a high rate capability and excellent capacity retention (Figure 9d).¹³⁸ Using the nanowire as a template, ultralong semihollow bicontinuous graphene scrolls self-coated on the V_3O_7 nanowires, which was reported by Yan et al. (Figure 9e).¹³⁹ Different from the physical mixture with metal oxides and graphene, their strategy provided the possibility to enhance the electrical transport of metal oxide electrodes at an individual nanowire level. Moreover, the semihollow graphene scrolls could allow for volume expansion of metal oxides and restrain dissolution of vanadium oxides, which resulted in enhanced electrochemical performance for lithium-ion batteries (Figure 9f).

Assembling the nanoscale building blocks into ordered nanowire architectures, where nanowires are vertically or horizontally aligned on conductive substrates, offers another way to overcome the self-aggregation issue.^{140–142} As each nanowire is fixed in a certain position and separated from each other, such architecture brings several advantages. First, the detached state of nanowires can greatly avoid self-aggregation, and free space between them could promote facile strain relaxation during battery operation. Second, nanowires are attached to the current collector for good adhesion and form continuous conducting pathways for electrons. Third, ordered nanowire architectures, compared with free-standing nanowires with disordered form, show a larger specific surface area and lower average concentration of structural defects and grain boundaries, resulting in an increased Li^+ -ion insertion/extraction rate and electron transport.

4. INTERFACES OF NANOWIRE ELECTRODES

The interfaces of nanowire electrodes have a great impact on the performance of electrochemical energy storage. In this review, we mainly focus on the nanowire electrode interfaces in two parts, which are summarized in this section. The first part is the interfaces between electrodes and electrolytes, where the solid electrolyte interphase layers form.^{143–149} The other part is the interfaces inside the heterostructured composite nanowires.

4.1. Interfaces between Electrodes and Electrolytes

Traditionally, electrolyte decomposition occurs when the potential of the electrode is relatively lower during battery charging, which results in formation of passivating layers, named SEI.¹⁴³ The SEI layer is an insulator for electrons but conductor for Li^+ ions. Formation of the SEI layers occurs on the electrode surface ($\sim 0.8 \text{ V}$)^{143,150,151} at potentials more positive than that for Li^+ ions to intercalate into the anode material ($\sim 0.1–0.4 \text{ V}$),^{100,152} which is an irreversible reaction that is associated with loss of cell capacity. Additionally, exposure of active material from electrode expansion during cycling results in continual SEI formation,¹⁰⁰ as the SEI layers cannot undergo a similar expansion with the electrode and cracking of the SEI layers can be severe.¹⁵³ As nanowires have a larger surface, the influence of SEI becomes more remarkable; thus, it is more important to reduce or even get rid of the influences brought by formation of SEI. Recently, some scientists showed great interest in formation of SEI on the surface of the 1D nanostructure such as carbon nanofibers (nanotubes),^{154–157} silicon nanowires (nanotubes),^{25,125} CoO nanowires,¹⁵⁸ MnO_2 nanowires,¹⁵⁹ and SnO_2 nanowires.¹⁶⁰

Among these materials, silicon shows the highest gravimetric capacity ($\sim 4200 \text{ mAh g}^{-1}$). Formation of SEI layers is one of the key issues to obtain the long cycle life of a silicon electrode's batteries. It was confirmed, by Chan and Ruffo,^{96,161}

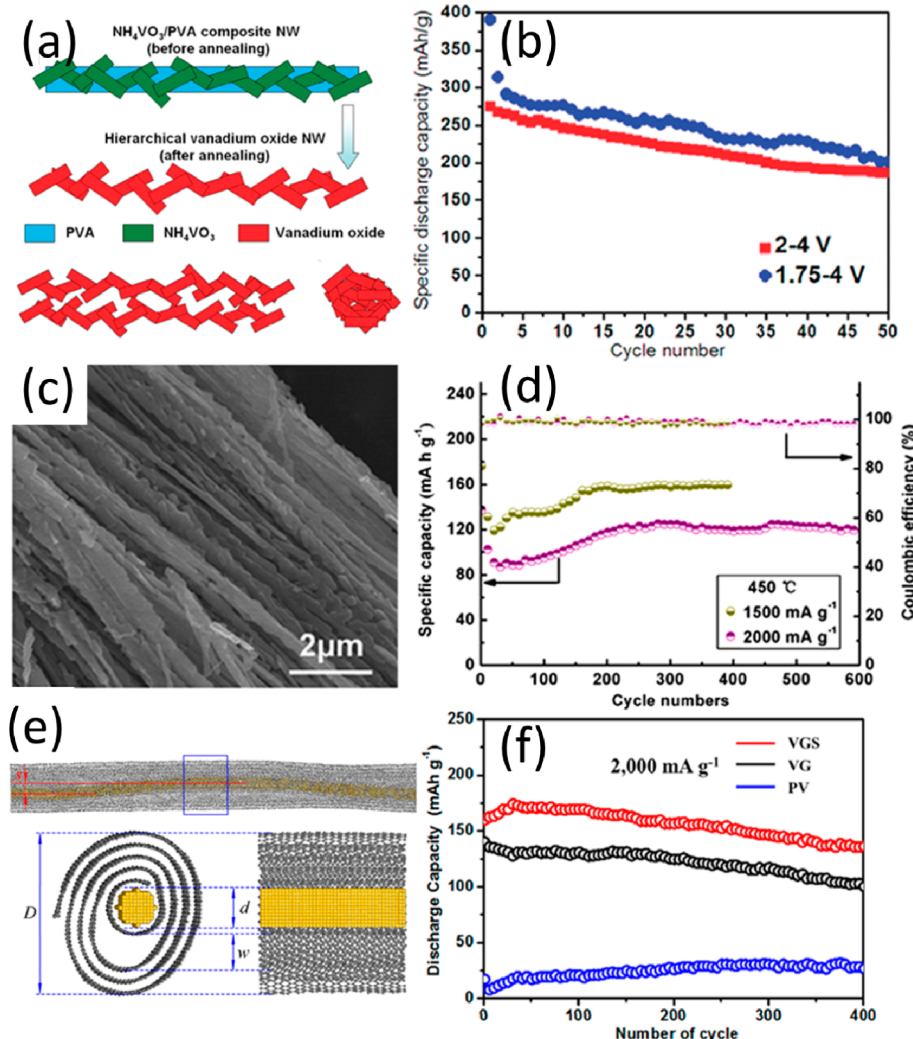


Figure 9. (a) Schematic of formation of the ultralong hierarchical V_2O_5 nanowires. (b) Cycling performance of the ultralong hierarchical V_2O_5 nanowires. (c) SEM image of the ultralong LiV_3O_8 nanowires. (d) Cycling performance of the ultralong LiV_3O_8 nanowires. (e) Schematic of the structure of V_3O_7 nanowires templated semihollow bicontinuous graphene scrolls (VGS). (f) Cycling performance of VGS, V_3O_7 nanowire/graphene structure without nanowire-templated graphene scrolls and pure V_3O_7 nanowires. (a and b) Reprinted with permission from ref 137. Copyright 2010 American Chemical Society. (c and d) Reprinted with permission from ref 138. Copyright 2012, Rights Managed by Nature Publishing Group. (e and f) Reprinted with permission from ref 139. Copyright 2013 American Chemical Society.

that SEI layer formation was greatly related with the surface composition and morphology. The SEI layers mainly consist of salt degradation products and an organic component which is a reduction products of electrolyte, such as hydrocarbon, Li alkyl carbonates, Li fluoride, Li ethers, PEO oligomers, LiPF_6 , Li hydroxide, and so forth. They found that the electrodes were able to limit the impedance increase and have good capacity retention by adjusting the charged and discharged potential window between 0.07 and 0.7 V. Modification of the surface with conductive agents also turns out to be a feasible approach. The conductive agents include carbon,^{124,162–165} reduced graphene oxide (rGO),¹⁶⁶ carbon nanotubes,¹⁶⁷ SiO_x ,⁸⁵ metals,^{168,169} and metal oxides.¹⁷⁰ Coating of the materials above can decrease the contact area between the silicon nanowire and the electrolyte, prevent breakdown of SEI layers, suppress SEI layer thickness, and enhance surface conductivity, which can reduce the irreversible capacity effectively.

Wu et al. reported a double-walled Si- SiO_x nanotube (DWSiNT) electrode where the active silicon and confined SiO_x served as the inner wall and outer wall, respectively.⁸⁵ In

the Li^+ -ion insertion process, the ions from the electrolyte penetrated across the confined SiO_x and reacted with the active silicon, which would expand inward into the hollow space. In the opposite process, the inner silicon shrank with small formation of a SEI layer. Figure 10 shows the advantages of this structure over nanowires and nanotubes during the charge and discharge processes. The as-synthesized DWSiNT exhibited excellent electrochemical performance, with no obvious capacity loss even after 6000 cycles. Park et al. utilized another method, a carbon coating approach to modify the surface of silicon nanotubes, which stabilized the interface of silicon and electrolyte and resulted in the high specific capacity and superior capacity retention.¹²⁵

There are other promising approaches, such as precoating a thin artificial SEI layer on SiNWs,¹⁷¹ prelithiated,¹⁷² surface modified,¹⁷³ atomic layer deposition.¹⁷⁴ These modification methods are also used for reducing the irreversible capacity of other materials like SnO_2 ¹⁷⁵ and MnO_2 ¹⁷⁶ nanowires which are on account of the SEI layers.

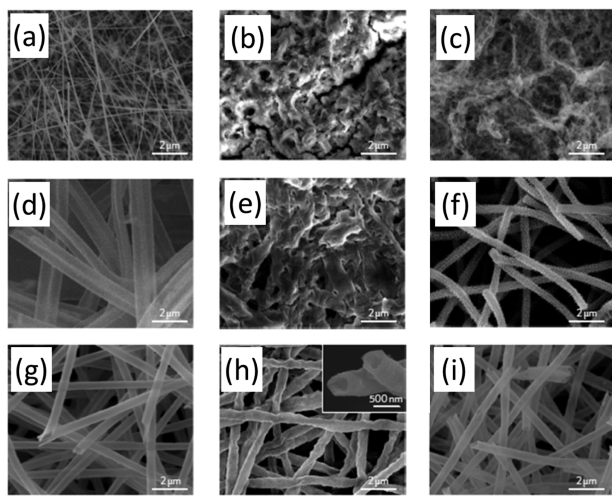


Figure 10. (a–i) SEM images of different silicon nanostructures before and after cycling. SEM images of initial silicon nanowires (a), silicon nanotubes (d), and DWSiNTs (g). SEM images of silicon nanowires (b), silicon nanotubes (e), and DWSiNTs (h) after 200 cycles. SEM images of nanowires (c), nanotubes (f), and DWSiNTs (i) after cycling 200, 200, and 2,000 times, respectively. Reprinted with permission from Macmillan Publishers Ltd.: *Nature Nanotechnology*, ref 85. Copyright 2012.

If the voltage of materials falls within the stable voltage window of the electrolyte, formation of the SEI layers will be limited; then the advantages of nanowires may more easily be exploited. Such an example is lithium titanium oxide, $\text{Li}_4\text{Ti}_5\text{O}_{12}$ (LTO). The voltage level of LTO is higher than those of conventional graphite, i.e., 1.5 versus 0.05 V, which prevents

SEI layer formation. Lee et al. synthesized $\text{Li}_4\text{Ti}_5\text{O}_{12}$ nanostructures using the calculation and solvothermal methods, in which the ethanol amounts were 60 (LT-E6) and 80 vol % (LT-E8) in the solvents.¹⁷⁷ It was confirmed by TEM images (Figure 11a and 11b) that the surface of the nanowires was attached with nanoparticles, where the heterogeneous nanostructures were formed. Heterogeneous $\text{Li}_4\text{Ti}_5\text{O}_{12}$ nanostructures were measured to deliver the higher specific capacity and better cycling performance, compared with $\text{Li}_4\text{Ti}_5\text{O}_{12}$ nanowires (Figure 11c and 11d). Lee et al. synthesized spinel $\text{Li}_4\text{Ti}_5\text{O}_{12}$ nanotubes via heat treatment and alkali-hydrothermal reactions through simple structural rearrangement, and the $\text{Li}_4\text{Ti}_5\text{O}_{12}$ nanotubes showed a well-performed reversible capacity of $\sim 156 \text{ mAh g}^{-1}$ at a rate of 0.1 C.¹⁷⁸

Compared with LTO, TiO_2 is also a promising alternative as it has a relatively higher theoretical capacity up to 335 mAh g^{-1} . The TiO_2 nanowires reported by Armstrong et al. changed into $\text{Li}_{0.91}\text{TiO}_2$ when delivering a high specific capacity as high as 305 mAh g^{-1} . Its capacity could still be retained at a high level after 50 cycles, which is twice that of TiO_2 nanoparticles. These results illustrated the significance of the control of nanostructures' dimensions for electrochemical optimization of electrodes.^{99,179} The other TiO_2 crystals such as anatase¹⁸⁰ and rutile¹⁸¹ are also good candidates, but the irreversible phase transition from TiO_2 to LiTiO_2 of rutile TiO_2 was the main problem of the capacity loss.¹⁵²

4.2. Interfaces Inside the Heterostructured Composite Nanowires

The other important interface is the one inside the heterostructured composite nanowires. The interface mismatch issues of heterostructured composite nanowires raise a series of problems like strain deformation and conductivity decrease.

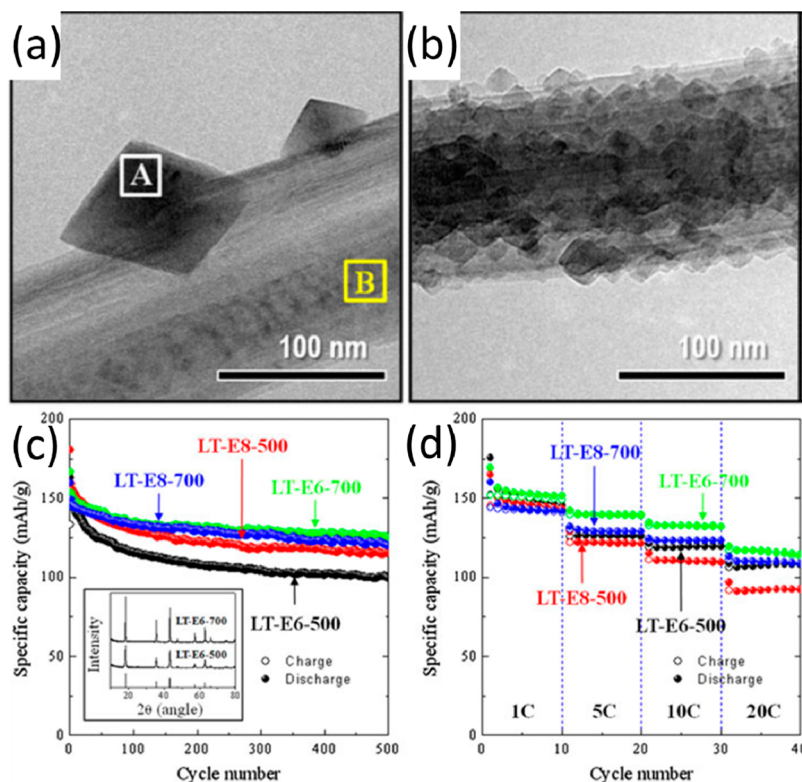


Figure 11. TEM images of LT-E6 (a) and LT-E8 powders (b). Cycling performance (c) and rate performance (d) of synthesized samples. (Inset in c) XRD patterns of the LT-E6-500 and LT-E8-500 powders. Reprinted with permission from ref 177. Copyright 2012 Springer.

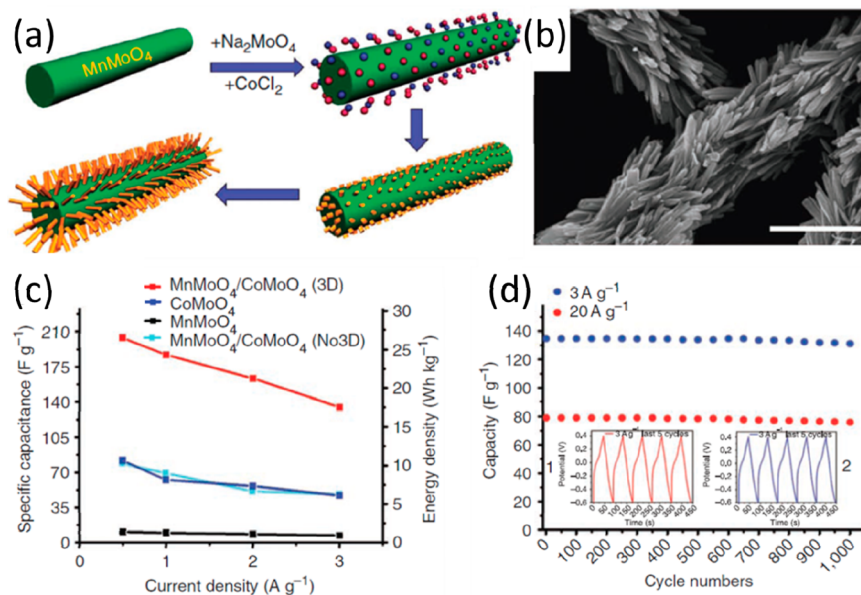


Figure 12. Schematic (a) and SEM image (b) of hierarchical $\text{MnMoO}_4/\text{CoMoO}_4$ heterostructured nanowires. (c) Specific capacitance of different electrodes at different current densities. (d) Cycling performance of $\text{MnMoO}_4/\text{CoMoO}_4$ electrodes. (Inset) Galvanostatic charge–discharge cyclic curves of the first and last five cycles at 3 A g^{-1} . Reprinted with permission from ref 40. Copyright 2011, Rights Managed by Nature Publishing Group.

Some effective approaches are adopted like concentration-gradient^{182,183} and hierarchical structure.^{41,50,184}

Sun et al. reported a concentration-gradient cathode for Li-ion batteries.¹⁸³ This material consisted of Ni-rich material of $\text{Li}(\text{Ni}_{0.8}\text{Co}_{0.1}\text{Mn}_{0.1})\text{O}_2$ surrounded by the concentration-gradient outer layer of $\text{Li}(\text{Ni}_{0.46}\text{Co}_{0.23}\text{Mn}_{0.31})\text{O}_2$. Both the concentration and the oxidation state of Ni, Co, and Mn changed from the core to the surface. Such structure avoided the loss contact between the core and the shell structure and had an excellent electrochemical performance. Mai et al. synthesized a three-dimensional (3D) multicomponent oxide, $\text{MnMoO}_4/\text{CoMoO}_4$ (Figure 12a and 12b).⁴⁰ On the basis of the hierarchical $\text{MnMoO}_4/\text{CoMoO}_4$ materials, the asymmetric supercapacitors were fabricated and a high capacitance of up to 181.1 F g^{-1} was achieved. After 1000 cycles, the 98% capacitance was maintained, showing the high reversibility (Figure 12c and 12d).

In many kinds of hierarchical structures, the branched nanowires usually own the smallest lattice mismatch due to induced nonperpendicular orientation. This can be seen in the combinations of $\text{SnO}_2/\text{Fe}_2\text{O}_3$ ⁴¹ and $\text{SnO}_2/\text{TiO}_2$ ¹⁸⁴ with 6-fold point symmetry and 2-fold symmetry, respectively. Zhou et al. constructed the novel branched heterostructured nanomaterials where SnO_2 nanowire and $\alpha\text{-Fe}_2\text{O}_3$ nanorod served as the stem and branches, respectively (Figure 13a and 13b).⁴¹ They found that when the precursors (FeOOH) branches grew slantwise instead of growing perpendicular, the interfacial lattice mismatch reduced from 47% to 4.6% (Figure 13c and 13d).

5. NANO CHEMISTRY FOR CONTROLLED SYNTHESIS OF NANOWIRE ELECTRODES

The chemical and physical properties of nanowires usually turn out different when using various synthesis strategies. It is confirmed that the crystal forms, compositions, dimensions, and morphologies of synthesized electrodes are important factors influencing their electrochemical performance in energy storage applications. There exist some techniques that are

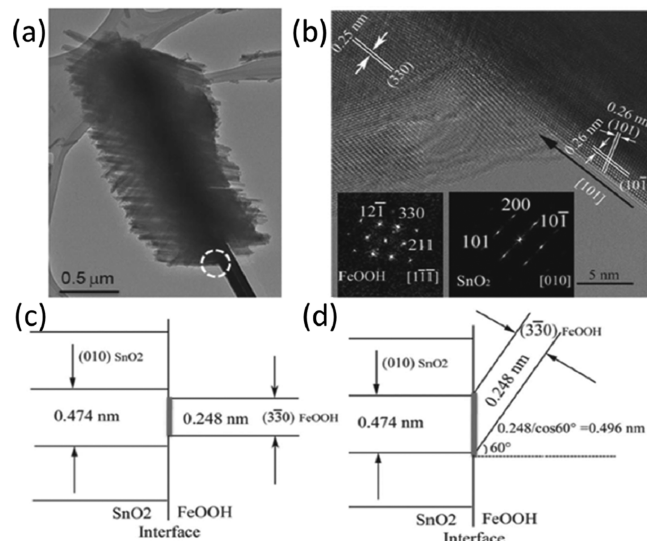


Figure 13. TEM image (a) and HRTEM image (b) of $\text{FeOOH}/\text{SnO}_2$ -branched nanostructure. (Inset in a) Corresponding fast Fourier transformation (FFT) patterns. (c,d) Schematic of the interface of the SnO_2 plane of the stem and FeOOH plane of the branch in different growing directions. Reprinted with permission from ref 41. Copyright 2011 WILEY-VCH Verlag GmbH&Co. KGaA, Weinheim.

widely used for growth of nanowires. They are divided into two basic categories: top-down and bottom-up approaches. In a top-down approach, the entire part is broken into small segments by different methods such as lithography and ball milling.^{185–188} The bottom-up assembly starts with individual atoms and molecules and builds up the desired nanostructures, which provides a low-cost and effective method for nanomaterial synthesis.^{21,189,190} This review mainly focuses on the solution-phase route, hard template method, and oriented-attachment method, which are the most widely used methods for nanowire electrodes, as they can provide facile ways to

Table 2. Typical Synthesis Strategies of Nanowire Electrodes for Energy Storage Devices

synthesis strategies	materials	typical geometry	applications	typical performance	ref
hydrothermal strategy	MnCo ₂ O ₄	nanowire arrays	anode for Li-ion batteries	1288.6 mAh g ⁻¹ at 100 mA g ⁻¹	191
	ZnCo ₂ O ₄	hierarchical nanowire arrays	anode for Li-ion batteries	1530 mAh g ⁻¹ at 200 mA g ⁻¹	88, 192
	α -CuV ₂ O ₆	nanowires	cathode for Li-ion batteries	447–514 mAh g ⁻¹ at 20 mA g ⁻¹	92
	β -AgVO ₃	nanowires	cathode for Li-ion batteries	320 mAh g ⁻¹ at 1 C	193
	V ₂ O ₅	ultralong nanowires	cathode for Li-ion batteries	412 mAh g ⁻¹ at 50 mA g ⁻¹	194–198
	Co ₃ O ₄	hollow nanowire arrays	electrode for pseudocapacitors	599 F g ⁻¹ at 2 A g ⁻¹	199
		mesoporous nanowire arrays	anode for Li-ion batteries	859 mAh g ⁻¹ at 1 C	87
	MoO ₃	nanobelts	cathode for Li-ion batteries	301 mAh g ⁻¹ at 30 mA g ⁻¹	105
	MnO ₂	nanowires	electrode for supercapacitors	360.3 F g ⁻¹ at 0.5 A g ⁻¹	200
	VN	porous nanowires	electrode for supercapacitors	298.5 F g ⁻¹ at 10 mV s ⁻¹	201
solvothermal strategy	LiMn ₂ O ₄	ultrathin nanowires	cathode for Li-ion batteries	100 mAh g ⁻¹ at 60 C	202
	TiO ₂	nanowires, nanotubes	anode for Li-ion batteries	232 mAh g ⁻¹ at 110 mA g ⁻¹	203, 204
template filling strategy	LiFePO ₄	hollow nanowires	cathode for Li-ion batteries	137 mAh g ⁻¹ at 15 C	205
	LiMn ₂ O ₄	nanotubes/porous nanowires	cathode for Li-ion batteries	138 mAh g ⁻¹ at 10 mA g ⁻¹	30, 206, 207
	ZnCo ₂ O ₄	porous nanowires	anode for Li-ion batteries	1197 mAh g ⁻¹ at 100 mA g ⁻¹	208
	LiCoO ₂	nanotubes	cathode for Li-ion batteries	185 mAh g ⁻¹ at 10 mA g ⁻¹	206
microemulsion strategy	MnMoO ₄ /CoMoO ₄	hierarchical nanowires	electrode for supercapacitors	187.1 F g ⁻¹ at 1 A g ⁻¹	40
electrospinning strategy	LiFePO ₄	nanowires	cathode for Li-ion batteries	140 mAh g ⁻¹ at 1 C	209–212
electrochemical deposition	Na ₃ V ₂ (PO ₄) ₃ /C	nanofibers	cathode for Na-ion batteries	103 mAh g ⁻¹ at 0.1 C	213
electrophoretic deposition	RuO ₂ ·xH ₂ O	nanotubular array	electrode for supercapacitors	4320 kW kg ⁻¹ and 7.5 W h kg ⁻¹	214
VLS method	ZnCo ₂ O ₄	nanowire arrays	anode for Li-Ion batteries	960 mA h g ⁻¹ at 60 mA g ⁻¹	215
oriented-attachment method	Si	core–shell nanowires	anode for Li-ion batteries	4277 mAh g ⁻¹ at C/20	25, 128, 216
	Li ₃ V ₂ (PO ₄) ₃ /C	mesoporous nanowires	cathode for Li-ion batteries	128 mAh g ⁻¹ at 1 C	217

precisely control the morphology. Table 2 is a summary of typical examples in synthesis strategies of nanowire electrodes for energy storage devices, which will be discussed below.

5.1. Solution-Phase Route

The solution-phase route has been widely used in nanowires growth due to its good dispersibility of nanowires, control of nanowire diameters, and large-scale production. However, the crystal structures and growth orientations of the nanowire are not easy to be readily controlled by the solution-phase route. Here we highlight some important progress of the solution-phase route.

5.1.1. Hydro(solvo)thermal Strategy. The hydro(solvo)thermal method can be defined as a kind of strategy to synthesize crystalline substances that rely on the solubility of the material under high temperatures and pressures. Formation of crystal typically follows three stages, that is, formation of the supersaturated solution, nucleation, and crystal growth.

The hydrothermal method is widely used to synthesize nanowires as it can create unstable crystalline phases at the melting point.^{202,203,218} Moreover, the hydrothermal approach is very efficient to grow high-quality crystals with less defects and high orientation. Meanwhile, it can realize good control over their composition and morphology by altering the procedure parameters, such as temperature, pressure, and so forth. In many cases, the hydrothermal method is in combination with the uncomplicated sol–gel processing method that produces the most desirable nanostructures with remarkable reliability, efficiency, selectivity, and variety.^{191,219–223}

On the basis of the advantages mentioned above, many materials have been successfully prepared through the hydrothermal method, such as Ag₂V₄O₁₁,^{193,224} Na₃V₂O₁₆·3H₂O,^{225,226} Ag₄V₂O₆,^{227,228} MnO₂,^{221,229,230} WO₃,^{231,232} VO₂,^{233,234} and so forth. Ding et al. synthesized V₂O₅ nanofibers and three vanadium-based oxides (MnV₂O₆ nanosheets, FeVO₄·0.92H₂O nanoneedles, and Sn₂VO₆·0.78H₂O

nanoparticles) under the same hydrothermal conditions and finally get different structures.²³⁵ It could be explained that the properties of the precursor were very important to formation of the final product. α -CuV₂O₆ nanowires were simply fabricated by Ma et al.⁹³

During the reaction the microrods would transfer to nanowires when the reaction parameters such as the reagent ratio and dwell time were controlled via “ripening-splitting” mechanisms.

In addition to disordered nanowires, nanowire arrays can also be fabricated by the hydrothermal method as the substrates are introduced to the solution for growth of nanowires. Li et al. investigated the electrochemical properties of a MnCo₂O₄ nanowire array prepared by a facile hydrothermal method coupled with an annealing treatment (Figure 14a and 14b).²³⁶

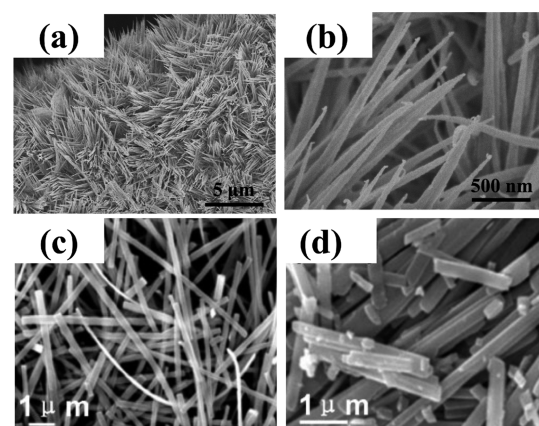


Figure 14. (a, b) SEM images of MnCo₂O₄ nanowire arrays. (c, d) SEM characterization of the nanobelts before and after lithiation, respectively. (a and b) Reprinted with permission from ref 236. Copyright 2014 Elsevier. (c and d) Reprinted with permission from ref 105. Copyright 2007 WILEY-VCH Verlag GmbH&Co. KGaA, Weinheim.

The MnCo_2O_4 nanowire array electrode was grown directly on nickel foam without organic binders or conductive additives and achieved good cohesiveness and electrical conductivities. The MnCo_2O_4 nanowire array presented high specific capacitance and rate capability, showing promising potential as the pseudocapacitive material. Hu et al. prepared highly entangled TiO_2 nanowires grown on Ti substrates at 180 °C utilizing various organic solvents to oxidize Ti.²³⁷ Nanoforest-like hierarchical ZnO nanowires grown on the substrate were reported by Ko et al.²⁶ ZnO ^{238,239} and Bi_2S_3 ²⁴⁰ arrays on the substrate were also prepared.

Notably, the hydrothermal reaction can be used for modification of the nanowires. Mai et al. synthesized $\alpha\text{-MoO}_3$ nanobelts which were prelithiated with LiCl solution through a secondary hydrothermal process. After the prelithiation process the crystal structure and surface morphology of nanobelts could be retained (Figure 14c and 14d).¹⁰⁵ Compared to that of nonlithiated nanobelts, the electrical conductivity of the prelithiated MoO_3 nanobelts was enhanced approximately 2 orders of magnitude. In addition, the lithiated MoO_3 nanobelts showed great cycling stability.

Lu et al. assembled a quasi-solid-state asymmetric supercapacitor with high energy density and cycling performance, which was composed of porous VO_x nanowire cathode and VN nanowire anode. Each individual carbon fiber was wrapped by hydrothermally grown interlaced VO_x nanowires (Figure 15).²⁰¹

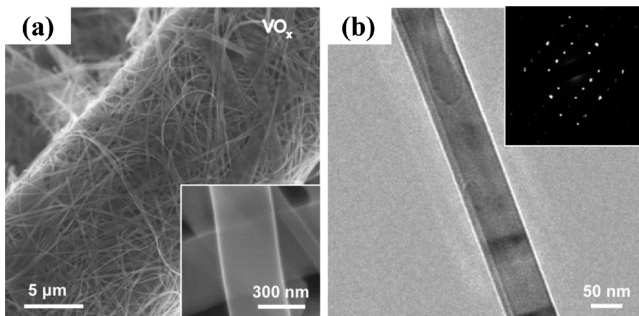


Figure 15. (a) SEM image of VO_x nanowires grown on carbon cloth substrate. (Inset) Corresponding magnified SEM image. (b) TEM image of a VO_x nanowire. (Inset) Corresponding SAED pattern. Reprinted with permission from ref 201. Copyright 2013 American Chemical Society.

The hydrothermal growth method can be also used together with the “soft template”. Xu et al. reported the synthesis process of two kinds of conductive polyaniline (PANI) hierarchical nanowires combined with graphene oxide (GO) nanosheets. By changing the content of aniline, the PANI nanowires exhibited different morphologies due to the varied nucleation mechanism. The heterogeneous nucleation growth direction of PANI nanowires was demonstrated to be vertical on GO substrate. In the homogeneous nucleation process, aniline micelles acted as the “soft template” to produce random connected PANI nanowires. Figure 16 illustrates the formation mechanism of PANI–GO nanocomposites.²⁴¹

The solvothermal strategy is also widely employed for preparation of nanowires.^{202,242,243} Su et al. deposited ordered nanowire upon fluorine-doped tin oxide (FTO) coated glass through the solvothermal technique. A WO_3 seed layer was used to initiate growth, with the geometries tailored by

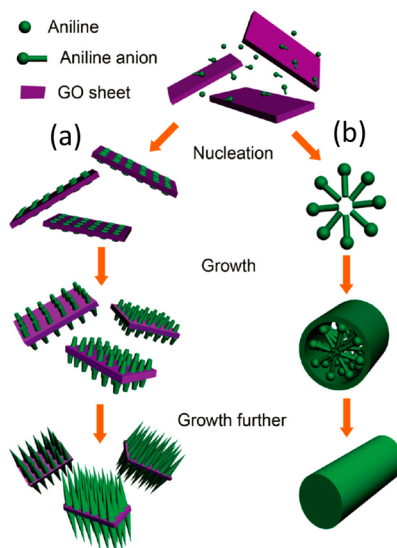


Figure 16. Schematic of the nucleation and growth mechanism of PANI nanowires for heterogeneous nucleation on GO nanosheets (a) and homogeneous nucleation in bulk solution (b). Reprinted with permission from ref 241. Copyright 2010 American Chemical Society.

adjusting the hydrothermal precursor composition. By adjustment of the amount of water and oxalic acid in the precursor, nanowire arrays were selectively deposited.²⁴⁴

5.1.2. Microemulsion Strategy. The microemulsion strategy has been widely used in the synthesis of a 1D nanostructure due to its facility, low consumption, and efficiency.²⁰⁴ In this route, nanosized water droplets, which act as reactors for nanoparticle formation, form in the core of spontaneously aggregated surfactant molecules. The water-in-oil droplets will get together rapidly inside droplets because of the systematic kinetics, resulting in the droplets precipitation and nanoparticles formation. Accordingly, the kinetics can be in the control of ions interactions in microemulsion reactions.²⁴⁵ The major superiority in this approach is that the controlled shapes and size distributions of particles can be realized with the different reactant concentrations, water to surfactant ratios, and aging time.²⁰⁴ The main disadvantage is the poor stability of microemulsion systems.

Jang et al. prepared size-tunable SiO_2 nanotubes using the reverse-microemulsion-mediated sol–gel strategy.²⁴⁶ Figure 17

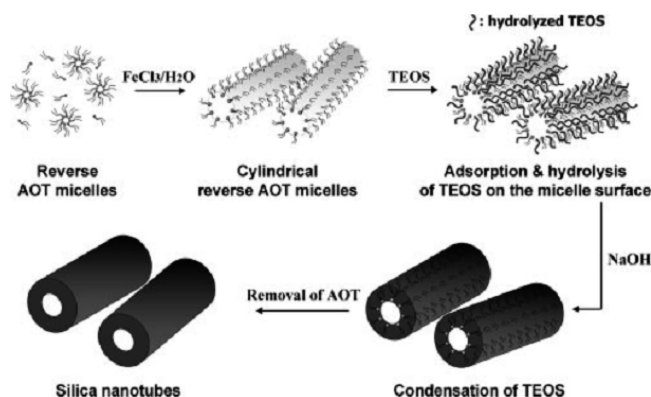


Figure 17. Schematic of the fabrication process of SiO_2 nanotubes. Reprinted with permission from ref 246. Copyright 2004 WILEY-VCH Verlag GmbH&Co. KGaA, Weinheim.

is the schematic illustration of the fabrication process. In this process, the cylindrical reverse micelles acted as the soft template where the sol–gel reaction happened, forming silica nanotubes at the water–oil interface.

Du et al. used a simple microemulsion-based method to synthesize $ZnCo_2(C_2O_4)_3$ nanowires, and it could be transformed to porous $ZnCo_2O_4$ nanowires under annealing conditions.²⁰⁸ Figure 18a and 18b presents the SEM images

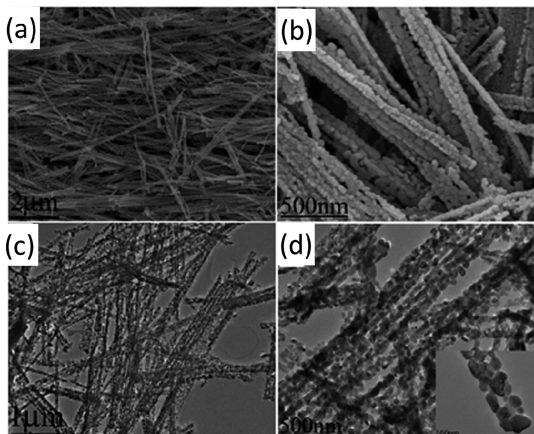


Figure 18. SEM images (a, b) and TEM images (c, d) of $ZnCo_2O_4$ nanowires. Reprinted with permission from ref 208. Copyright 2011 American Chemical Society.

of $ZnCo_2O_4$ nanowires synthesized via annealing of $ZnCo_2(C_2O_4)_3$ nanowires at 700 °C. As observed from the TEM images (Figure 18c and 18d), there were plenty of nanopores inside the nanowires. This study showed that the porous nanowires morphology changed along with the different annealing temperatures. Notably, the as-prepared electrodes exhibited a high initial capacity of 1331.5 mAh g⁻¹ and good cycling performance for lithium batteries.

5.2. Hard Template Methods

The template method has been widely utilized to synthesize the nonoriented and oriented nanowires, which exhibit outstanding properties, especially superconducting and electrochemical properties. Many templates are used for formation of nanowires, in which the anodized alumina membrane (AAM)^{247–249} and radiation track-etched polycarbonate (PC) membranes become the most popular choices.²⁵⁰ Meanwhile, many other templates are applied for formation of nanowires.²⁵¹ Current developments show that application of a template can be divided into four types, namely, template filling strategy, electrochemical deposition, electrophoretic deposition, and electrospinning strategy.

5.2.1. Template Filling Strategy. Template filling represents a most direct way to get 1D nanostructured arrays, although it appears difficult to fill the materials in template pores completely. The final morphology of the filling materials turns out different with different adhesive force between the pores and the materials. When the force is weak or solidification occurs at the pores center, it is most likely to get the solid nanowires. Otherwise, hollow nanotubes are likely to be obtained.²⁵¹ Lu et al. synthesized SBA-15 nanorod arrays in AAM (Figure 19).²⁵² The as-prepared SBA-15 exhibited vertical alignment in the hard template. Tao et al. demonstrated that template synthesis could be used to create arrays of nanowires from the biocompatible, biodegradable polymer

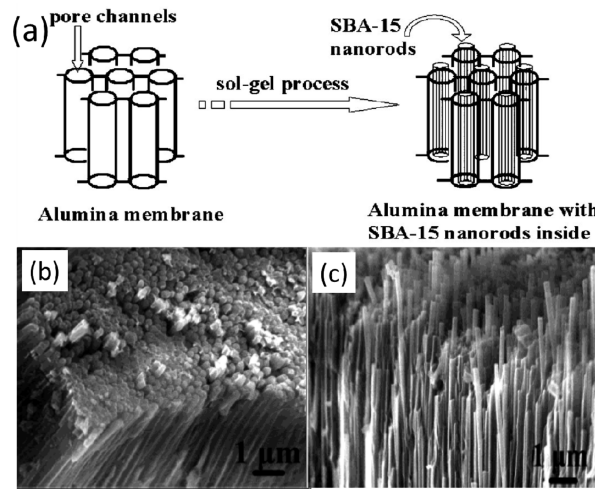


Figure 19. (a) Schematic of the fabrication process of SBA-15 nanorods. Top view (b) and side view (c) SEM image of SBA-15 with AAM. Reprinted with permission from ref 252. Copyright 2004 American Chemical Society.

poly(ϵ -caprolactone).²⁵³ They also found that nanostructure morphology could be controlled, and complex patterning could be achieved.

5.2.2. Electrochemical Deposition. In the electrochemical deposition process, the template disperses in the solution and attaches to the cathode while the anode is parallel to the template. Under the influence of the electric field, the nanowires grow inside the template pores through diffusion of cations toward the cathode. After removal of template membrane, nanorod or nanowire arrays are prepared.^{117,254,255}

The triblock copolymer-assisted hard-template method was applied by Tao et al. to construct an ordered array of nickel nanotubes.³⁵ Figure 20a and 20b shows the SEM images of nickel nanotube arrays after removal of AAM. The annealed

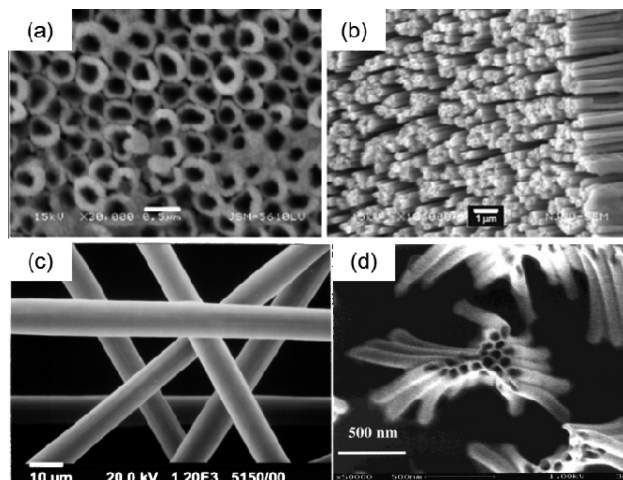


Figure 20. Top view (a) and side view (b) SEM images of Ni nanotubes array after partial removal of the AAM. (c) SEM image of a composite deposit prepared from a 5 mM $ZrOCl_2$ + 0.4 g L⁻¹ PEI solution on a carbon felt. (d) SEM image of PPy nanotubes. (a and b) Reprinted with permission from ref 35. Copyright 2006 WILEY-VCH Verlag GmbH&Co. KGaA, Weinheim. (c) Reprinted with permission from ref 257. Copyright 2004 American Chemical Society. (d) Reprinted with permission from ref 258. Copyright 2001 American Chemical Society.

$\text{RuO}_2 \cdot x\text{H}_2\text{O}$ nanotubes with a 3D arrayed architecture were successfully designed and tailored by Hu et al.²¹⁴ The material presented excellent electrochemical performance (ultra-high-power characteristics and high capacity) required for next-generation energy storage devices. Molares et al. reported direct current potentiostatic deposition of single-crystalline Cu nanowires using an ion track membrane,²⁵⁶ which showed the possibility to compare the effects of the transport process in poly- and single-crystalline nanowires.

5.2.3. Electrophoretic Deposition. The electrophoretic deposition technique is useful for applying materials to any electrically conductive surface, especially for ceramics and organoceramics deposition in colloidal dispersion.^{259,260} The electrical charge occurred on the surface of nanomaterials through one or more of the following mechanisms: (1) dissolution along preferential directions, (2) charges/charged species deposition, (3) reduction or oxidation along preferential directions, and (4) charged species physical adsorption.²⁵¹ Pang et al. prepared composite films by electrophoretic deposition of poly(ethyleneimine) or poly(allylamine hydrochloride) combined with cathode precipitation of zirconia (Figure 20c).²⁵⁷ The obtained results pave the way for fabrication of other composites based on weak cationic polyelectrolyte and metal oxides or hydroxides. Nanotubes are commonly observed for polymer materials. Dauginet et al. succeeded to modify the charge state and hydrophilicity of the PET and PC films by a two-step sequence involving hydrolysis of ester or carbonate bonds under basic conditions followed by adsorption of a polyelectrolyte (Figure 20d).²⁵⁸

5.2.4. Electrospinning Strategy. Electrospinning is widely used to generate very fine fibers from a liquid using an electrical charge. It can be used to synthesize a rich variety of materials that includes polymers, composites, and so forth. An illustration of the basic setup for electrospinning is shown in Figure 21.

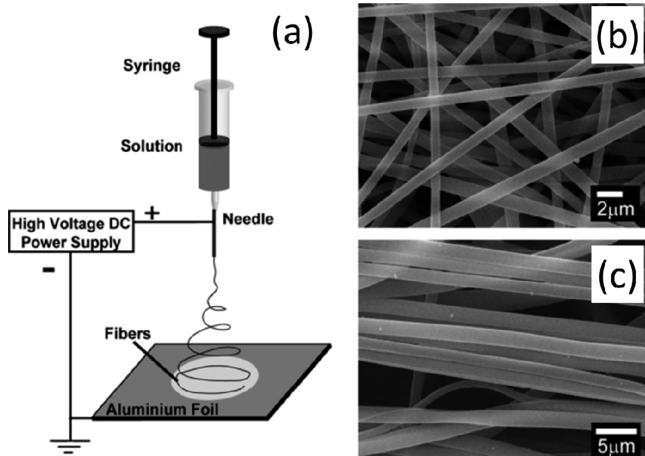


Figure 21. (a) Schematic of electrospinning approaches. SEM images of electrospun polymer nanofibers without (b) and with (c) preferential orientation. Reprinted with permission from ref 262. Copyright 2011 Elsevier.

With the use of a syringe pump, the solution can be fed through the spinneret at a constant and controllable rate. The liquid droplets are distorted into a conical object (Taylor cone) under a sufficiently high voltage. The electrified jet then undergoes a stretching and whipping process, dries in flight, and eventually is deposited on the grounded collector. The charge fibers are often constituted of randomly oriented nanowires with a big

length to diameter ratio, high surface area, complex pore structure, and alignment on the molecular level. As a result, many kinds of nanowires have been fabricated by the electrospinning method.²⁶¹

As there are some intrinsic properties requirements for the electrospinning precursor, such as viscosity, elasticity, electrical conductivity, and so on, as a result, the electrospinning method is first applied to synthesize polymer nanowires.^{263–267} Li et al. reported the fabrication of uniform and homogeneous MEH-PPV/PVP fibers through cospinning (Figure 22a).²⁶⁸ The

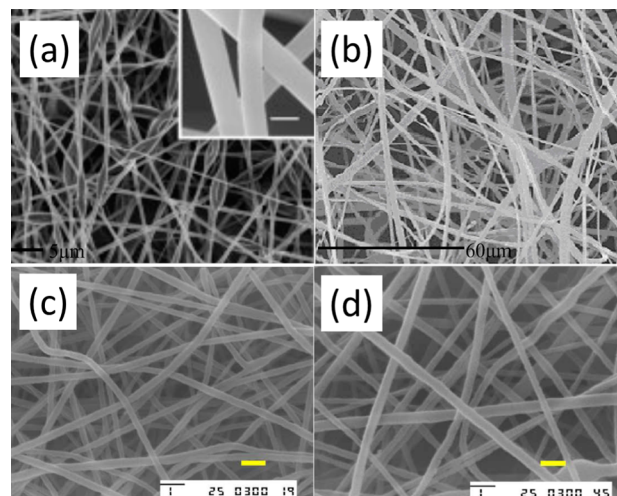


Figure 22. (a) SEM image of MEH-PPV/PVP fibers. (b) SEM image of CSA-doped POA-PS composite fibers. SEM images of PPy nanofibers from aqueous solutions of 1.5 wt % PEO and 62.5 wt % (c) and 71.5 wt % (d) PEO. Scale bar, 1 μm (ref 271). (a) Reprinted with permission from ref 268. Copyright 2004 WILEY-VCH Verlag GmbH&Co. KGaA, Weinheim. (b) Reprinted with permission from ref 269. Copyright 2011 Elsevier. (c and d) Reprinted with permission from ref 271. Copyright 2006 Elsevier.

results indicated that the morphology of the resultant MEH-PPV fibers could be tuned by adjusting the concentration and its feed rate. Also, the extent of mixing was dependent on the volume of solvent contained in the compound jet. Aussawasathien et al. produced camphorsulfonic acid (CSA)-doped poly(oanisidine) (POA)-polystyrene (PS) composite fibers in the nonwoven mat form (Figure 22b).²⁶⁹ Compared to the other two components, POA and CSA, variation in PS content had a greater influence on fiber features. Norris et al. prepared the CSA and poly(ethylene oxide) (PEO)-doped PANI ultrafine fibers through electrospinning. In these fibers, the diameter ranged from 950 nm to 2.1 mm, and the same widths were shown along the fiber.²⁷⁰ Chronakis et al. reported the synthesis of conducting polypyrrole (PPy) nanofibers with 70–300 nm diameters by electrospinning (Figure 22c and 22d).²⁷¹ In the nanofibers, PEO was added to enhance the processability of PPy. Moreover, electrical transport and diameters of nanofibers could be tuned by changing PEO concentrations.

Except for the pure polymer nanowires mentioned above, polymers are also applied to fabrication of inorganic nanowires which would increase the viscosity of the precursor, thus realizing successful electrospinning of inorganic nanowires. Kanjwal et al. combined the electrospinning process with a hydrothermal technique to produce a new hierarchical nanostructure that consists of cobalt oxide (Co_3O_4) and zinc oxide (ZnO).²⁷² Shim et al. reported the fabrication of

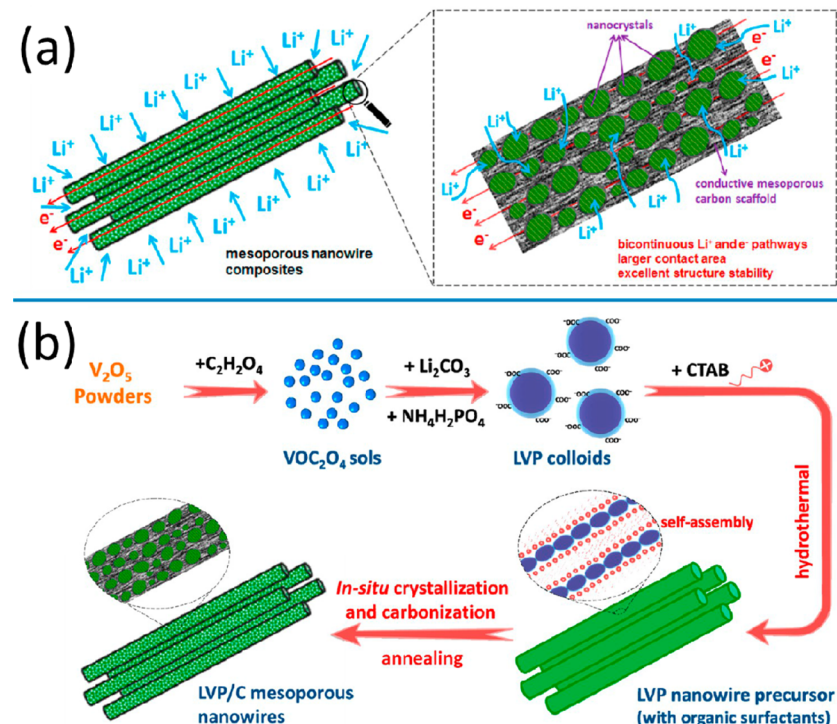


Figure 23. (a) Schematic of the hierarchical nanowires with bicontinuous electron/ion transport pathways. (b) Schematic of the fabrication mechanism of LVP/C-M-NWs. Reprinted with permission from ref 217. Copyright 2014 American Chemical Society.

polycrystalline WO₃ nanowire electrodes prepared on an indium tin oxide (ITO)-coated substrate by the electrospinning method.²⁷³ The 1D WO₃ nanowires had faster charge transfer. Xu et al. prepared porous In₂O₃ nanotubes and nanowires in cubic phase via electrospinning.²⁷⁴ A novel nanowire network catalyst made of highly dispersed Pt nanoparticles into an electrospun Pt nanowire network was prepared by Kim et al.²⁷⁵

As an important nanofiber fabrication method, electrospinning holds significant promise due to its relatively low cost and high production rate. Also, the operation parameters can be readily reconfigured to produce fibers with various structures. The catalog of electrospun nanofiber products, such as ceramics, metals, alloys, and composites fibers, has attracted much attention for its potential application in energy devices like fuel cells, solar cells, and lithium-ion batteries.

5.3. Oriented-Attachment Method

Currently, the present continued research efforts are directed toward the oriented attachment method to synthesize nanowires with controlled morphology and dimensions.^{276–279} The oriented attachment route is based on the crystallization process that occurred naturally for the nanomaterials.^{280,282} It is demonstrated that nanoparticles can join together either with perfect aligned lattice planes by sharing specific crystallographic orientation or with dislocations by slight misorientation at the interface, requiring only similar surface symmetries²⁸¹ and a nearly zero kinetic barrier.²⁷⁶

Mai et al. used oriented-attachment technique to achieve the 3D hierarchical MnMoO₄/CoMoO₄ heterostructure, exhibiting a high specific capacitance.⁴⁰ Wei et al. reported a facile way to obtain the hierarchical lithium vanadium phosphate/C mesoporous nanowires (LVP/C-M-NWs).²¹⁷ In this synthesis process the surfactants self-assembled together and the Li₃V₂(PO₄)₃ colloids attached on them, forming hierarchical nanowires (Figure 23). It was noted that the charged

homogeneous micelles played important roles in controlling the curvature of the surface.

With the further development in the oriented attachment method, deeper understanding in the reaction mechanism is very urgent for highly ordered nanowires self-assembly.²⁸² The ordered nanowires with controllable structures, morphologies, and hierarchies will be of great potential for energy storage devices in consideration of their unique arrangements.

6. NANOWIRE ELECTRODES FOR ADVANCED AND NEXT-GENERATION ENERGY STORAGE DEVICES

Electrochemical energy storage devices are undergoing a period of rapid development. On one hand, they are optimized for conventional use. On the other hand, along with the new requirements of applications, some new types of energy storage devices emerge and develop quickly. As mentioned above, nanowire electrodes possess many unique properties in this field. In this section, advanced and next-generation energy storage devices, including advanced lithium batteries and sodium batteries, Li–air batteries, Li–S batteries, and micro/nanoscale energy storage devices, are summarized and discussed in detail. Figure 24 shows the typical applications of nanowires for energy storage devices, which are discussed below.

6.1. Nanowire Electrodes for Advanced Lithium-Ion Batteries

As a typical kind of energy storage device, lithium-ion batteries exhibit high-energy performance compared with electrochemical capacitors. However, there is still strong demand for high-power batteries and some new types of batteries. Herein, we mainly focus on the ultrafast and flexible lithium-ion batteries in this subsection.

6.1.1. Nanowire Electrodes for Ultrafast Lithium-Ion Batteries.

As an important feature for lithium-ion batteries,

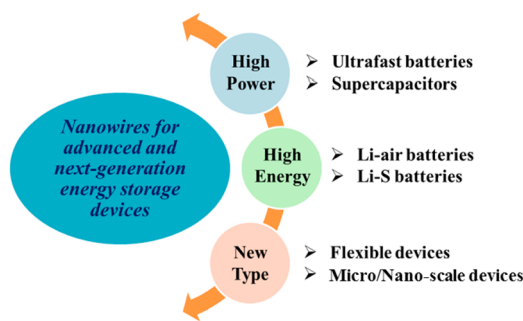


Figure 24. Schematic of general advanced and next-generation energy storage devices.

ultrafast charging–discharging has become one of the most serious limitations for further development of electric vehicles and portable devices especially with high power density and high power consumption, respectively.²⁸³ In the research of lithium-ion batteries, the rate of charging–discharging is mainly determined by (i) the kinetics of Li^+ -ion diffusion, (ii) electrical conductivity, and (iii) structure stability of electrode materials. To realize the ultrafast charging–discharging or improve the rate capability in batteries, a general strategy is using nanoscale materials, such as nanowires with large surface area, short Li^+ -ion diffusion distances, enhanced electron transport, and better accommodated internal strain. In addition, some other specific strategies based on nanowires could further improve the rate capability.

To shorten the Li^+ -ion intercalation/deintercalation time, decreasing the Li^+ -ion diffusion distance and increasing the reactivity of the intercalating/deintercalating sites can be considered as efficient methods. To achieve these two points, decreasing the diameter can satisfy both. Lee et al. successfully obtained improved power density on ultrathin cubic spinel.

LiMn_2O_4 nanowires.²⁰² With several micrometers in length and less than 10 nm in diameter (Figure 25a), the fabricated nanowires showed excellent kinetic performance. At ultrahigh rates of 60 and 150 C, the ultrathin nanowires still delivered high capacities of 100 and 78 mAh g^{-1} , respectively, and exhibited outstanding capacity retention. It was inferred that this morphology allowed for structural transformation between the tetragonal and the cubic phase (Figure 25b). Compared with the LiMn_2O_4 nanorods,²⁸⁴ the electrochemical performance is much better. Decreasing the diameter of nanowires can shorten the distance from the surface into the inside along the radial direction; furthermore, the surface area can be improved and provide more intercalation/deintercalation sites of Li^+ ions, so the rate performance is improved. With increased surface area, the porous nanowires are also applied in lithium-ion batteries.^{180,285,286} Actually, the porous nanowires have a similar function in decreasing the diffusion distance and increasing the reactive sites. In addition, for the lithium-ion battery electrode materials diffusion can sometimes happen in specific planes or the diffusion barrier in different planes is different.²⁸⁷ Thus, when the nanowires are grown along a specific orientation, diffusion of lithium ions will be much faster.

To increase the electrical conductivity, combining the electrode materials with conductors, including graphene,²⁸⁸ carbon nanotube,^{289–292} and conductive substrate,^{22,25,141,243,293,294} is commonly reported. VO_2 –graphene nanoribbons (Figure 25c) were reported to demonstrate a less than 7% capacity loss after 1000 cycles at 190 °C. Even at 75 °C, it can also show good cycling performance at 28 °C (Figure 25d).²⁸⁸ By combining $\text{FePO}_4 \cdot \text{H}_2\text{O}$ or LiFePO_4 with a carbon nanotube, the rate capability is also enhanced.²⁹¹ Conductive substrates are most widely used to improve the rate capability for nanowire arrays. It can not only provide facile transfer of electrons but also avoid the aggregation of nanowires and

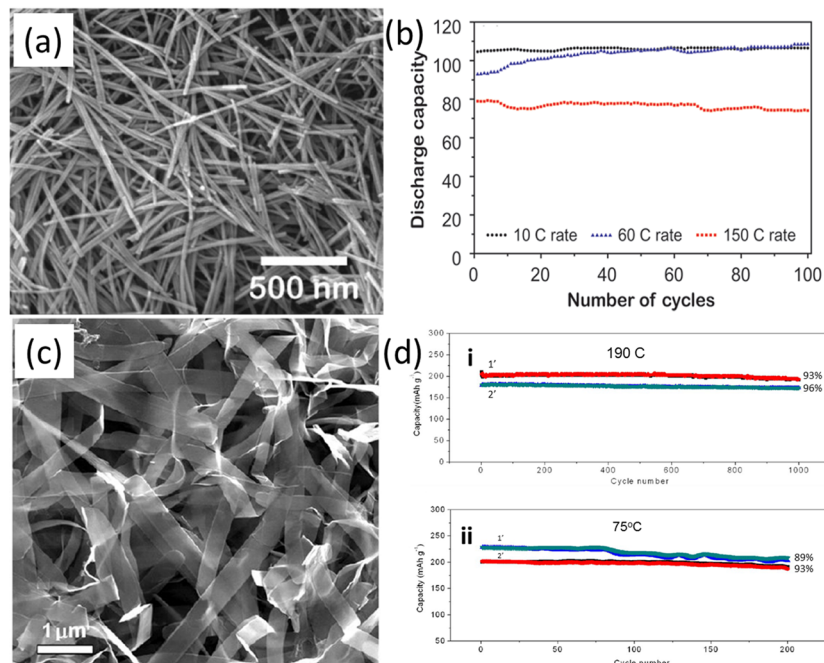


Figure 25. (a) SEM image of ultrathin LiMn_2O_4 nanowires. (b) Cycling stability of ultrathin LiMn_2O_4 nanowire in different potential ranges (10 C 3.1/4.3 V, 60 C 2.4/4.4 V, 150 C 1.5/4.5 V). (c) SEM image of VO_2 –graphene ribbons. (d) Cycling stability of VO_2 –graphene ribbons under different temperatures and rates. (a and b) Reprinted with permission from ref 202. Copyright 2010 American Chemical Society. (c and d) Reprinted with permission from ref 288. Copyright 2013 American Chemical Society.

maintain the surface area. Self-supported hydrogenated $\text{Li}_4\text{Ti}_5\text{O}_{12}$ nanoarrays (H-LTO NAWs) were fabricated on Ti foil (Figure 26a and 26b), it can deliver a relatively high

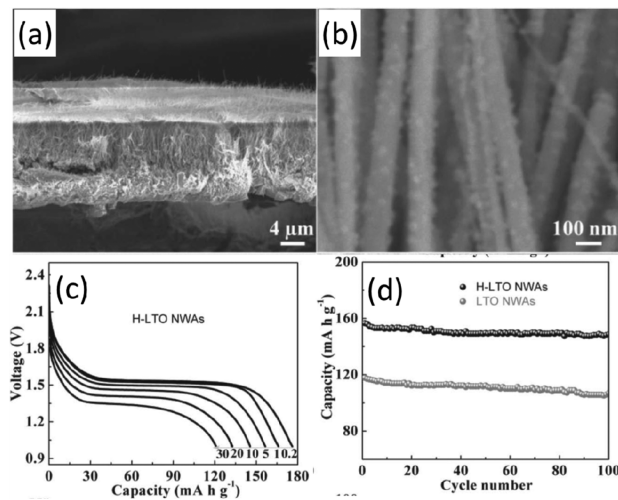


Figure 26. (a, b) Cross-sectional SEM image of H-LTO NAWs. (c) Discharge curves at various C rates. (d) Cycling performance of H-LTO NAWs at 5 C. Reprinted with permission from ref 243. Copyright 2012 WILEY-VCH Verlag GmbH&Co. KGaA, Weinheim.

capacitance and 5% loss of capacity after 100 cycles at a rate of 5 C (Figure 26c and 26d), revealing a good cycling performance at high current. Most electrode materials are chalcogen compounds, which are usually semiconductors or even insulators, showing low conductivity.²⁴³ Thus, the conductivity is considered as a limitation for ultrafast charge and discharge rate. When the electrode materials are combined with the conductors, the electron can be delivered to nanowires, electron diffusion on the electrode surface will be much faster, and rate capability will be enhanced.

During the charge and discharge processes most electrode materials will suffer a structure change except some zero-strain materials like $\text{Li}_4\text{Ti}_5\text{O}_{12}$, and this structure change in the conversion reaction is more severe. To maintain the structure of electrode materials, the core/shell architecture can be considered as an efficient approach.^{76,295,296} SnO_2 is one of the highest capacity anodes, but a large volume change during charge and discharge exists. Yan et al. coated SnO_2 nanowires with V_2O_5 (Figure 27a and 27b), which revealed an excellent rate performance at high current densities, and the power density of as-prepared electrodes could reach 60 kW kg^{-1} . In addition, it also exhibited good performance at low temperature.²⁹⁷ It was found that for SnO_2 nanowires the carbon, aluminum, or copper coating could result in an improvement of about 10 times in charging rate. Through TEM observation (Figure 27c and 27d) the coating layer could completely suppress radial expansion of the nanowires; thus, their structural change can be restrained and the rate capability can be promoted.⁷⁶ When nanowires are coated by other materials, the interior of the shell material can be considered as the nanoreactor chamber and can avoid collapse of the core, further improving the rate capability. Besides, the structure of the electrode can be maintained through constructing buffered structures;²⁹⁸ a buffered section between the nanowires will prevent volume swelling during lithiation/delithiation and offer facile strain relaxation, so good rate performance can be

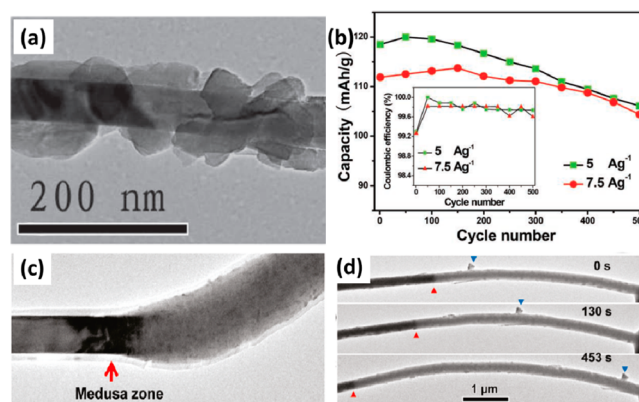


Figure 27. (a) TEM image of V_2O_5 -coated SnO_2 nanowire. (b) Cycling stability of V_2O_5 -coated SnO_2 nanowires at different current densities. (c) TEM image of uncoated SnO_2 nanowire in the charging process. (d) TEM image of carbon-coated SnO_2 nanowire in the charging process. (a and b) Reprinted with permission from ref 297. Copyright 2011 WILEY-VCH Verlag GmbH&Co. KGaA, Weinheim. (c and d) Reprinted with permission from ref 76. Copyright 2011 American Chemical Society.

achieved. In addition, the conductivity can be improved through doping with supervalent ions or low-valent ions, resulting in an improvement of rate capability.²⁹⁹

Through modification of nanowires, the rate capability can be greatly enhanced. Aforementioned modification methods are available to promote the rate performance, such as fabricating a core/shell structure^{300–302} or hierarchical heterostructure.⁷⁶ In some conditions, some architectures are able to achieve the enhanced kinetics of lithium-ion diffusion and electrical conductivity at the same time, such as the VO_2 –graphene nanoribbons when the ribbons become thinner. Notably, an important factor is the delivery of Li^+ ions and electrons to the surface of the electrode,³⁰³ where the Li^+ ions and electrons first diffuse from the electrolyte and the current collector, respectively. It could be the limitation for further improving the rate capability, and modifying the surface of the nanowires may further enhance Li^+ -ion and electrons transport rate which is seldom reported.

6.1.2. Nanowire Electrodes for Flexible Lithium-Ion Batteries. Flexible energy storage devices possess great potential in practical applications of portable electronic devices, such as roll-up displays, electronic paper, mobile phones, and computers.^{304–306} A variety of flexible polymers are usually selected as supporters to achieve the mechanical flexibility for sheet-like and cable-type flexible batteries. Nanowire electrodes have excellent electrochemical performance and good contact with conductive thin films coated on supporters. Moreover, in the bending processes the nanowire electrodes can provide a continuous electronic transport pathway compared with nanoparticle electrodes, which enables continuous high-energy output of fabricated flexible energy storage devices.^{87,192}

Nam et al. assembled macroscopically ordered Co_3O_4 viral nanowires at room temperature, which were driven by electrostatic forces, polyelectrolyte interdiffusion, and viruses' anisotropic character (Figure 28a and 28b).³⁰⁷ As-prepared ordered nanowires enabled the high flexibility and transparency of the constructed energy storage films through a facile dipping method (Figure 28c). Electrochemical measurements showed that at a rate of 1.12 C the macroscopically ordered Co_3O_4 viral nanowires could deliver as high as 94% of the theoretical

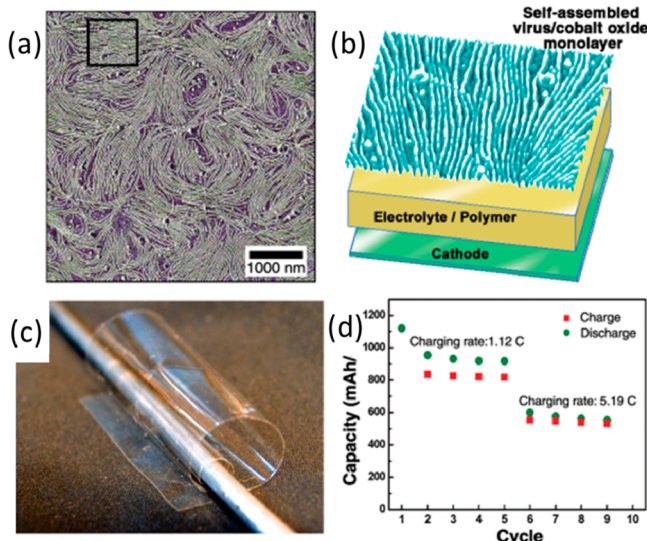


Figure 28. (a) Optical image of driven Co_3O_4 nanowires. (b) Phase-mode atomic force microscope image of a macroscopically ordered monolayer of Co_3O_4 -coated viruses. (c) Digital camera image of the flexible and transparent free-standing film of assembled nanostructured monolayer of Co_3O_4 viral nanowires. (d) Charging/discharging cycling curves of the assembled monolayer of Co_3O_4 nanowires. Reprinted with permission from ref 307. Copyright 2006 AAAS.

capacity and exhibit great cycling stability (Figure 28d). Their results demonstrate great advantages and potentials of nanowire-based films in the application of flexible energy storage devices.

It is worth noting that the wire-shaped batteries, which can be easily woven into textiles or other structures, become an important part in flexible energy storage devices.^{308–310} To fabricate highly flexible and wire-shaped lithium-ion batteries, the novel MWCNT/Si composite fiber was developed and reported by Peng's group (Figure 29a and 29b).³⁰⁸ The twisted MWCNT in the fiber showed high alignment, which largely improved the electrical transport of Si and the mechanical strength of the device. Moreover, the flexible 1D-shaped design could even be made into a knot and utilized as an effective electrode for flexible lithium-ion batteries when the Li wire was

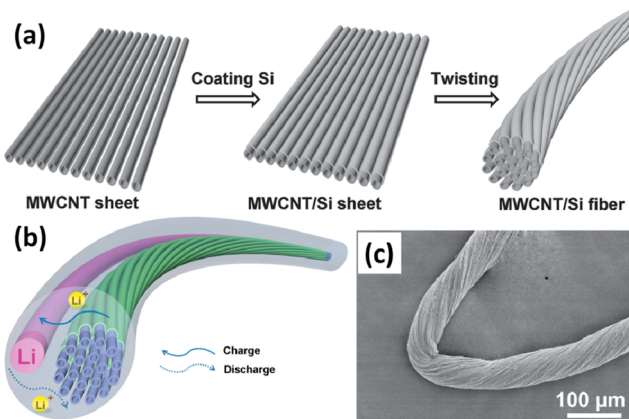


Figure 29. (a) Schematic of the fabrication process of the aligned MWCNT/Si composite fiber. (b) Schematic of the wire-shaped lithium-ion battery. (c) SEM images of the bent aligned MWCNT/Si composite fiber. Reprinted with permission from ref 308. Copyright 2013 WILEY-VCH Verlag GmbH&Co. KGaA, Weinheim.

used as the counter electrode (consult Figure 29b). For this kind of energy storage device nanowires are believed to have great potential because of their natural geometric advantages in electrical and ion transport.

6.2. Nanowire Electrodes for Advanced Sodium-Ion Batteries

Recently, sodium-ion batteries have received widespread attention.^{311–318} Although lithium-ion batteries have been commercialized for more than 20 years and widely applied in portable electronics,³¹⁹ the limitation of the Li resource and its high cost has made it not suitable for large-scale storage systems in the future.^{320,321} In comparison, because of the large availability of sodium, the low price and its similar electrochemical process with Li-ion chemistry, Na-ion batteries are regarded as one of the most promising candidates for large-scale energy storage such as an electrical grid.^{322–325}

However, since the radius of the Na^+ ion is approximately 70% larger than that of the Li^+ ion,⁹ the diffusion resistance of Na ions is much larger in the charge–discharge process,^{326–328} and the volume expansion problem is also more conspicuous especially for conversion and alloying reaction electrodes.^{329,330} In this case, nanomaterials, especially 1D nanostructures with a short ion diffusion distance and facile stress release, are essential for long-life and high-rate sodium-ion batteries.³³¹

Cao et al. utilized the advantages of nanowires to sodium-ion batteries for the first time.³³² They prepared single-crystalline $\text{Na}_4\text{Mn}_9\text{O}_{18}$ nanowires with high crystallinity and homogeneous structure (Figure 30a and 30b). The $\text{Na}_4\text{Mn}_9\text{O}_{18}$ nanowire electrode showed not only outstanding rate capability but also excellent cyclability. It exhibited high capacities of 128 and 82 mAh g^{-1} at rates of 0.1 and 2 C, respectively, demonstrating facile kinetic characteristics. In addition, its capacity retention reached up to 77% even after 1000 cycles at 0.5 C (Figure 30c), much better than that of $\text{Na}_4\text{Mn}_9\text{O}_{18}$ prepared by the solid-state reaction. The superior electrochemical performance is attributed to their nanowire morphology and high crystallinity, ensuring fast Na^+ -ion diffusion and good structural stability during intercalation and extraction.

Afterward, numerous 1D electrode materials with different types began to be used for sodium-ion batteries constantly, such as hollow nanowires,³³³ nanotubes,^{334,335} core–shell nanoforests,³³⁶ porous nanowires,³³⁷ and carbon-coated nanofibers.³³⁸ Compared to single nanowires, these complex constructions show more versatile features and better performance. Wang et al. synthesized microspheric $\text{Na}_2\text{Ti}_3\text{O}_7$ consisting of tiny nanotubes with a size of about 8 nm in the outer diameter (Figure 30d and 30e).³³⁴ This structure can provide an ultrashort ionic and electronic diffusion distance and increase the specific surface area; most importantly, it can allow Na^+ ions to insert not only into the crystal lattice of $\text{Na}_2\text{Ti}_3\text{O}_7$ but also into the nanotubes and form an electrical double-layer capacitor. Thus, the tiny nanotubes are equal to the combination of battery electrodes and capacitor electrodes, which should exhibit a good rate performance. A significant result was that even at the high current density of 3540 mA g^{-1} (about 10 C), the discharge capacity was still maintained at 85 mAh g^{-1} after 100 cycles (Figure 30f), which could be used in rapid charging and discharging energy storage systems.

1D nanostructural electrodes show great advantages in the electrochemical performance for sodium-ion batteries, and in addition, since nanowires can be easily used to assemble electrochemical nanodevices,^{34,339} study of 1D electrode

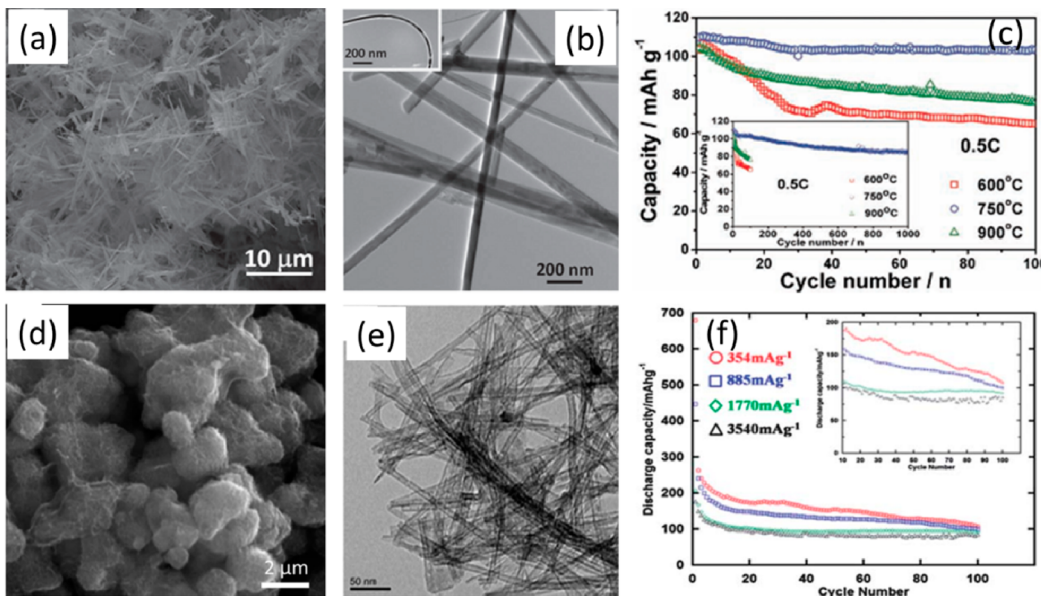


Figure 30. (a) SEM images of Na₄Mn₉O₁₈ samples. (b) TEM image of dispersed Na₄Mn₉O₁₈ nanowires (inset shows the single nanowire). (c) Cycling performance of Na₄Mn₉O₁₈ samples calcined at various temperatures at 0.5 C. SEM image (d) and TEM image (e) of Na₂Ti₃O₇ nanotubes. (f) Cycling performance of Na₂Ti₃O₇ nanotubes at different current densities for 100 cycles (inset is the cycling performance from the 11–100th cycles). (a–c) Reprinted with permission from ref 332. Copyright 2011 WILEY-VCH Verlag GmbH&Co. KGaA, Weinheim. (d–f) Reprinted with permission from ref 334. Copyright 2013 Royal Society of Chemistry.

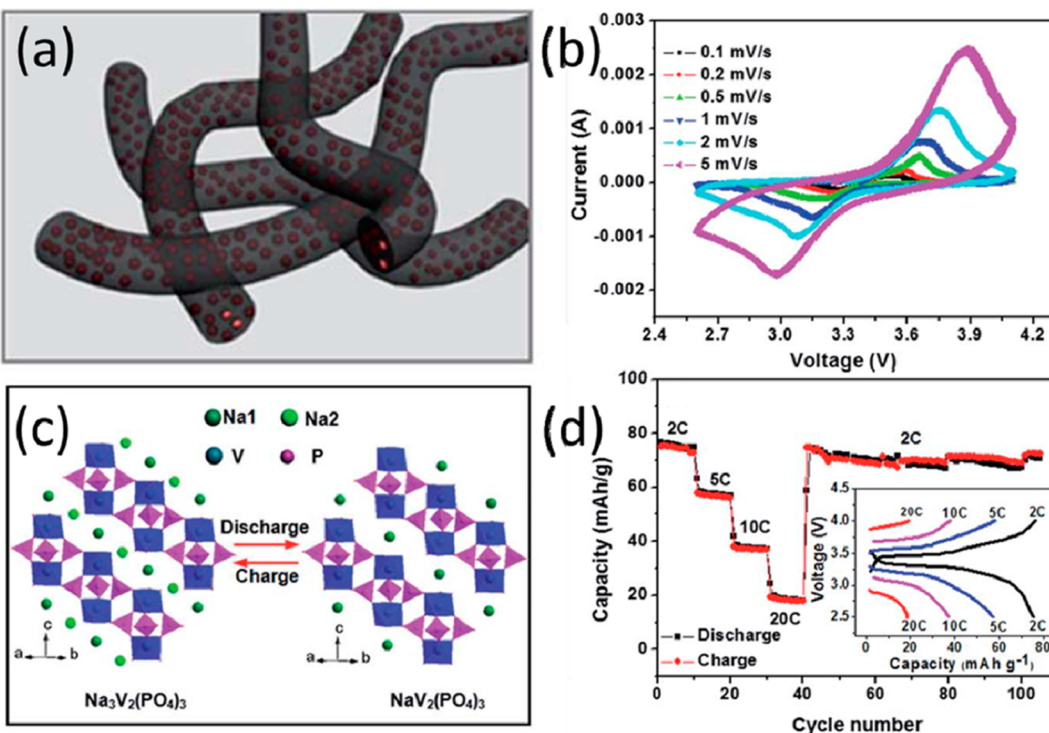


Figure 31. (a) Schematic of the Na₃V₂(PO₄)₃/C nanofiber cathode. (b) CV curves at various scan rates. (c) Unit cell structures of Na₃V₂(PO₄)₃ during discharge and charge processes. (d) Cycling performance of the Na₃V₂(PO₄)₃/C cathode at different current densities, and (inset) charge–discharge curves of the Na₃V₂(PO₄)₃/C nanofiber cathode at these different rates. Reprinted with permission from ref 213. Copyright 2014 Royal Society of Chemistry.

materials is an effective way for promotion of performance and deepening of fundamental research. However, a problem is that it is not very easy for some promising electrode materials to get 1D structure. A typical example is for phosphates,^{340–343} such as Na₃V₂(PO₄)₃; although much work has been published about its outstanding sodium storage performance, none of

them are based on 1D structure.^{344–346} To meet this challenge, Liu et al. recently brought an important step toward this target.²¹³ They used a simple electrospinning method to fabricate a 1D Na₃V₂(PO₄)₃/C cathode electrode where 20–30 nm Na₃V₂(PO₄)₃ nanoparticles were uniformly wrapped into the carbon nanofibers (Figure 31a and 31c). As-prepared 1D

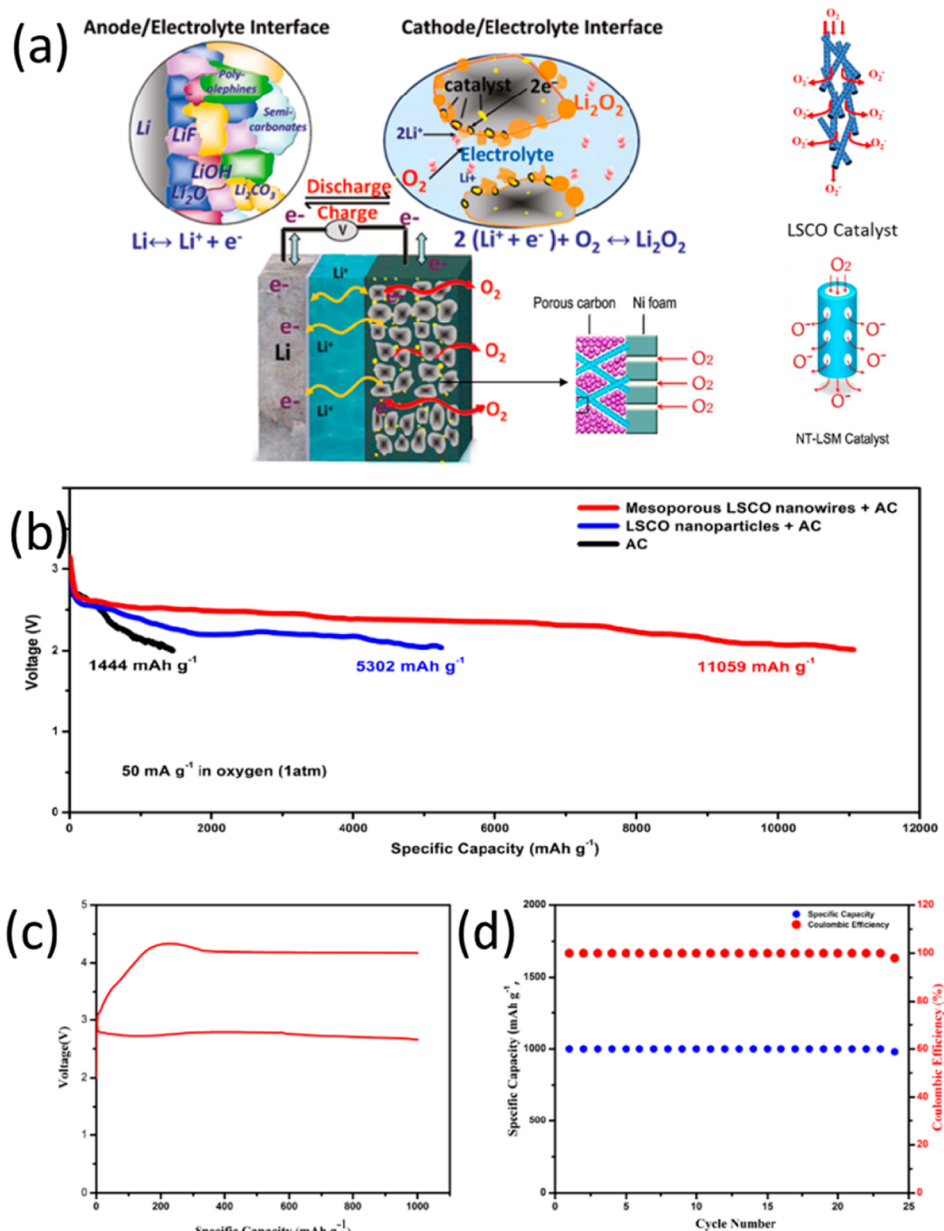


Figure 32. (a) Schematic of the structure of the rechargeable Li–air batteries. (b) Discharge curves of various catalysts. (c, d) Charge/discharge curve and cycling performance of LSCO for Li–air batteries. Reprinted with permission from ref 362. Copyright 2013 ESG.

$\text{Na}_3\text{V}_2(\text{PO}_4)_3/\text{C}$ composite delivered very high discharge capacity and rate performance (Figure 31b and 31d). This work reveals the possibility and necessity of getting 1D sodium phosphate electrodes.

6.3. Nanowire Electrodes for Li–Air Batteries

Li–air batteries have attracted worldwide interest and shown great potential for their highest gravimetric capacities, although practical applications have been limited by some problems such as poor cyclability and sluggish kinetic performance.^{7,8,10,347–354} To enhance the kinetic and cycling performance, porous nanowire catalysts have been applied to provide continuous free oxygen diffusion channels and enhance catalytic properties in Li–air batteries.^{355–358}

The reaction in Li–air batteries corresponds to the oxygen reduction reaction (ORR) and the oxygen evolution reaction (OER) in nonaqueous electrolyte. However, there still exist

many challenges that need to be solved in rechargeable Li–air batteries: (1) the overpotential is very high because of the terrible ORR/OER kinetics of the cathode, which cause poor rechargeability and low rate capability; (2) precipitation of reaction products on the catalyst/electrode hinders the diffusion channels of oxygen, which leads to the limited capacity and poor cycling performance of Li–air batteries (Figure 32a, left). Therefore, it is important to develop highly efficient catalysts for both the ORR and the OER and construct structures with continuous oxygen diffusion channels to realize rechargeable Li–air batteries. Porous catalytic nanowires are good candidates to enhance the catalytic and cycling properties in Li–air batteries according to intensive research (Figure 32a, right).^{359,360,363}

Nanowires could be directly utilized as a highly efficient catalyst of Li–air batteries due to their high catalytically active site and continuous electronic pathway. Water-dispersed

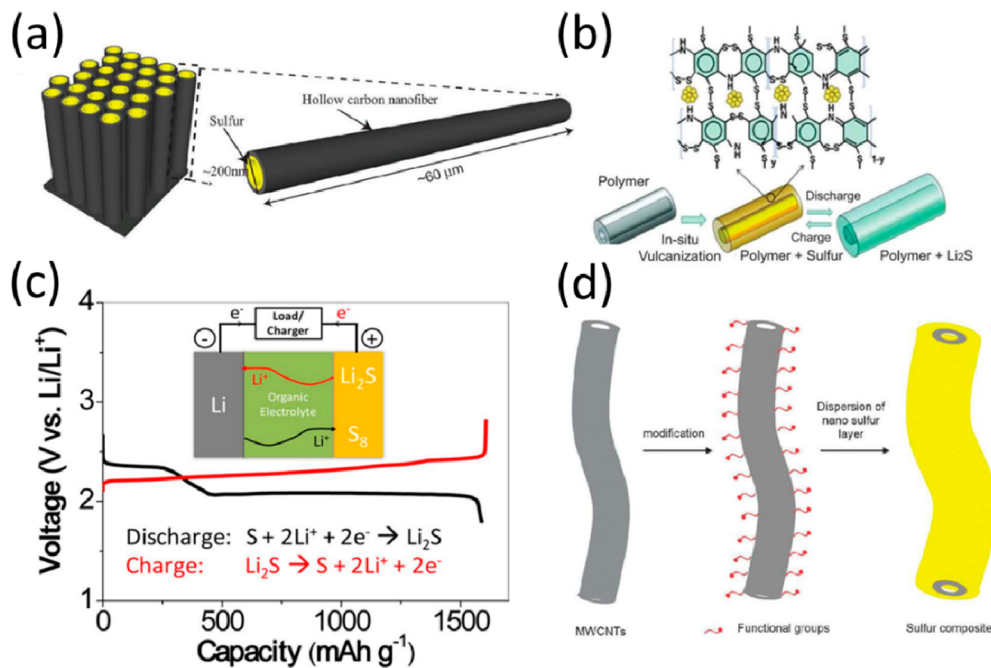


Figure 33. Schematic of the hollow carbon nanofibers/sulfur composite structure (a), fabrication and discharge/charge process of the SPANI-NT/S composite (b), Li–S battery and its initial discharge and charge cycle (c), and how the groups on MWCNT surface influence the dispersion of sulfur layer (d). (a) Reprinted with permission from ref 373. Copyright 2011 American Chemical Society. (b) Reprinted with permission from ref 374. Copyright 2012 WILEY-VCH Verlag GmbH&Co. KGaA, Weinheim. (c) Reprinted with permission from ref 46. Copyright 2012 American Chemical Society. (d) Reprinted with permission from ref 375. Copyright 2012 Royal Society of Chemistry.

conductive PANI nanofibers have been synthesized and employed in Li–air batteries.³⁶¹ The discharge reaction could be catalyzed by this easily produced material. In the first three charge–discharge processes the discharge capacity decreased from 3260 to 2320 mAh g⁻¹ at a current density of 0.05 mA cm⁻². Then, in the following 27 cycles, the capacity retention of PANI became very high at 96% compared with that of the third cycle, which showed the promising prospect to realize practical application of high-capacity rechargeable Li–air batteries.

However, there are still big problems that the surface area and porosity of the air electrodes continuously decreased during discharge–charge cycling. Further research indicated that nanowires could also be used as a skeleton of catalysts. Zheng's group reported the electrodes made with a mixture of carbon nanotube (CNT)/carbon nanofiber (CNF) and α-MnO₂ nanorods, in which the α-MnO₂ catalysts were well distributed in the entangled CNT/CNF networks.³⁶³ The first discharge capacity for cells of CNT/CNF could reach about 1400 mAh g⁻¹, much higher than that of an identical cell with α-MnO₂ catalyst. Similarly, Zhang et al. utilized the long γ-MnOOH nanowires as the skeleton to support Kejetenblack carbon catalyst, making the electrode loose and porous.¹² This porosity can not only provide large contact area of the catalyst and much space for discharge products but also keep diffusion of oxygen and soaking of the electrolyte at a high level, which results in the greatly improved capacity and cycling performance.

Porous nanowire catalysts are becoming a hot field in research because it not only is an excellent catalyst as itself but also provides continuous free oxygen diffusion channels to enhance catalytic and cycling properties in Li–air batteries. To maximize the catalytic sites and facilitate reactants diffusion, the perovskite-based porous La_{0.75}Sr_{0.25}MnO₃ nanotubes (PNT-LSM) were prepared.³⁶⁰ Due to the porous and hollow

channels, as-prepared 1D nanomaterials could enable the high ORR and OER catalytic activity, which makes high-capacity, high-rate, and good-cyclability Li–air batteries. High-aspect-ratio γ-MnOOH nanowires were also successfully synthesized; when used as catalysts in Li–air batteries, great improvements in discharge capacity, cycling stability, and rate retention were obtained, which were attributed to the high catalyst efficiency and cathode porosity.¹² Mai's group synthesized hierarchical mesoporous perovskite-structured La_{0.5}Sr_{0.5}CoO_{2.91} (LSCO) nanowires as catalysts which exhibited an ultrahigh capacity over 11 000 mAh g⁻¹, showing a 1 order of magnitude improvement over LSCO nanoparticles.^{359,362} In addition, 25 charge/discharge cycles with a stable specific capacity of 1000 mAh g⁻¹ were achieved in follow-up work (Figure 32b–d).³⁶² This structure can provide continuous oxygen diffusion channels that contribute to its electrocatalytic performance.

6.4. Nanowire Electrodes for Li–S Batteries

Li–S batteries have captured much attention in recent years because they can offer high theoretical gravimetric (2500 Wh kg⁻¹) and volumetric (2800 Wh L⁻¹) energy density and 1 order of magnitude higher capacity (1675 mAh g⁻¹) than that of conventional lithium-ion batteries.^{7,9,48,364–370} The common Li–S batteries are made up of sulfur composite cathode, metallic lithium anode, and organic electrolyte. During discharging, the sulfur–sulfur bonds are broken, opening the S₈ ring and forming soluble lithium polysulfides (Li₂S_x, 2 < x < 8) intermediates and at last insoluble lithium sulfide (Li₂S) products (Figure 33c).⁴⁶ The overall discharge reaction of Li–S batteries is S₈ + 16Li → 8Li₂S, which has a voltage of 2.15 V.⁴⁸ There are several fatal disadvantages impeding commercialization of Li–S batteries. First, the volume changes of sulfur particles during electrochemical cycles lead to structure changes of active materials and cause low capacity.³⁷¹ Second, sulfur and

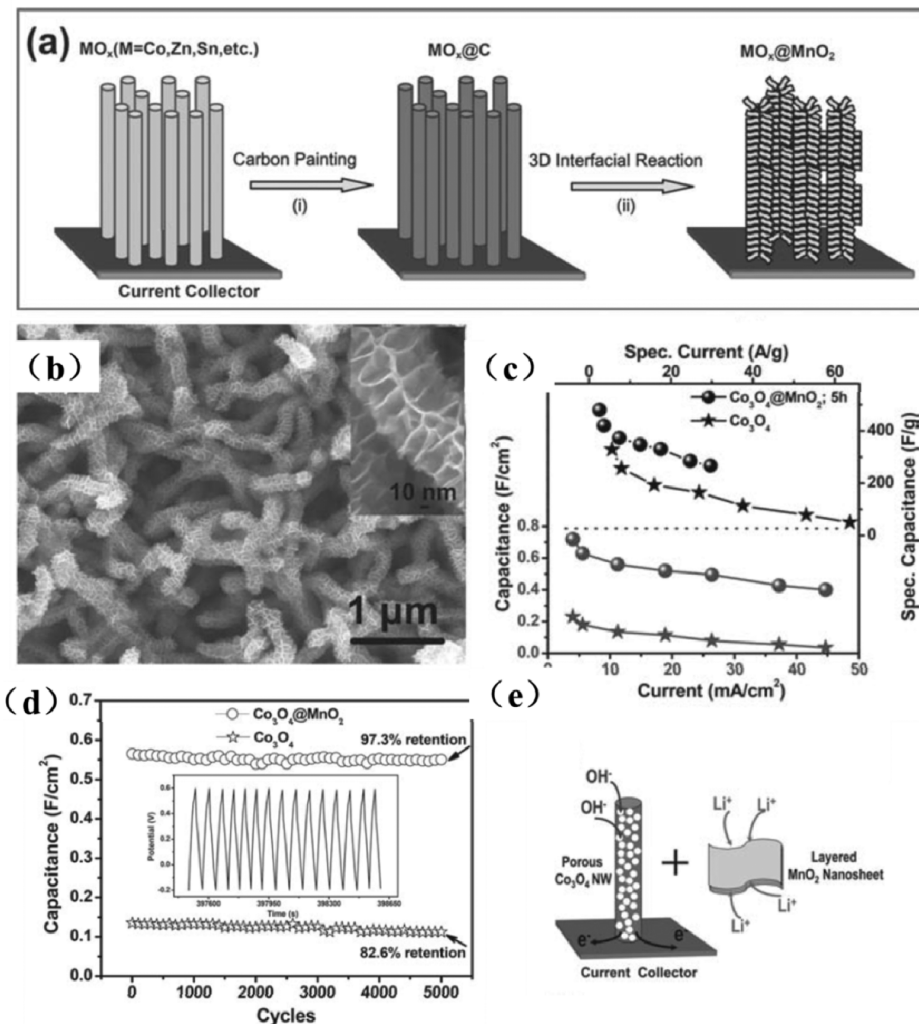


Figure 34. (a) Schematic of the electrode fabrication processes. (b) SEM image of Co₃O₄@MnO₂ hierarchical nanowire arrays (inset is enlarged image). (c) Areal capacitance and specific capacitance vs current densities of the electrodes. (d) Cycling performance of the hybrid and pristine Co₃O₄ arrays. (Inset) Charge–discharge curves of the last 15 cycles for the hybrid arrays. (e) Schematic of the charge storage processes of the hybrid nanowire arrays. Reprinted with permission from ref 396. Copyright 2011 WILEY-VCH Verlag GmbH&Co. KGaA, Weinheim.

Li₂S are both insulating, resulting in sluggish electrochemical kinetics. Third, polysulfides are easy to dissolve in the electrolyte, which is the main cause of the “shuttle phenomenon”.^{364,372}

In order to solve the problems mentioned above, efforts have been paid into the use of nanowire structure-based sulfur cathodes.^{373,376,377} Zheng et al. used 1D carbon nanostructures as the sulfur holder to get this structure (Figure 33a).³⁷³ On one hand, polysulfides could be efficiently trapped in the hollow carbon nanofibers. On the other hand, the high aspect ratio nanofiber arrays enabled the short charge transport pathways, which is beneficial for enhanced reaction kinetics. The electrochemical test showed that this kind of sulfur cathode with around 75% sulfur loading delivered the high initial capacity of around 1400 mAh g⁻¹, retaining the reversible capacity of around 730 mAh g⁻¹ after 150 charge–discharge cycles. Recently, they obtained an improved cycling stability of Li–S batteries by amphiphilic surface-modified hollow carbon fibers with the use of PVP.³⁷⁶

Self-assembled polyaniline nanotubes (PANI-NTs) were also reported to encapsulate sulfur by a soft approach (Figure 33b).³⁷⁴ At a temperature of 280 °C, sulfur reacted with the

polymer, which resulted in the interconnected structure. In the sulfur-PANI-NT composites, sulfur and polysulfide were confined in the nanotubes whose soft encapsulation was at the molecular level compared with mesoporous carbon.⁹ At a rate of 0.1 C, a capacity of 755 mAh g⁻¹ was achieved and the specific capacity increased in the first several cycles, which then became stable in the next cycles. It was inferred by the authors that initially the low surface area prevented full penetration of the electrolyte, which resulted in the relatively low specific capacity in the first cycle. It is also confirmed that MWCNT is also a good choice for 1D sulfur composite synthesis.^{375,378} After surface modification of MWCNTs, the thin uniform sulfur coating could be achieved (Figure 33d).³⁷⁵ Compared to the sulfur encapsulation structure, it may not effectively decrease the polysulfides dissolution. However, the shortened charge transport pathways could result in the high interface kinetics reaction. Even though the 1D structure provides better electrical connection of the matrix and sulfur in the Li–S batteries, it still has trouble in many aspects, such as a relatively high synthesis temperature, low activity material loading, and so on. Despite the fact that these nanowires have improved the battery performance to some extent, development of Li–air

batteries and Li–S is still in its infancy period and great efforts are urgently needed.

6.5. Nanowire Electrodes for Supercapacitors

Supercapacitors are widely known electrochemical devices for their high power density and fast charge/discharge kinetics compared to batteries.^{11,379,380} Different from batteries, the energy storage of most supercapacitors mainly depends on the reaction occurring on/near the electrode surface. Nanowires can provide a high specific area, direct electron pathway, and high electrolyte–electrode contact area, making transport of electrolyte ions faster and utilization of electrodes higher, resulting in the high power-energy density storage.

Traditional EDLCs are mainly carbon-based materials, like activated carbon,^{381,382} mesoporous carbons,³⁸³ graphene,^{384–386} and carbon nanotubes (CNTs).^{387,388} CNTs possess excellent conductivity and exceptional chemical and thermal stability, but the capacitance of CNTs is still low because of its low specific surface area (less than $600 \text{ m}^2 \text{ g}^{-1}$). Several attempts have been made to improve the specific surface area, such as chemical and plasma activation.^{388,389} Lu et al. increased the specific surface area of CNTs through oxygen plasma treatment, resulting in opening of CNT end tips, the specific surface area was increased to $400 \text{ m}^2 \text{ g}^{-1}$, and the activated CNTs showed a high capacitance ($\sim 440 \text{ F g}^{-1}$).³⁸⁸

Although carbon-based materials are easily available and have high surface area, the capacitance and energy density are still relatively low compared with batteries. Therefore, to further improve the electrochemical energy storage performance of supercapacitors, electrochemically active materials with high pseudocapacitance are used, such as RuO₂,^{214,390} MnO₂,^{36,117} Co₃O₄,^{199,391} Co(OH)₂,^{392,393} Ni(OH)₂,^{394,395} and so forth. In addition, to further improve the performance, the combination of these materials is also proposed; promotion of electrochemical performance is attributed to the so-called “synergistic effect”.^{40,50,396,397} Liu et al. synthesized Co₃O₄@MnO₂ ultrathin nanosheet core/shell arrays;³⁹⁶ they deposited the carbon on the Co₃O₄ nanowires followed by growing the MnO₂ nanosheets on the backbone nanowires; the coated carbon as the reactant helped MnO₂ deposit on the nanowires (Figure 34a and 34b). Both components were electrochemically active compounds, while the Co₃O₄ nanowires provided a direct electron transport pathway, and the highly porous MnO₂ nanosheets, where each nanosheet was attached with others, provided the high surface contact with electrolyte and enabled the infiltration of the surface. The electrochemical experiments were tested in LiOH solution. The Co₃O₄@MnO₂ hierarchical nanowire arrays exhibited 480 F g^{-1} at 2.67 A g^{-1} and 267 F g^{-1} at 29.8 A g^{-1} (Figure 34c), its capacitance retention was 97.3% after 5000 cycles (Figure 34d), demonstrating a good rate and cycling performance, and the electrochemical performance was much better than that of single Co₃O₄. The enhancement of the electrochemical performance can be ascribed to the following two reasons (Figure 34e): (1) the MnO₂ nanosheets grown on Co₃O₄ nanowire are separated from each other, making the Li⁺ ions more accessible to the electrode; (2) a highly porous structure on Co₃O₄ nanowire is constructed by MnO₂ nanosheets. Besides the above, many similar structures, such as NiO–MnO₂ hybrid tubular array³⁹⁸ and branched Co₃O₄/NiO nanowire arrays,⁴³ have also been fabricated. To increase the conductivity of the electrodes, the conductive polymer nanowires are also applied in supercapacitors by

combining with metal oxides or metal hydroxides. For example, MnO₂-enriched PEDOT nanowires,³⁹⁹ RuO₂/PEDOT nanotubes,⁴⁰⁰ and PANI/MnO₂ coaxial nanofibers⁴⁰¹ were constructed and exhibited good electrochemical energy storage performance for supercapacitors.

Supercapacitors have rapid power delivery and recharging, but to make the supercapacitors achieve an energy density equivalent to batteries, optimization of the electrochemical energy storage performance of supercapacitors is still needed. For constructing better supercapacitors, many feasible strategies have been proposed, such as free-standing or binder-free structure,^{402,403} which provide reliable electrical connections between the electrochemically active materials and the current collectors and decrease the internal resistance of the electrode, facilitating fast electron pathways and maximum utilization of materials, and combination of electrochemically active materials with CNTs or graphene oxides will also improve the conductivity of materials.^{139,403,404} Apart from further increasing the specific surface area and electron transport, there are some approaches worthy of attention: (1) Modifying the surface of nanowires together with using redox additive/active electrolytes,^{403,405} the synergistic interaction between electrode and electrolyte can deliver an ultrahigh capacitance, and a battery-level energy density; (2) constructing metal cations intercalation nanowires supercapacitors⁴⁰⁶ as well as metal-ion capacitors, these supercapacitors follow the working mechanism like LIBs, with improved electrochemical performance. Furthermore, making the nanowires expose specific facets, which allow fast ion intercalation/deintercalation, will improve the capacitance and power density. The supercapacitors based on conductive polymer nanowires and CNTs have potential in lightweight, portable, and wire-shaped devices applications, because of their highly flexible and stretchable mechanical properties.^{407–409}

6.6. Nanowire Electrodes for Micro/Nanoscale Energy Storage Devices

Micro/nanoscale energy storage units, including microbatteries and microsupercapacitors, have been increasingly investigated for microelectronic devices such as digital integrated circuits and implantable medical chips.^{410–413} There are mainly two types of microsized energy storage devices: conventional sandwich structures and interdigitated structures. 3D microbatteries and microsupercapacitors are designed with high integration density to fully utilize the limited space available in microelectronic devices. 3D nanowire arrays with efficient and continuous 1D electron transport pathway have attracted much interest as the electrode for energy storage devices, because of their higher area and volumetric energy density.^{412,414}

Microbatteries have shown great advantages for higher energy density and operating voltages compared with microsupercapacitors. Ajayan's group developed and reported novel energy storage devices engineered on single nanowires (Figure 35a).⁴¹⁵ The devices were fabricated predominantly by the methods of electrodeposition and infiltration, which enabled construction onto single nanowires at room temperature. Figure 35c–e shows the structure of the device where PANI and Ni–Sn served as the cathode and anode, respectively, and the LiPF₆-based electrolyte was employed. During the charge process in the single nanowire, alloying occurred at the Ni–Sn electrode, and the PF₆[−] ions doping happened in the PANI electrode (Figure 35b). The ultrathin electrolyte layer, with approximately 20 nm, allowed for the ultrashort ion diffusion

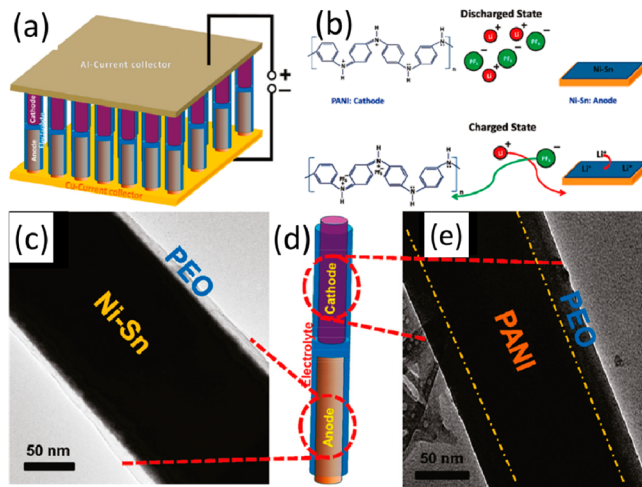


Figure 35. Schematic (a) and charge and discharge processes (b) of the single-nanowire-based microbatteries. TEM image of the anode/electrolyte (c) and cathode/electrolyte (e) core/shell nanowires. (d) Schematic of the structure of a single nanowire for microbatteries. Reprinted with permission from ref 415. Copyright 2011 American Chemical Society.

pathway and excellent Li^+ -ion insertion and deinsertion processes, resulting in a high areal capacitance of $\sim 3 \mu\text{Ah cm}^{-2}$. The high areal capacity is demonstrated to be highly related to skillful design of nanowire electrodes. Min et al. reported another type of 3D microbatteries.⁴¹⁶ The 3D arrays of dodecylbenzenesulfonate-doped PPy and carbon were selected as the cathode and anode, respectively, where these two electrodes were arranged interdigitated at the microscale level by the carbon-microelectromechanical (C-MEMS) approach. These interdigitated microbatteries delivered much higher reversible capacity compared with the electrodeposited 2D films, confirming the advantages of the 3D configuration, which enabled diffusion of ions in multidirections.

Another kind of micro-sized energy storage device, a microsupercapacitor, is able to store energy in a very short time.⁴¹⁷ Wang et al. reported the high-performance all-solid-state microsupercapacitors of PANI nanowire arrays,⁴¹⁸ and the fabrication process is shown in Figure 36a where the photolithography technique was also utilized to get the interdigitated microscale electrodes like that of microbatteries. It is clearly seen that obtained microsupercapacitors showed good flexibility (Figure 36b and 36c). Vertically aligned nanowire arrays provided a high surface contact with electrolyte and good electrical contact with current collectors at every nanowire level (Figure 36d and 36e). According to the electrochemical test results, the ultrahigh volumetric capacitance of 500 F cm^{-3} was achieved due to the high utilization of active materials. Moreover, it is also worth noting that the volumetric capacitance increases when the width of each interdigitated finger decreased. This work demonstrates that the nanowire arrays can serve as excellent candidates for high-performance microsupercapacitors.

3D self-supported nanowire arrays have been considered an excellent part for microbatteries and microsupercapacitors because they possess combined advantages of various merits including high surface areas, continuous charge transport, and low aggregation, which are beneficial to the high capacitance and better volume change resistance. Moreover, unlike other nanostructures, such as nanoparticles where the active materials

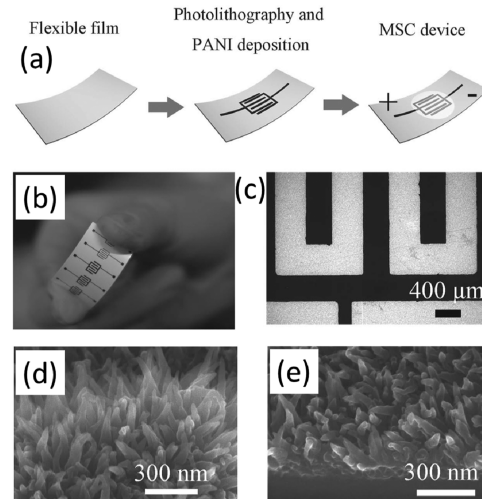


Figure 36. (a) Schematic of the fabrication process of all-solid-state microsupercapacitors. Photograph (b) and optical microscopy (c) image of the flexible microsupercapacitor. (d, e) SEM images of unit arrays. Reprinted with permission from ref 418. Copyright 2011 WILEY-VCH Verlag GmbH&Co. KGaA, Weinheim.

are usually sprayed on the current collectors, nanowire arrays are generally directly grown on the current collectors, which ensures the direct charge transport pathway between the electrodes and the current collectors. It can be seen that the nanowire electrodes possess great potential for constructing high-performance micro-sized energy storage devices.

With the development of next-generation nanotechnology, nanowire electrodes will play a vital role in next-generation micro/nanoscale energy storage devices with ultrahigh energy density, such as Li-air batteries, Li-S batteries, and so forth. Nanowire arrays with high surface area and a continuous electron pathway along the axial direction would be a desirable catalyst supporter for the ORR and OER of Li-air batteries. Moreover, the micro/nanoscale Li-S batteries with ultrahigh energy storage will also be developed by effective design of nanowire structures.

7. CONCLUDING REMARKS

Compared with bulk electrode materials, nanowire electrodes with short path lengths for ion insertion/extraction and electronic transport, facile strain relaxation upon electrochemical cycling, and very large surface to volume ratio are playing more and more important roles in the development of energy storage devices. To look more deeply into the energy storage devices and explore the fundamental mechanism of capacity fading of nanowire electrode materials, a single-nanowire electrode can be considered as a nanoscale probe either ex situ or in situ to detect the electrochemical devices in the process of charge and discharge, making giant strides forward in progress of the nanowires in energy applications. On the basis of the fundamental mechanism, some challenges, optimized strategies, interfaces, controlled synthesis, and next-generation devices have been reviewed in detail in each section, which can help researchers push the development of energy storage devices. Here we want to emphasize some important future directions which can result in significant progress in the field of energy storage.

- (1) It is believed that a single nanowire for in-situ probing can more actually reflect the dynamic nature of

electrochemical device operation under more realistic conditions than that of ex-situ probing. Multiple characterization techniques would be applied at the same time to get a more comprehensive approach for better understanding of the nanowire energy storage mechanism.

- (2) Considering that nanowire electrodes possess versatile redox-dependent characteristics, there are still great possibilities and potential in fabricating high-energy-power, hybrid, and multifunctional electrochemical devices by exploring new nanowire materials and structures based on further understanding the intrinsic electroactivity of nanowire electrodes.
- (3) For Li–air batteries, the nanowire electrodes can serve as the ORR/OER catalyst. To further improve the electrochemical energy storage of Li–air batteries, there are still some directions which would be of great potential: (i) Synthesizing a high catalytic activity nanowire electrode would lower the overpotential of Li–air batteries between charge and discharge; (ii) Improving the conductivity of nanowires by constructing free-standing nanowire arrays would be an approach to increase the electron transport and contribute fast decomposition of Li_2O_2 on the electrode surface; (iii) Modifying the surface of nanowires, such as decorating with Pt, Pd, or Au nanoparticles/crystalline, could tailor the morphology of Li_2O_2 and examine the influence on rechargeability.
- (4) For the Li–S batteries, the “shuttle phenomenon” will be suppressed and even prevented through the following strategies: (i) Constructing micropores on the nanowires electrode would store the S in a small molecular form rather than S_8 ; (ii) the 1D core/shell structure electrodes for Li–S batteries would be further developed, where the shell materials are usually conductive polymers or CNTs because these materials are highly flexible and possess potential in bendable or wearable batteries.
- (5) It can be expected that with the increased utilization of nanowire structures the novel flexible, wearable, transparent energy storage devices will be deeply developed. Moreover, together with the high-performance nanowire-based energy storage devices, it will become an emerging and important technique to integrate energy storage devices with a range of novel functional electronic and mechanical micro/nanodevices. Evolution of nanowire electrode-based energy storage devices will impact many fields and open up a whole new area in the future.

AUTHOR INFORMATION

Corresponding Author

*E-mail: mlq518@whut.edu.cn; mlq@cmliris.harvard.edu.

Notes

The authors declare no competing financial interest.

Biographies



Liqiang Mai received his Ph.D. degree from Wuhan University of Technology in 2004. He then carried out postdoctoral research in the laboratory of Professor Zhonglin Wang at Georgia Institute of Technology in 2006–2007 and worked as an advanced research scholar in the laboratory of Professor Charles M. Lieber at Harvard University in 2008–2011. He is Chair Professor of Materials Science and Engineering at Wuhan University of Technology and Executive Director of the WUT-Harvard Joint Nano Key Laboratory. He has published more than 90 papers tagged by SCI in peer-reviewed journals such as *Nature Nanotechnology*, *Nature Communications*, *Proceedings of the National Academy of Sciences*, *Journal of the American Chemical Society*, *Nano Letters*, *Advanced Materials*. His interests include nanowire materials, micro/nanoenergy storage devices, and energy-based nano–bio interface.



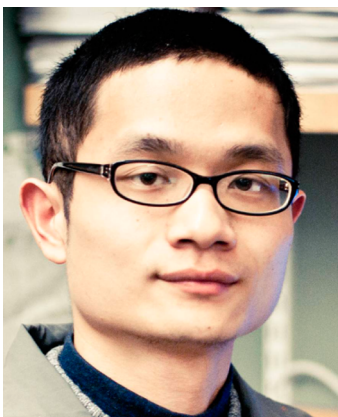
Xiaocong Tian received his first B.S. degree in Material Physics from Wuhan University of Technology in 2011 and second B.S. degree in English from Huazhong University of Science & Technology in the same year. He is pursuing his Ph.D. degree at the WUT-Harvard Joint Nano Key Laboratory. His current research interests are mainly focused on novel electrochemical energy storage materials and devices.



Xu Xu received his B.S. degree in Material Chemistry from Wuhan University of Technology in 2009. He is pursuing his Ph.D. degree under Professors Qingjie Zhang and Liqiang Mai at WUT-Harvard Joint Nano Key Laboratory. Now he works as a research scholar in Professor Xiangfeng Duan's group at University of California, Los Angeles. His current research interests are mainly focused on energy storage materials and devices.



Liang Chang received her M.S. degree in Material Science from Wuhan University of Technology, and she is currently working toward her Ph.D. degree under Professor Yun Hang Hu at the School of Material Science and Engineering, Michigan Technological University. Her current research interests include nanoenergy materials.



Lin Xu received his Ph.D. degree cosupervised by Professors Liqiang Mai and Qingjie Zhang at Wuhan University of Technology and Professor Charles M. Lieber at Harvard University. He is currently a postdoctoral fellow at Harvard University in the group of Professor Charles M. Lieber. His research is mainly focused on new energy nanomaterials and devices and nanobioelectronics.

ACKNOWLEDGMENTS

This work was supported by the National Basic Research Program of China (2013CB934103, 2012CB933003), International Science & Technology Cooperation Program of China (2013DFA50840), the National Science Fund for Distinguished Young Scholars, National Natural Science Foundation of China (51272197, 51302203), and Fundamental Research Funds for the Central Universities (143201003, 2013-VII-028). We are deeply thankful to Professor M. Stanley Whittingham of State University of New York at Binghamton for his support and very valuable input. We also thank Professor Charles M. Lieber of Harvard University, Professor Dongyuan Zhao of Fudan University, and Professor Jun Liu of Pacific Northwest National Laboratory for their stimulating discussion and kind help.

REFERENCES

- (1) Goodenough, J. B.; Park, K.-S. *J. Am. Chem. Soc.* **2013**, *135*, 1167.
- (2) Chu, S.; Majumdar, A. *Nature* **2012**, *488*, 294.
- (3) Soloveichik, G. L. *Annu. Rev. Chem. Biomol.* **2011**, *2*, 503.
- (4) Thackeray, M. M.; Wolverton, C.; Isaacs, E. D. *Energy Environ. Sci.* **2012**, *5*, 7854.
- (5) Vu, A.; Qian, Y.; Stein, A. *Adv. Energy Mater.* **2012**, *2*, 1056.
- (6) Cabana, J.; Monconduit, L.; Larcher, D.; Palacin, M. R. *Adv. Mater.* **2010**, *22*, E170.
- (7) Bruce, P. G.; Freunberger, S. A.; Hardwick, L. J.; Tarascon, J.-M. *Nat. Mater.* **2012**, *11*, 19.
- (8) Peng, Z.; Freunberger, S. A.; Chen, Y.; Bruce, P. G. *Science* **2012**, *337*, 563.
- (9) Ji, X.; Lee, K. T.; Nazar, L. F. *Nat. Mater.* **2009**, *8*, 500.
- (10) Thotiyil, M. M. O.; Freunberger, S. A.; Peng, Z.; Chen, Y.; Liu, Z.; Bruce, P. G. *Nat. Mater.* **2013**, *12*, 1050.
- (11) Simon, P.; Gogotsi, Y.; Dunn, B. *Science* **2014**, *343*, 1210.
- (12) Zhang, L.; Zhang, X.; Wang, Z.; Xu, J.; Xu, D.; Wang, L. *Chem. Commun.* **2012**, *48*, 7598.
- (13) Jiang, H.; Ma, J.; Li, C. *Adv. Mater.* **2012**, *24*, 4197.
- (14) Wei, W.; Cui, X.; Chen, W.; Ivey, D. G. *Chem. Soc. Rev.* **2011**, *40*, 1697.
- (15) Choi, N. S.; Chen, Z.; Freunberger, S. A.; Ji, X.; Sun, Y. K.; Amine, K.; Yushin, G.; Nazar, L. F.; Cho, J.; Bruce, P. G. *Angew. Chem., Int. Ed.* **2012**, *51*, 9994.
- (16) Yang, P.; Tarascon, J.-M. *Nat. Mater.* **2012**, *11*, 560.
- (17) Barth, S.; Hernandez-Ramirez, F.; Holmes, J. D.; Romano-Rodriguez, A. *Prog. Mater. Sci.* **2010**, *55*, 563.
- (18) (a) Bruce, P. G.; Scrosati, B.; Tarascon, J. M. *Angew. Chem., Int. Ed.* **2008**, *47*, 2930. (b) Zhao, Y.; Feng, J.; Liu, X.; Wang, F.; Wang, L.; Shi, C.; Huang, L.; Feng, X.; Chen, X.; Xu, L.; Yan, M.; Zhang, Q.; Bai, X.; Wu, H.; Mai, L. *Nat. Commun.* **2014**, *5*, 4565.
- (19) Dasgupta, N. P.; Sun, J.; Liu, C.; Brittman, S.; Andrews, S. C.; Lim, J.; Gao, H.; Yan, R.; Yang, P. *Adv. Mater.* **2014**, *26*, 2137.
- (20) Yan, R.; Gargas, D.; Yang, P. *Nat. Photonics* **2009**, *3*, 569.
- (21) Kempa, T. J.; Day, R. W.; Kim, S.-K.; Park, H.-G.; Lieber, C. M. *Energy Environ. Sci.* **2013**, *6*, 719.
- (22) Jiang, J.; Li, Y.; Liu, J.; Huang, X. *Nanoscale* **2011**, *3*, 45.
- (23) Wang, Y.; Cao, G. *Adv. Mater.* **2008**, *20*, 2251.
- (24) Xia, Y.; Yang, P.; Sun, Y.; Wu, Y.; Mayers, B.; Gates, B.; Yin, Y.; Kim, F.; Yan, H. *Adv. Mater.* **2003**, *15*, 353.
- (25) Chan, C. K.; Peng, H.; Liu, G.; McIlwrath, K.; Zhang, X. F.; Huggins, R. A.; Cui, Y. *Nat. Nanotechnol.* **2008**, *3*, 31.
- (26) Ko, S. H.; Lee, D.; Kang, H. W.; Nam, K. H.; Yeo, J. Y.; Hong, S. J.; Grigoropoulos, C. P.; Sung, H. J. *Nano Lett.* **2011**, *11*, 666.
- (27) Yodyingyong, S.; Zhang, Q.; Park, K.; Dandeneau, C. S.; Zhou, X.; Triampo, D.; Cao, G. *Appl. Phys. Lett.* **2010**, *96*, 073115.
- (28) Hochbaum, A. I.; Yang, P. *Chem. Rev.* **2009**, *110*, 527.
- (29) Aricò, A. S.; Bruce, P.; Scrosati, B.; Tarascon, J.-M.; Van Schalkwijk, W. *Nat. Mater.* **2005**, *4*, 366.

- (30) Hosono, E.; Kudo, T.; Honma, I.; Matsuda, H.; Zhou, H. *Nano Lett.* **2009**, *9*, 1045.
- (31) Hosono, E.; Saito, T.; Hoshino, J.; Okubo, M.; Saito, Y.; Nishio-Hamane, D.; Kudo, T.; Zhou, H. *J. Power Sources* **2012**, *217*, 43.
- (32) Chen, H. M.; Chen, C. K.; Liu, R.-S.; Zhang, L.; Zhang, J.; Wilkinson, D. P. *Chem. Soc. Rev.* **2012**, *41*, 5654.
- (33) Szczech, J. R.; Jin, S. *Energy Environ. Sci.* **2011**, *4*, 56.
- (34) Meduri, P.; Pendyala, C.; Kumar, V.; Sumanasekera, G. U.; Sunkara, M. K. *Nano Lett.* **2009**, *9*, 612.
- (35) Tao, F.; Guan, M.; Jiang, Y.; Zhu, J.; Xu, Z.; Xue, Z. *Adv. Mater.* **2006**, *18*, 2161.
- (36) Chou, S.-L.; Wang, J.-Z.; Chew, S.-Y.; Liu, H.-K.; Dou, S.-X. *Electrochim. Commun.* **2008**, *10*, 1724.
- (37) DiLeo, R. A.; Frisco, S.; Ganter, M. J.; Rogers, R. E.; Raffaelle, R. P.; Landi, B. *J. Phys. Chem. C* **2011**, *115*, 22609.
- (38) Shen, L.; Zhang, X.; Li, H.; Yuan, C.; Cao, G. *J. Phys. Chem. Lett.* **2011**, *2*, 3096.
- (39) Wang, Y.; Wang, Y.; Jia, D.; Peng, Z.; Xia, Y.; Zheng, G. *Nano Lett.* **2014**, *14*, 1080.
- (40) Mai, L.-Q.; Yang, F.; Zhao, Y.-L.; Xu, X.; Xu, L.; Luo, Y.-Z. *Nat. Commun.* **2011**, *2*, 381.
- (41) Zhou, W.; Cheng, C.; Liu, J.; Tay, Y. Y.; Jiang, J.; Jia, X.; Zhang, J.; Gong, H.; Hng, H. H.; Yu, T. *Adv. Funct. Mater.* **2011**, *21*, 2439.
- (42) Cui, L.-F.; Yang, Y.; Hsu, C.-M.; Cui, Y. *Nano Lett.* **2009**, *9*, 3370.
- (43) Xia, X.; Tu, J.; Zhang, Y.; Wang, X.; Gu, C.; Zhao, X.-b.; Fan, H. *J. ACS Nano* **2012**, *6*, 5531.
- (44) Huang, J. Y.; Zhong, L.; Wang, C. M.; Sullivan, J. P.; Xu, W.; Zhang, L. Q.; Mao, S. X.; Hudak, N. S.; Liu, X. H.; Subramanian, A. *Science* **2010**, *330*, 1515.
- (45) Liu, X. H.; Huang, J. Y. *Energy Environ. Sci.* **2011**, *4*, 3844.
- (46) Manthiram, A.; Fu, Y.; Su, Y.-S. *Acc. Chem. Res.* **2012**, *46*, 1125.
- (47) Chen, X.; Li, C.; Grätzel, M.; Kostecki, R.; Mao, S. S. *Chem. Soc. Rev.* **2012**, *41*, 7909.
- (48) Evers, S.; Nazar, L. F. *Acc. Chem. Res.* **2012**, *46*, 1135.
- (49) Peng, K.-Q.; Wang, X.; Li, L.; Hu, Y.; Lee, S.-T. *Nano Today* **2013**, *8*, 75.
- (50) Cheng, C.; Fan, H. *J. Nano Today* **2012**, *7*, 327.
- (51) Yao, J.; Yan, H.; Das, S.; Klemic, J. F.; Ellenbogen, J. C.; Lieber, C. M. *Proc. Natl. Acad. Sci. U.S.A.* **2014**, *111*, 2431.
- (52) Qing, Q.; Jiang, Z.; Xu, L.; Gao, R.; Mai, L.; Lieber, C. M. *Nat. Nanotechnol.* **2014**, *9*, 142.
- (53) Zhou, C.; Mai, L.; Liu, Y.; Qi, Y.; Dai, Y.; Chen, W. *J. Phys. Chem. C* **2007**, *111*, 8202.
- (54) Zheng, G.; Patolsky, F.; Cui, Y.; Wang, W. U.; Lieber, C. M. *Nat. Biotechnol.* **2005**, *23*, 1294.
- (55) Mai, L.; Xu, X.; Xu, L.; Han, C.; Luo, Y. *J. Mater. Res.* **2011**, *26*, 2175.
- (56) Wang, Y.; Wang, T.; Da, P.; Xu, M.; Wu, H.; Zheng, G. *Adv. Mater.* **2013**, *25*, 5177.
- (57) Xu, J.; Wu, H.; Wang, F.; Xia, Y.; Zheng, G. *Adv. Energy Mater.* **2013**, *3*, 286.
- (58) (a) Ghassemi, H.; Au, M.; Chen, N.; Heiden, P. A.; Yassar, R. S. *ACS Nano* **2011**, *5*, 7805. (b) Wang, L.; Liu, D.; Yang, S.; Tian, X.; Zhang, G.; Wang, W.; Wang, E.; Xu, Z.; Bai, X. *ACS Nano* **2014**, *8*, 8249.
- (59) Liu, Y.; Hudak, N. S.; Huber, D. L.; Limmer, S. J.; Sullivan, J. P.; Huang, J. Y. *Nano Lett.* **2011**, *11*, 4188.
- (60) McDowell, M. T.; Ryu, I.; Lee, S. W.; Wang, C.; Nix, W. D.; Cui, Y. *Adv. Mater.* **2012**, *24*, 6034.
- (61) Liu, N.; Wu, H.; McDowell, M. T.; Yao, Y.; Wang, C.; Cui, Y. *Nano Lett.* **2012**, *12*, 3315.
- (62) McDowell, M. T.; Lee, S. W.; Harris, J. T.; Korgel, B. A.; Wang, C.; Nix, W. D.; Cui, Y. *Nano Lett.* **2013**, *13*, 758.
- (63) Zhong, L.; Mitchell, R. R.; Liu, Y.; Gallant, B. M.; Thompson, C. V.; Huang, J. Y.; Mao, S. X.; Shao-Horn, Y. *Nano Lett.* **2013**, *13*, 2209.
- (64) Gu, M.; Li, Y.; Li, X.; Hu, S.; Zhang, X.; Xu, W.; Thevuthasan, S.; Baer, D. R.; Zhang, J.-G.; Liu, J. *ACS Nano* **2012**, *6*, 8439.
- (65) Kushima, A.; Huang, J. Y.; Li, J. *ACS Nano* **2012**, *6*, 9425.
- (66) Karki, K.; Epstein, E.; Cho, J.-H.; Jia, Z.; Li, T.; Picraux, S. T.; Wang, C.; Cumings, J. *Nano Lett.* **2012**, *12*, 1392.
- (67) McDowell, M. T.; Woo Lee, S.; Wang, C.; Cui, Y. *Nano Energy* **2012**, *1*, 401.
- (68) Liu, X. H.; Zhang, L. Q.; Zhong, L.; Liu, Y.; Zheng, H.; Wang, J. W.; Cho, J.-H.; Dayeh, S. A.; Picraux, S. T.; Sullivan, J. P. *Nano Lett.* **2011**, *11*, 2251.
- (69) Liu, X. H.; Huang, S.; Picraux, S. T.; Li, J.; Zhu, T.; Huang, J. Y. *Nano Lett.* **2011**, *11*, 3991.
- (70) Gu, M.; Parent, L. R.; Mehdi, B. L.; Unocic, R. R.; McDowell, M. T.; Sacci, R. L.; Xu, W.; Connell, J. G.; Xu, P.; Abellan, P. *Nano Lett.* **2013**, *13*, 6106.
- (71) Wang, C.-M.; Li, X.; Wang, Z.; Xu, W.; Liu, J.; Gao, F.; Kovarik, L.; Zhang, J.-G.; Howe, J.; Burton, D. J. *Nano Lett.* **2012**, *12*, 1624.
- (72) Liu, X. H.; Wang, J. W.; Huang, S.; Fan, F.; Huang, X.; Liu, Y.; Krylyuk, S.; Yoo, J.; Dayeh, S. A.; Davydov, A. V. *Nat. Nanotechnol.* **2012**, *7*, 749.
- (73) Liu, X. H.; Zheng, H.; Zhong, L.; Huang, S.; Karki, K.; Zhang, L. Q.; Liu, Y.; Kushima, A.; Liang, W. T.; Wang, J. W. *Nano Lett.* **2011**, *11*, 3312.
- (74) Gregorczyk, K. E.; Liu, Y.; Sullivan, J. P.; Rubloff, G. W. *ACS Nano* **2013**, *7*, 6354.
- (75) Wang, C.-M.; Xu, W.; Liu, J.; Zhang, J.-G.; Saraf, L. V.; Arey, B. W.; Choi, D.; Yang, Z.-G.; Xiao, J.; Thevuthasan, S. *Nano Lett.* **2011**, *11*, 1874.
- (76) Zhang, L. Q.; Liu, X. H.; Liu, Y.; Huang, S.; Zhu, T.; Gui, L.; Mao, S. X.; Ye, Z. Z.; Wang, C. M.; Sullivan, J. P. *ACS Nano* **2011**, *5*, 4800.
- (77) Kushima, A.; Liu, X. H.; Zhu, G.; Wang, Z. L.; Huang, J. Y.; Li, J. *Nano Lett.* **2011**, *11*, 4535.
- (78) Wang, X.; Tang, D.-M.; Li, H.; Yi, W.; Zhai, T.; Bando, Y.; Golberg, D. *Chem. Commun.* **2012**, *48*, 4812.
- (79) Lee, S.; Oshima, Y.; Hosono, E.; Zhou, H.; Kim, K.; Chang, H. M.; Kanno, R.; Takayanagi, K. *J. Phys. Chem. C* **2013**, *117*, 24236.
- (80) Liu, X. H.; Liu, Y.; Kushima, A.; Zhang, S.; Zhu, T.; Li, J.; Huang, J. Y. *Adv. Energy Mater.* **2012**, *2*, 722.
- (81) Misra, S.; Liu, N.; Nelson, J.; Hong, S. S.; Cui, Y.; Toney, M. F. *ACS Nano* **2012**, *6*, 5465.
- (82) Boles, S. T.; Sedlmayr, A.; Kraft, O.; Mönig, R. *Appl. Phys. Lett.* **2012**, *100*, 243901.
- (83) Ogata, K.; Salager, E.; Kerr, C.; Fraser, A.; Ducati, C.; Morris, A.; Hofmann, S.; Grey, C. *Nat. Commun.* **2014**, *5*, 3217.
- (84) Mai, L.; Dong, Y.; Xu, L.; Han, C. *Nano Lett.* **2010**, *10*, 4273.
- (85) Wu, H.; Chan, G.; Choi, J. W.; Ryu, I.; Yao, Y.; McDowell, M. T.; Lee, S. W.; Jackson, A.; Yang, Y.; Hu, L. *Nat. Nanotechnol.* **2012**, *7*, 310.
- (86) Kim, H.; Cho, J. *J. Mater. Chem.* **2008**, *18*, 771.
- (87) Li, Y.; Tan, B.; Wu, Y. *Nano Lett.* **2008**, *8*, 265.
- (88) Kim, S.-W.; Lee, H.-W.; Muralidharan, P.; Seo, D.-H.; Yoon, W.-S.; Kim, D. K.; Kang, K. *Nano Res.* **2011**, *4*, 505.
- (89) Kim, H.; Son, Y.; Park, C.; Cho, J.; Choi, H. C. *Angew. Chem., Int. Ed.* **2013**, *125*, 6113.
- (90) Ge, M.; Rong, J.; Fang, X.; Zhou, C. *Nano Lett.* **2012**, *12*, 2318.
- (91) Yang, Y.; Xie, C.; Ruffo, R.; Peng, H.; Kim, D. K.; Cui, Y. *Nano Lett.* **2009**, *9*, 4109.
- (92) Reddy, A. L. M.; Shajumon, M. M.; Gowda, S. R.; Ajayan, P. M. *Nano Lett.* **2009**, *9*, 1002.
- (93) Ma, H.; Zhang, S.; Ji, W.; Tao, Z.; Chen, J. *J. Am. Chem. Soc.* **2008**, *130*, 5361.
- (94) Etacheri, V.; Haik, O.; Goffer, Y.; Roberts, G. A.; Stefan, I. C.; Fasching, R.; Aurbach, D. *Langmuir* **2011**, *28*, 965.
- (95) Kim, M. G.; Jo, M.; Hong, Y.-S.; Cho, J. *Chem. Commun.* **2009**, *218*.
- (96) Chan, C. K.; Ruffo, R.; Hong, S. S.; Huggins, R. A.; Cui, Y. J. *Power Sources* **2009**, *189*, 34.
- (97) Park, C.-M.; Sohn, H.-J. *Chem. Mater.* **2008**, *20*, 6319.
- (98) TaeáLee, K. *Energy Environ. Sci.* **2011**, *4*, 425.
- (99) Armstrong, A. R.; Armstrong, G.; Canales, J.; García, R.; Bruce, P. G. *Adv. Mater.* **2005**, *17*, 862.

- (100) Wu, H.; Cui, Y. *Nano Today* **2012**, *7*, 414.
- (101) Broussely, M.; Biensan, P.; Bonhomme, F.; Blanchard, P.; Herreyre, S.; Nechev, K.; Staniewicz, R. *J. Power Sources* **2005**, *146*, 90.
- (102) Chan, C. K.; Peng, H.; Twesten, R. D.; Jarausch, K.; Zhang, X. F.; Cui, Y. *Nano Lett.* **2007**, *7*, 490.
- (103) Huang, X.; Tu, J.; Xia, X.; Wang, X.; Xiang, J. *Electrochim. Commun.* **2008**, *10*, 1288.
- (104) Gowda, S. R.; Reddy, A. L. M.; Shaijumon, M. M.; Zhan, X.; Ci, L.; Ajayan, P. M. *Nano Lett.* **2010**, *11*, 101.
- (105) Mai, L. Q.; Hu, B.; Chen, W.; Qi, Y.; Lao, C.; Yang, R.; Dai, Y.; Wang, Z. L. *Adv. Mater.* **2007**, *19*, 3712.
- (106) Mai, L.; Xu, L.; Hu, B.; Gu, Y. *J. Mater. Res.* **2010**, *25*, 1413.
- (107) Garcia, B.; Millet, M.; Pereira-Ramos, J. P.; Baffier, N.; Bloch, D. *J. Power Sources* **1999**, *81–82*, 670.
- (108) Mai, L.; Gao, Y.; Guan, J.; Hu, B.; Xu, L.; Jin, W. *Int. J. Electrochem. Sci.* **2009**, *4*, 755.
- (109) Zhang, Z.; Yang, J.; Nuli, Y.; Wang, B.; Xu, J. *Solid State Ionics* **2005**, *176*, 693.
- (110) Kim, D.-W.; Hwang, I.-S.; Kwon, S. J.; Kang, H.-Y.; Park, K.-S.; Choi, Y.-J.; Choi, K.-J.; Park, J.-G. *Nano Lett.* **2007**, *7*, 3041.
- (111) Fu, L.; Liu, H.; Li, C.; Wu, Y.; Rahm, E.; Holze, R.; Wu, H. *Solid State Sci.* **2006**, *8*, 113.
- (112) Limthongkul, P.; Jang, Y.-I.; Dudney, N. J.; Chiang, Y.-M. *Acta Mater.* **2003**, *51*, 1103.
- (113) Tarascon, J.-M.; Armand, M. *Nature* **2001**, *414*, 359.
- (114) Shao-Horn, Y.; Croguennec, L.; Delmas, C.; Nelson, E. C.; O'Keefe, M. A. *Nat. Mater.* **2003**, *2*, 464.
- (115) Lee, S. H.; Kim, Y. H.; Deshpande, R.; Parilla, P. A.; Whitney, E.; Gillaspie, D. T.; Jones, K. M.; Mahan, A.; Zhang, S.; Dillon, A. C. *Adv. Mater.* **2008**, *20*, 3627.
- (116) Kuwabata, S.; Masui, S.; Yoneyama, H. *Electrochim. Acta* **1999**, *44*, 4593.
- (117) Liu, R.; Lee, S. B. *J. Am. Chem. Soc.* **2008**, *130*, 2942.
- (118) Murugan, A. V.; Kwon, C.-W.; Campet, G.; Kale, B.; Mandale, A.; Sainker, S.; Gopinath, C. S.; Vijayamohanan, K. *J. Phys. Chem. B* **2004**, *108*, 10736.
- (119) Mai, L.; Xu, X.; Han, C.; Luo, Y.; Xu, L.; Wu, Y. A.; Zhao, Y. *Nano Lett.* **2011**, *11*, 4992.
- (120) Li, S.; Han, C.-H.; Mai, L.-Q.; Han, J.-H.; Xu, X.; Zhu, Y.-Q. *Int. J. Electrochem. Sci.* **2011**, *6*, 4504.
- (121) Mai, L.; Yang, F.; Zhao, Y.; Xu, X.; Xu, L.; Hu, B.; Luo, Y.; Liu, H. *Mater. Today* **2011**, *14*, 346.
- (122) Chen, W.; Mai, L.; Qi, Y.; Dai, Y. *J. Phys. Chem. Solids* **2006**, *67*, 896.
- (123) Murugan, A. V.; Muraliganth, T.; Manthiram, A. *J. Phys. Chem. C* **2008**, *112*, 14665.
- (124) Kim, H.; Cho, J. *Nano Lett.* **2008**, *8*, 3688.
- (125) Park, M.-H.; Kim, M. G.; Joo, J.; Kim, K.; Kim, J.; Ahn, S.; Cui, Y.; Cho, J. *Nano Lett.* **2009**, *9*, 3844.
- (126) Li, H.; Zhou, H. *Chem. Commun.* **2012**, *48*, 1201.
- (127) Wang, Q.; Li, J. *J. Phys. Chem. C* **2007**, *111*, 1675.
- (128) Cui, L.-F.; Ruffo, R.; Chan, C. K.; Peng, H.; Cui, Y. *Nano Lett.* **2008**, *9*, 491.
- (129) Gu, X.; Chen, L.; Ju, Z.; Xu, H.; Yang, J.; Qian, Y. *Adv. Funct. Mater.* **2013**, *23*, 4049.
- (130) Magasinski, A.; Dixon, P.; Hertzberg, B.; Kvit, A.; Ayala, J.; Yushin, G. *Nat. Mater.* **2010**, *9*, 353.
- (131) Hu, L.; Wu, H.; Hong, S. S.; Cui, L.; McDonough, J. R.; Bohy, S.; Cui, Y. *Chem. Commun.* **2011**, *47*, 367.
- (132) Wu, H.; Xu, M.; Wang, Y.; Zheng, G. *Nano Res.* **2013**, *6*, 167.
- (133) Ren, Y.; Armstrong, A. R.; Jiao, F.; Bruce, P. G. *J. Am. Chem. Soc.* **2009**, *132*, 996.
- (134) Song, Y.; Qin, S.; Zhang, Y.; Gao, W.; Liu, J. *J. Phys. Chem. C* **2010**, *114*, 21158.
- (135) Kim, J. G.; Nam, S. H.; Lee, S. H.; Choi, S. M.; Kim, W. B. *ACS Appl. Mater. Interfaces* **2011**, *3*, 828.
- (136) Jiang, J.; Zhu, J.; Feng, Y.; Liu, J.; Huang, X. *Chem. Commun.* **2012**, *48*, 7471.
- (137) Mai, L.; Xu, L.; Han, C.; Xu, X.; Luo, Y.; Zhao, S.; Zhao, Y. *Nano Lett.* **2010**, *10*, 4750.
- (138) Xu, X.; Luo, Y.-Z.; Mai, L.-Q.; Zhao, Y.-L.; An, Q.-Y.; Xu, L.; Hu, F.; Zhang, L.; Zhang, Q.-J. *NPG Asia Mater.* **2012**, *4*, e20.
- (139) Yan, M.; Wang, F.; Han, C.; Ma, X.; Xu, X.; An, Q.; Xu, L.; Niu, C.; Zhao, Y.; Tian, X. *J. Am. Chem. Soc.* **2013**, *135*, 18176.
- (140) Chan, C. K.; Zhang, X. F.; Cui, Y. *Nano Lett.* **2008**, *8*, 307.
- (141) Lai, C.-H.; Huang, K.-W.; Cheng, J.-H.; Lee, C.-Y.; Hwang, B.-J.; Chen, L.-J. *J. Mater. Chem.* **2010**, *20*, 6638.
- (142) Kim, J.-H.; Ayalasomayajula, T.; Gona, V.; Choi, D. *J. Power Sources* **2008**, *183*, 366.
- (143) Verma, P.; Maire, P.; Novák, P. *Electrochim. Acta* **2010**, *55*, 6332.
- (144) Zhang, W.-J. *J. Power Sources* **2011**, *196*, 13.
- (145) Li, Z.; Huang, J.; Yann Liaw, B.; Metzler, V.; Zhang, J. *J. Power Sources* **2014**, *254*, 168.
- (146) Nie, M.; Abraham, D. P.; Chen, Y.; Bose, A.; Lucht, B. L. *J. Phys. Chem. C* **2013**, *117*, 13403.
- (147) Peled, E. *J. Electrochim. Soc.* **1979**, *126*, 2047.
- (148) Chan, C. K.; Ruffo, R.; Hong, S. S.; Cui, Y. *J. Power Sources* **2009**, *189*, 1132.
- (149) Kim, S.-P.; Van Duin, A. C.; Shenoy, V. B. *J. Power Sources* **2011**, *196*, 8590.
- (150) Bryngelsson, H.; Stjerndahl, M.; Gustafsson, T.; Edström, K. *J. Power Sources* **2007**, *174*, 970.
- (151) Edström, K.; Herstedt, M.; Abraham, D. P. *J. Power Sources* **2006**, *153*, 380.
- (152) Reddy, M.; Subba Rao, G.; Chowdari, B. *Chem. Rev.* **2013**, *113*, 5364.
- (153) Choi, N.-S.; Yao, Y.; Cui, Y.; Cho, J. *J. Mater. Chem.* **2011**, *21*, 9825.
- (154) Lee, B.-S.; Son, S.-B.; Park, K.-M.; Yu, W.-R.; Oh, K.-H.; Lee, S.-H. *J. Power Sources* **2012**, *199*, 53.
- (155) Zou, G.; Zhang, D.; Dong, C.; Li, H.; Xiong, K.; Fei, L.; Qian, Y. *Carbon* **2006**, *44*, 828.
- (156) Bulusheva, L.; Okotrub, A.; Kurenya, A.; Zhang, H.; Zhang, H.; Chen, X.; Song, H. *Carbon* **2011**, *49*, 4013.
- (157) Qie, L.; Chen, W. M.; Wang, Z. H.; Shao, Q. G.; Li, X.; Yuan, L. X.; Hu, X. L.; Zhang, W. X.; Huang, Y. H. *Adv. Mater.* **2012**, *24*, 2047.
- (158) Jiang, J.; Liu, J.; Ding, R.; Ji, X.; Hu, Y.; Li, X.; Hu, A.; Wu, F.; Zhu, Z.; Huang, X. *J. Phys. Chem. C* **2009**, *114*, 929.
- (159) Wu, M.-S.; Chiang, P.-C. J.; Lee, J.-T.; Lin, J.-C. *J. Phys. Chem. B* **2005**, *109*, 23279.
- (160) Han, Y.; Wu, X.; Ma, Y.; Gong, L.; Qu, F.; Fan, H. *CrystEngComm* **2011**, *13*, 3506.
- (161) Ruffo, R.; Hong, S. S.; Chan, C. K.; Huggins, R. A.; Cui, Y. *J. Phys. Chem. C* **2009**, *113*, 11390.
- (162) Chan, C. K.; Patel, R. N.; O'Connell, M. J.; Korgel, B. A.; Cui, Y. *ACS Nano* **2010**, *4*, 1443.
- (163) Huang, R.; Fan, X.; Shen, W.; Zhu, J. *Appl. Phys. Lett.* **2009**, *95*, 133119.
- (164) Cho, Y. J.; Kim, H. S.; Im, H.; Myung, Y.; Jung, G. B.; Lee, C. W.; Park, J.; Park, M.-H.; Cho, J.; Kang, H. S. *J. Phys. Chem. C* **2011**, *115*, 9451.
- (165) Gao, P.; Fu, J.; Yang, J.; Lv, R.; Wang, J.; Nuli, Y.; Tang, X. *Phys. Chem. Chem. Phys.* **2009**, *11*, 11101.
- (166) Wang, B.; Li, X.; Zhang, X.; Luo, B.; Jin, M.; Liang, M.; Dayeh, S. A.; Picraux, S.; Zhi, L. *ACS Nano* **2013**, *7*, 1437.
- (167) Hertzberg, B.; Alexeev, A.; Yushin, G. *J. Am. Chem. Soc.* **2010**, *132*, 8548.
- (168) Chen, H.; Xiao, Y.; Wang, L.; Yang, Y. *J. Power Sources* **2011**, *196*, 6657.
- (169) Föll, H.; Carstensen, J.; Ossei-Wusu, E.; Cojocaru, A.; Quirogá-González, E.; Neumann, G. *J. Electrochim. Soc.* **2011**, *158*, A580.
- (170) Qiu, M.; Yang, L.; Qi, X.; Li, J.; Zhong, J. *ACS Appl. Mater. Interfaces* **2010**, *2*, 3614.
- (171) Pan, Q.; Wang, H.; Jiang, Y. *Electrochim. Commun.* **2007**, *9*, 754.

- (172) Liu, N.; Hu, L.; McDowell, M. T.; Jackson, A.; Cui, Y. *ACS Nano* **2011**, *5*, 6487.
- (173) Xu, W.; Vegunta, S. S. S.; Flake, J. C. *J. Power Sources* **2011**, *196*, 8583.
- (174) Meng, X.; Yang, X. Q.; Sun, X. *Adv. Mater.* **2012**, *24*, 3589.
- (175) (a) Kim, J. G.; Lee, S. H.; Nam, S. H.; Choi, S. M.; Kim, W. B. *RSC Adv.* **2012**, *2*, 7829. (b) Guan, C.; Wang, X.; Zhang, Q.; Fan, Z.; Zhang, H.; Fan, H. *J. Nano Lett.* **2014**, *14*, 4852.
- (176) Lee, S.; Ha, J.; Cheng, H.; Lee, J. W.; Jang, T. S.; Jung, Y. G.; Huang, Y.; Rogers, J. A.; Paik, U. *Adv. Energy Mater.* **2014**, *4*, 1.
- (177) Lee, D. K.; Shim, H.-W.; An, J. S.; Cho, C. M.; Cho, I.-S.; Hong, K. S.; Kim, D.-W. *Nanoscale Res. Lett.* **2010**, *5*, 1585.
- (178) Lee, S. C.; Lee, S. M.; Lee, J. W.; Lee, J. B.; Lee, S. M.; Han, S. S.; Lee, H. C.; Kim, H. J. *J. Phys. Chem. C* **2009**, *113*, 18420.
- (179) Armstrong, A. R.; Armstrong, G.; Canales, J.; Bruce, P. G. *Angew. Chem., Int. Ed.* **2004**, *43*, 2286.
- (180) Shim, H.-W.; Lee, D. K.; Cho, I.-S.; Hong, K. S.; Kim, D.-W. *Nanotechnology* **2010**, *21*, 255706.
- (181) Zhou, W.; Liu, X.; Cui, J.; Liu, D.; Li, J.; Jiang, H.; Wang, J.; Liu, H. *CrystEngComm* **2011**, *13*, 4557.
- (182) Sun, Y.-K.; Myung, S.-T.; Kim, M.-H.; Prakash, J.; Amine, K. J. *Am. Chem. Soc.* **2005**, *127*, 13411.
- (183) Sun, Y.-K.; Myung, S.-T.; Park, B.-C.; Prakash, J.; Belharouak, I.; Amine, K. *Nat. Mater.* **2009**, *8*, 320.
- (184) Cheng, C.; Tay, Y. Y.; Hng, H. H.; Fan, H. *J. J. Mater. Res.* **2011**, *26*, 2254.
- (185) Hu, S.; Weng, W.; Wan, Y. *Solid State Commun.* **2004**, *130*, 111.
- (186) Fan, H.; Knez, M.; Scholz, R.; Nielsch, K.; Pippel, E.; Hesse, D.; Gösele, U.; Zacharias, M. *Nanotechnology* **2006**, *17*, 5157.
- (187) McCarthy, E.; Garry, S.; Byrne, D.; McGlynn, E.; Mosnier, J.-P. *J. Appl. Phys.* **2011**, *110*, 124324.
- (188) Glushenkov, A.; Zhang, H.; Zou, J.; Lu, G.; Chen, Y. *Nanotechnology* **2007**, *18*, 175604.
- (189) Yang, P.; Yan, R.; Fardy, M. *Nano Lett.* **2010**, *10*, 1529.
- (190) Weiss, N. O.; Duan, X. *Proc. Natl. Acad. Sci. U.S.A.* **2013**, *110*, 15171.
- (191) Li, L.; Zhang, Y.; Liu, X.; Shi, S.; Zhao, X.; Zhang, H.; Ge, X.; Cai, G.; Gu, C.; Wang, X. *Electrochim. Acta* **2014**, *116*, 467.
- (192) Liu, B.; Zhang, J.; Wang, X.; Chen, G.; Chen, D.; Zhou, C.; Shen, G. *Nano Lett.* **2012**, *12*, 3005.
- (193) Sauvage, F.; Bodenez, V.; Tarascon, J.-M.; Poepelmeier, K. R. *J. Am. Chem. Soc.* **2010**, *132*, 6778.
- (194) Liu, H.; Yang, W. *Energy Environ. Sci.* **2011**, *4*, 4000.
- (195) Xiong, C.; Aliev, A. E.; Gnade, B.; Balkus, K. J., Jr. *ACS Nano* **2008**, *2*, 293.
- (196) Wu, X.; Tao, Y.; Dong, L.; Hong, J. *J. Mater. Chem.* **2004**, *14*, 901.
- (197) Li, X.; Li, W.; Ma, H.; Chen, J. *J. Electrochem. Soc.* **2007**, *154*, A39.
- (198) André, R.; Natálio, F.; Humanes, M.; Leppin, J.; Heinze, K.; Wever, R.; Schröder, H. C.; Müller, W. E.; Tremel, W. *Adv. Funct. Mater.* **2011**, *21*, 501.
- (199) Xia, X.-h.; Tu, J.-p.; Mai, Y.-j.; Wang, X.-l.; Gu, C.-d.; Zhao, X.-b. *J. Mater. Chem.* **2011**, *21*, 9319.
- (200) Yan, J.; Fan, Z.; Sun, W.; Ning, G.; Wei, T.; Zhang, Q.; Zhang, R.; Zhi, L.; Wei, F. *Adv. Funct. Mater.* **2012**, *22*, 2632.
- (201) Lu, X.; Yu, M.; Zhai, T.; Wang, G.; Xie, S.; Liu, T.; Liang, C.; Tong, Y.; Li, Y. *Nano Lett.* **2013**, *13*, 2628.
- (202) Lee, H.-W.; Muralidharan, P.; Ruffo, R.; Mari, C. M.; Cui, Y.; Kim, D. K. *Nano Lett.* **2010**, *10*, 3852.
- (203) Wang, Q.; Wen, Z.; Li, J. *Inorg. Chem.* **2006**, *45*, 6944.
- (204) Khomane, R. B. *J. Colloid Interface Sci.* **2011**, *356*, 369.
- (205) Lim, S.; Yoon, C. S.; Cho, J. *Chem. Mater.* **2008**, *20*, 4560.
- (206) Li, X.; Cheng, F.; Guo, B.; Chen, J. *J. Phys. Chem. B* **2005**, *109*, 14017.
- (207) Qu, Q.; Fu, L.; Zhan, X.; Samuelis, D.; Maier, J.; Li, L.; Tian, S.; Li, Z.; Wu, Y. *Energy Environ. Sci.* **2011**, *4*, 3985.
- (208) Du, N.; Xu, Y.; Zhang, H.; Yu, J.; Zhai, C.; Yang, D. *Inorg. Chem.* **2011**, *50*, 3320.
- (209) Wang, G.; Shen, X.; Yao, J. *J. Power Sources* **2009**, *189*, 543.
- (210) Zhu, C.; Yu, Y.; Gu, L.; Weichert, K.; Maier, J. *Angew. Chem., Int. Ed.* **2011**, *50*, 6278.
- (211) Hosono, E.; Wang, Y.; Kida, N.; Enomoto, M.; Kojima, N.; Okubo, M.; Matsuda, H.; Saito, Y.; Kudo, T.; Honma, I. *ACS Appl. Mater. Interfaces* **2009**, *2*, 212.
- (212) Li, M.; Sun, L.; Sun, K.; Yu, S.; Wang, R.; Xie, H. *J. Solid State Electr. Chem.* **2012**, *16*, 3581.
- (213) Liu, J.; Tang, K.; Song, K.; Van Aken, P. A.; Yu, Y.; Maier, J. *Nanoscale* **2014**, *6*, 5081.
- (214) Hu, C.-C.; Chang, K.-H.; Lin, M.-C.; Wu, Y.-T. *Nano Lett.* **2006**, *6*, 2690.
- (215) Sharma, Y.; Sharma, N.; Subba Rao, G.; Chowdari, B. *Adv. Funct. Mater.* **2007**, *17*, 2855.
- (216) Kang, K.; Lee, H.-S.; Han, D.-W.; Kim, G.-S.; Lee, D.; Lee, G.; Kang, Y.-M.; Jo, M.-H. *Appl. Phys. Lett.* **2010**, *96*, 053110.
- (217) Wei, Q.; An, Q.; Chen, D.; Mai, L.; Chen, S.; Zhao, Y.; Hercule, K. M.; Xu, L.; Minhas-Khan, A.; Zhang, Q. *Nano Lett.* **2014**, *14*, 1042.
- (218) Muraliganth, T.; Vadivel Murugan, A.; Manthiram, A. *Chem. Commun.* **2009**, 7360.
- (219) Wang, Y.; Cao, G. *Chem. Mater.* **2006**, *18*, 2787.
- (220) Wang, X.; Yan, C.; Sumboja, A.; Lee, P. S. *Nano Energy* **2014**, *3*, 119.
- (221) Dai, K.; Lu, L.; Liang, C.; Dai, J.; Liu, Q.; Zhang, Y.; Zhu, G.; Liu, Z. *Electrochim. Acta* **2014**, *116*, 111.
- (222) Shakir, I.; Shahid, M.; Rana, U. A.; Nashef, I. M. A.; Hussain, R. *Electrochim. Acta* **2014**, *129*, 28.
- (223) Lee, K.-H.; Lee, Y.-W.; Ko, A. R.; Cao, G.; Park, K.-W. *J. Am. Ceram. Soc.* **2013**, *96*, 37.
- (224) Zhang, S.; Li, W.; Li, C.; Chen, J. *J. Phys. Chem. B* **2006**, *110*, 24855.
- (225) Yu, J.; Yu, J. C.; Ho, W.; Wu, L.; Wang, X. *J. Am. Chem. Soc.* **2004**, *126*, 3422.
- (226) Zhou, G.-T.; Wang, X.; Yu, J. C. *Cryst. Growth Des.* **2005**, *5*, 969.
- (227) Sorensen, E. M.; Izumi, H. K.; Vaughey, J. T.; Stern, C. L.; Poepelmeier, K. R. *J. Am. Chem. Soc.* **2005**, *127*, 6347.
- (228) Albrecht, T. A.; Sauvage, F.; Bodenez, V.; Tarascon, J.-M.; Poepelmeier, K. R. *Chem. Mater.* **2009**, *21*, 3017.
- (229) Wang, X.; Li, Y. *J. Am. Chem. Soc.* **2002**, *124*, 2880.
- (230) Kim, I. Y.; Ha, H.-W.; Kim, T. W.; Paik, Y.; Choy, J.-H.; Hwang, S.-J. *J. Phys. Chem. C* **2009**, *113*, 21274.
- (231) Wang, J.; Khoo, E.; Lee, P. S.; Ma, J. *J. Phys. Chem. C* **2008**, *112*, 14306.
- (232) Gao, L.; Wang, X.; Xie, Z.; Song, W.; Wang, L.; Wu, X.; Qu, F.; Chen, D.; Shen, G. *J. Mater. Chem. A* **2013**, *1*, 7167.
- (233) (a) Ni, J.; Jiang, W.; Yu, K.; Gao, Y.; Zhu, Z. *Electrochim. Acta* **2011**, *56*, 2122. (b) Niu, C.; Meng, J.; Han, C.; Zhao, K.; Yan, M. *Nano Lett.* **2014**, *14*, 2873.
- (234) Son, J.-H.; Wei, J.; Cobden, D.; Cao, G.; Xia, Y. *Chem. Mater.* **2010**, *22*, 3043.
- (235) Ding, N.; Liu, S.; Feng, X.; Gao, H.; Fang, X.; Xu, J.; Tremel, W.; Lieberwirth, I.; Chen, C. *Cryst. Growth Des.* **2009**, *9*, 1723.
- (236) Li, L.; Zhang, Y. Q.; Liu, X. Y.; Shi, S. J.; Zhao, X. Y.; Zhang, H.; Ge, X.; Cai, G. F.; Gu, C. D.; Wang, X. L.; Tu, J. P. *Electrochim. Acta* **2014**, *116*, 467.
- (237) Hu, A.; Zhang, X.; Oakes, K. D.; Peng, P.; Zhou, Y. N.; Servos, M. R. *J. Hazard. Mater.* **2011**, *189*, 278.
- (238) Sun, Y.; Ndifor-Angwafor, N. G.; Riley, D. J.; Ashfold, M. N. *Chem. Phys. Lett.* **2006**, *431*, 352.
- (239) Kim, J.-Y.; Cho, J. W.; Kim, S. H. *Mater. Lett.* **2011**, *65*, 1161.
- (240) Tang, C.; Wang, G.; Wang, H.; Zhang, Y.; Li, G. *Mater. Lett.* **2008**, *62*, 3663.
- (241) Xu, J.; Wang, K.; Zu, S.; Han, B.; Wei, Z. *ACS Nano* **2010**, *4*, 5019.

- (242) Tang, K. B.; Qian, Y. T.; Zeng, J. H.; Yang, X. G. *Adv. Mater.* **2003**, *15*, 448.
- (243) Shen, L.; Uchaker, E.; Zhang, X.; Cao, G. *Adv. Mater.* **2012**, *24*, 6502.
- (244) Su, J.; Guo, L.; Bao, N.; Grimes, C. A. *Nano Lett.* **2011**, *11*, 1928.
- (245) Aman, D.; Zaki, T.; Mikhail, S.; Selim, S. *Catal. Today* **2011**, *164*, 209.
- (246) Jang, J.; Yoon, H. *Adv. Mater.* **2004**, *16*, 799.
- (247) Li, X.; Cai, K.; Li, H.; Yu, D.; Wang, X.; Wang, H. *Superlattices Microstruct.* **2010**, *47*, 710.
- (248) Yang, Z.; Li, Z.; Kong, L. *J. Alloys Compd.* **2010**, *501*, 173.
- (249) Yang, X.-C.; Zou, X.; Liu, Y.; Li, X.-N.; Hou, J.-W. *Mater. Lett.* **2010**, *64*, 1451.
- (250) Valizadeh, S.; George, J.; Leisner, P.; Hultman, L. *Thin Solid Films* **2002**, *402*, 262.
- (251) Cao, G.; Liu, D. *Adv. Colloid Interfaces* **2008**, *136*, 45.
- (252) Lu, Q.; Gao, F.; Komarneni, S.; Mallouk, T. E. *J. Am. Chem. Soc.* **2004**, *126*, 8650.
- (253) Tao, S. L.; Desai, T. A. *Nano Lett.* **2007**, *7*, 1463.
- (254) Li, X.; Wang, Y.; Song, G.; Peng, Z.; Yu, Y.; She, X.; Sun, J.; Li, J.; Li, P.; Wang, Z. *J. Phys. Chem. C* **2010**, *114*, 6914.
- (255) Wang, J.; Tian, M.; Mallouk, T. E.; Chan, M. H. *J. Phys. Chem. B* **2004**, *108*, 841.
- (256) Molares, M. T.; Buschmann, V.; Dobrev, D.; Neumann, R.; Scholz, R.; Schuchert, I. U.; Vetter, J. *Adv. Mater.* **2001**, *13*, 62.
- (257) Pang, X.; Zhitomirsky, I. *Langmuir* **2004**, *20*, 2921.
- (258) Dauginet, L.; Duwez, A.-S.; Legras, R.; Demoustier-Champagne, S. *Langmuir* **2001**, *17*, 3952.
- (259) Van der Biest, O. O.; Vandeperre, L. *J. Annu. Rev. Mater. Sci.* **1999**, *29*, 327.
- (260) Zhitomirsky, I. *Adv. Colloid Interfac* **2002**, *97*, 279.
- (261) Li, D.; Xia, Y. *Adv. Mater.* **2004**, *16*, 1151.
- (262) Long, Y.-Z.; Li, M.-M.; Gu, C.; Wan, M.; Duvail, J.-L.; Liu, Z.; Fan, Z. *Prog. Polym. Sci.* **2011**, *36*, 1415.
- (263) Huang, Z.-M.; Zhang, Y.-Z.; Kotaki, M.; Ramakrishna, S. *Compos. Sci. Technol.* **2003**, *63*, 2223.
- (264) Greiner, A.; Wendorff, J. *Self-Assembled Nanomaterials I*; Springer: Berlin Heidelberg, 2008, p 107.
- (265) Pinto, N.; Johnson, A., Jr; MacDiarmid, A.; Mueller, C.; Theofylaktos, N.; Robinson, D.; Miranda, F. *Appl. Phys. Lett.* **2003**, *83*, 4244.
- (266) Liu, H.; Reccius, C. H.; Craighead, H. *Appl. Phys. Lett.* **2005**, *87*, 253106.
- (267) Liu, H.; Kameoka, J.; Czaplewski, D. A.; Craighead, H. *Nano Lett.* **2004**, *4*, 671.
- (268) Li, D.; Babel, A.; Jenekhe, S. A.; Xia, Y. *Adv. Mater.* **2004**, *16*, 2062.
- (269) Aussawasathien, D.; Sahasithiwat, S.; Menbangpung, L.; Teerawattananon, C. *Sens. Actuators, B* **2011**, *151*, 341.
- (270) Norris, I. D.; Shaker, M. M.; Ko, F. K.; MacDiarmid, A. G. *Synth. Met.* **2000**, *114*, 109.
- (271) Chronakis, I. S.; Grapenson, S.; Jakob, A. *Polymer* **2006**, *47*, 1597.
- (272) Kanjwal, M. A.; Sheikh, F. A.; Barakat, N. A.; Chronakis, I. S.; Kim, H. Y. *Appl. Surf. Sci.* **2011**, *257*, 7975.
- (273) Shim, H.-S.; Kim, J. W.; Sung, Y.-E.; Kim, W. B. *Sol. Energy Mater. Sol. C* **2009**, *93*, 2062.
- (274) Xu, L.; Dong, B.; Wang, Y.; Bai, X.; Liu, Q.; Song, H. *Sens. Actuators, B: Chem.* **2010**, *147*, 531.
- (275) Kim, H. J.; Kim, Y. S.; Seo, M. H.; Choi, S. M.; Cho, J.; Huber, G. W.; Kim, W. B. *Electrochem. Commun.* **2010**, *12*, 32.
- (276) Leite, E.; Giraldi, T.; Pontes, F.; Longo, E.; Beltran, A.; Andres, J. *Appl. Phys. Lett.* **2003**, *83*, 1566.
- (277) Adachi, M.; Murata, Y.; Takao, J.; Jiu, J.; Sakamoto, M.; Wang, F. *J. Am. Chem. Soc.* **2004**, *126*, 14943.
- (278) Halder, A.; Ravishankar, N. *Adv. Mater.* **2007**, *19*, 1854.
- (279) Zhang, J.; Huang, F.; Lin, Z. *Nanoscale* **2010**, *2*, 18.
- (280) Liu, B.; Yu, S.-H.; Li, L.; Zhang, F.; Zhang, Q.; Yoshimura, M.; Shen, P. *J. Phys. Chem. B* **2004**, *108*, 2788.
- (281) Penn, R. L.; Banfield, J. F. *Science* **1998**, *281*, 969.
- (282) Zhang, Q.; Liu, S.-J.; Yu, S.-H. *J. Mater. Chem.* **2009**, *19*, 191.
- (283) Whittingham, M. S. *MRS Bull.* **2008**, *33*, 411.
- (284) Kim, D. K.; Muralidharan, P.; Lee, H.-W.; Ruffo, R.; Yang, Y.; Chan, C. K.; Peng, H.; Huggins, R. A.; Cui, Y. *Nano Lett.* **2008**, *8*, 3948.
- (285) Shaju, K. M.; Jiao, F.; Débart, A.; Bruce, P. G. *Phys. Chem. Chem. Phys.* **2007**, *9*, 1837.
- (286) Wang, Y.; Xia, H.; Lu, L.; Lin, J. *ACS Nano* **2010**, *4*, 1425.
- (287) Wang, L.; He, X.; Sun, W.; Wang, J.; Li, Y.; Fan, S. *Nano Lett.* **2012**, *12*, 5632.
- (288) Yang, S.; Gong, Y.; Liu, Z.; Zhan, L.; Hashim, D. P.; Ma, L.; Vajtai, R.; Ajayan, P. M. *Nano Lett.* **2013**, *13*, 1596.
- (289) Zhang, H.; Cao, G.; Wang, Z.; Yang, Y.; Shi, Z.; Gu, Z. *Electrochim. Acta* **2010**, *55*, 2873.
- (290) Zhang, H.; Cao, G.; Wang, Z.; Yang, Y.; Shi, Z.; Gu, Z. *Electrochem. Solid-State Lett.* **2008**, *11*, A223.
- (291) Jegal, J.-P.; Kim, J.-G.; Kim, K.-B. *Electrochem. Commun.* **2013**, *30*, 87.
- (292) Chen, G.; Wang, Z.; Xia, D. *Chem. Mater.* **2008**, *20*, 6951.
- (293) Park, K.-S.; Kang, J.-G.; Choi, Y.-J.; Lee, S.; Kim, D.-W.; Park, J.-G. *Energy Environ. Sci.* **2011**, *4*, 1796.
- (294) Han, C.; Pi, Y.; An, Q.; Mai, L.; Xie, J.; Xu, X.; Xu, L.; Zhao, Y.; Niu, C.; Khan, A. M. *Nano Lett.* **2012**, *12*, 4668.
- (295) Cho, J. *J. Mater. Chem.* **2008**, *18*, 2257.
- (296) Kim, H.-B.; Park, B.-C.; Myung, S.-T.; Amine, K.; Prakash, J.; Sun, Y.-K. *J. Power Sources* **2008**, *179*, 347.
- (297) Yan, J.; Sumboja, A.; Khoo, E.; Lee, P. S. *Adv. Mater.* **2011**, *23*, 746.
- (298) Mai, L.; Wei, Q.; An, Q.; Tian, X.; Zhao, Y.; Xu, X.; Xu, L.; Chang, L.; Zhang, Q. *Adv. Mater.* **2013**, *25*, 2969.
- (299) Herle, P. S.; Ellis, B.; Coombs, N.; Nazar, L. *Nat. Mater.* **2004**, *3*, 147.
- (300) Wang, J.; Du, N.; Zhang, H.; Yu, J.; Yang, D. *J. Mater. Chem.* **2012**, *22*, 1511.
- (301) Wang, J.; Du, N.; Zhang, H.; Yu, J.; Yang, D. *J. Power Sources* **2012**, *208*, 434.
- (302) Kim, H. S.; Kang, S. H.; Chung, Y. H.; Sung, Y.-E. *Electrochim. Solid-State Lett.* **2010**, *13*, A15.
- (303) Kang, B.; Ceder, G. *Nature* **2009**, *458*, 190.
- (304) (a) Li, N.; Chen, Z.; Ren, W.; Li, F.; Cheng, H.-M. *Proc. Natl. Acad. Sci. U.S.A.* **2012**, *109*, 17360. (b) Wang, X.; Lu, X.; Liu, B.; Chen, D.; Tong, Y.; Shen, G. *Adv. Mater.* **2014**, *26*, 4673.
- (305) Niu, Z.; Zhang, L.; Liu, L.; Zhu, B.; Dong, H.; Chen, X. *Adv. Mater.* **2013**, *25*, 4035.
- (306) Hu, L.; Wu, H.; La Mantia, F.; Yang, Y.; Cui, Y. *ACS Nano* **2010**, *4*, 5843.
- (307) Nam, K. T.; Kim, D.-W.; Yoo, P. J.; Chiang, C.-Y.; Meethong, N.; Hammond, P. T.; Chiang, Y.-M.; Belcher, A. M. *Science* **2006**, *312*, 885.
- (308) Lin, H.; Weng, W.; Ren, J.; Qiu, L.; Zhang, Z.; Chen, P.; Chen, X.; Deng, J.; Wang, Y.; Peng, H. *Adv. Mater.* **2014**, *26*, 1217.
- (309) Ren, J.; Li, L.; Chen, C.; Chen, X.; Cai, Z.; Qiu, L.; Wang, Y.; Zhu, X.; Peng, H. *Adv. Mater.* **2013**, *25*, 1155.
- (310) (a) Weng, W.; Lin, H.; Chen, X.; Ren, J.; Zhang, Z.; Qiu, L.; Guan, G.; Peng, H. *J. Mater. Chem. A* **2014**, *2*, 9306. (b) Zeng, W.; Shu, L.; Li, Q.; Chen, S.; Wang, F.; Tao, X.-M. *Adv. Mater.* **2014**, *26*, 5310.
- (311) Hong, S. Y.; Kim, Y.; Park, Y.; Choi, A.; Choi, N.-S.; Lee, K. T. *Energy Environ. Sci.* **2013**, *6*, 2067.
- (312) Ong, S. P.; Chevrier, V. L.; Hautier, G.; Jain, A.; Moore, C.; Kim, S.; Ma, X.; Ceder, G. *Energy Environ. Sci.* **2011**, *4*, 3680.
- (313) Ha, K.-H.; Woo, S. H.; Mok, D.; Choi, N.-S.; Park, Y.; Oh, S. M.; Kim, Y.; Kim, J.; Lee, J.; Nazar, L. F.; Lee, K. T. *Adv. Energy Mater.* **2013**, *3*, 770.

- (314) Yabuuchi, N.; Kajiyama, M.; Iwatate, J.; Nishikawa, H.; Hitomi, S.; Okuyama, R.; Usui, R.; Yamada, Y.; Komaba, S. *Nat. Mater.* **2012**, *11*, 512.
- (315) Kim, H.; Kim, D. J.; Seo, D.-H.; Yeom, M. S.; Kang, K.; Kim, D. K.; Jung, Y. *Chem. Mater.* **2012**, *24*, 1205.
- (316) Wang, Y.; Yu, X.; Xu, S.; Bai, J.; Xiao, R.; Hu, Y.-S.; Li, H.; Yang, X.-Q.; Chen, L.; Huang, X. *Nat. Commun.* **2013**, *4*, 2365.
- (317) Tang, K.; Fu, L.; White, R. J.; Yu, L.; Titirici, M.-M.; Antonietti, M.; Maier, J. *Adv. Energy Mater.* **2012**, *2*, 873.
- (318) Yao, M.; Kuratani, K.; Kojima, T.; Takeichi, N.; Senoh, H.; Kiyobayashi, T. *Sci. Rep.* **2014**, *4*, 3650.
- (319) Goodenough, J. B.; Kim, Y. *Chem. Mater.* **2010**, *22*, 587.
- (320) Ellis, B. L.; Nazar, L. F. *Curr. Opin. Solid State Mater. Sci.* **2012**, *16*, 168.
- (321) Pan, H.; Hu, Y.-S.; Chen, L. *Energy Environ. Sci.* **2013**, *6*, 2338.
- (322) Palomares, V.; Serras, P.; Villaluenga, I.; Hueso, K. B.; Carretero-González, J.; Rojo, T. *Energy Environ. Sci.* **2012**, *5*, 5884.
- (323) Kim, S.-W.; Seo, D.-H.; Ma, X.; Ceder, G.; Kang, K. *Adv. Energy Mater.* **2012**, *2*, 710.
- (324) Oh, S.-M.; Myung, S.-T.; Yoon, C. S.; Lu, J.; Hassoun, J.; Scrosati, B.; Amine, K.; Sun, Y.-K. *Nano Lett.* **2014**, *14*, 1620.
- (325) Park, Y.-U.; Seo, D.-H.; Kwon, H.-S.; Kim, B.; Kim, J.; Kim, H.; Kim, I.; Yoo, H.-I.; Kang, K. *J. Am. Chem. Soc.* **2013**, *135*, 13870.
- (326) Berthelot, R.; Carlier, D.; Delmas, C. *Nat. Mater.* **2011**, *10*, 74.
- (327) Guignard, M.; Didier, C.; Darriet, J.; Bordet, P.; Elkaïm, E.; Delmas, C. *Nat. Mater.* **2013**, *12*, 74.
- (328) Su, D.; Wang, G. *ACS Nano* **2013**, *7*, 11218.
- (329) Hariharan, S.; Saravanan, K.; Balaya, P. *Electrochim. Commun.* **2013**, *31*, 5.
- (330) Darwiche, A.; Marino, C.; Sougrati, M. T.; Fraisse, B.; Stievano, L.; Monconduit, L. *J. Am. Chem. Soc.* **2012**, *134*, 20805.
- (331) Jiang, J.; Li, Y.; Liu, J.; Huang, X.; Yuan, C.; Lou, X. W. D. *Adv. Mater.* **2012**, *24*, 5166.
- (332) Cao, Y.; Xiao, L.; Wang, W.; Choi, D.; Nie, Z.; Yu, J.; Saraf, L. V.; Yang, Z.; Liu, J. *Adv. Mater.* **2011**, *23*, 3155.
- (333) Cao, Y.; Xiao, L.; Sushko, M. L.; Wang, W.; Schwenzer, B.; Xiao, J.; Nie, Z.; Saraf, L. V.; Yang, Z.; Liu, J. *Nano Lett.* **2012**, *12*, 3783.
- (334) Wang, W.; Yu, C.; Lin, Z.; Hou, J.; Zhu, H.; Jiao, S. *Nanoscale* **2013**, *5*, 594.
- (335) Xiong, H.; Slater, M. D.; Balasubramanian, M.; Johnson, C. S.; Rajh, T. *J. Phys. Chem. Lett.* **2011**, *2*, 2560.
- (336) Liu, Y.; Xu, Y.; Zhu, Y.; Culver, J. N.; Lundgren, C. A.; Xu, K.; Wang, C. *ACS Nano* **2013**, *7*, 3627.
- (337) Wang, L.; Zhang, K.; Hu, Z.; Duan, W.; Cheng, F.; Chen, J. *Nano Res.* **2013**, *7*, 199.
- (338) Zhu, Y.; Han, X.; Xu, Y.; Liu, Y.; Zheng, S.; Xu, K.; Hu, L.; Wang, C. *ACS Nano* **2013**, *7*, 6378.
- (339) Gu, M.; Kushima, A.; Shao, Y.; Zhang, J.-G.; Liu, J.; Browning, N. D.; Li, J.; Wang, C. *Nano Lett.* **2013**, *13*, 5203.
- (340) Senguttuvan, P.; Rousse, G.; Arroyo y de Dompablo, M. E.; Vezin, H.; Tarascon, J. M.; Palacín, M. R. *J. Am. Chem. Soc.* **2013**, *135*, 3897.
- (341) Kim, H.; Shakoor, R. A.; Park, C.; Lim, S. Y.; Kim, J.-S.; Jo, Y. N.; Cho, W.; Miyasaka, K.; Kahraman, R.; Jung, Y.; Choi, J. W. *Adv. Funct. Mater.* **2013**, *23*, 1147.
- (342) Trad, K.; Carlier, D.; Crogueennec, L.; Wattiaux, A.; Ben Amara, M.; Delmas, C. *Chem. Mater.* **2010**, *22*, 5554.
- (343) Wang, W.; Jiang, B.; Hu, L.; Jiao, S. *J. Mater. Chem. A* **2014**, *2*, 1341.
- (344) Jian, Z.; Han, W.; Lu, X.; Yang, H.; Hu, Y.-S.; Zhou, J.; Zhou, Z.; Li, J.; Chen, W.; Chen, D.; Chen, L. *Adv. Energy Mater.* **2013**, *3*, 156.
- (345) Saravanan, K.; Mason, C. W.; Rudola, A.; Wong, K. H.; Balaya, P. *Adv. Energy Mater.* **2013**, *3*, 444.
- (346) Jian, Z.; Zhao, L.; Pan, H.; Hu, Y.-S.; Li, H.; Chen, W.; Chen, L. *Electrochim. Commun.* **2012**, *14*, 86.
- (347) Zhang, T.; Zhou, H. *Nat. Commun.* **2013**, *4*, 1817.
- (348) Jung, H.-G.; Hassoun, J.; Park, J.-B.; Sun, Y.-K.; Scrosati, B. *Nat. Chem.* **2012**, *4*, 579.
- (349) Oh, S. H.; Black, R.; Pomerantseva, E.; Lee, J.-H.; Nazar, L. F. *Nat. Chem.* **2012**, *4*, 1004.
- (350) Chen, Y.; Freunberger, S. A.; Peng, Z.; Fontaine, O.; Bruce, P. G. *Nat. Chem.* **2013**, *5*, 489.
- (351) Zhang, T.; Zhou, H. *Angew. Chem., Int. Ed.* **2012**, *124*, 11224.
- (352) Freunberger, S. A.; Chen, Y.; Drewett, N. E.; Hardwick, L. J.; Bardé, F.; Bruce, P. G. *Angew. Chem., Int. Ed.* **2011**, *50*, 8609.
- (353) Girishkumar, G.; McCloskey, B.; Luntz, A.; Swanson, S.; Wilcke, W. *J. Phys. Chem. Lett.* **2010**, *1*, 2193.
- (354) Kang, S.; Mo, Y.; Ong, S. P.; Ceder, G. *Chem. Mater.* **2013**, *25*, 3328.
- (355) (a) Ryu, W.-H.; Yoon, T.-H.; Song, S. H.; Jeon, S.; Park, Y.-J.; Kim, I.-D. *Nano Lett.* **2013**, *13*, 4190. (b) Oh, D.; Qi, J.; Han, B.; Zhang, G.; Carney, T. J.; Ohmura, J.; Zhang, Y.; Shao-Horn, Y.; Belcher, A. M. *Nano Lett.* **2014**, *14*, 4837.
- (356) Park, J.; Jun, Y.-S.; Lee, W.-r.; Gerbec, J. A.; See, K. A.; Stucky, G. D. *Chem. Mater.* **2013**, *25*, 3779.
- (357) Lim, H. D.; Park, K. Y.; Song, H.; Jang, E. Y.; Gwon, H.; Kim, J.; Kim, Y. H.; Lima, M. D.; Robles, R. O.; Lepró, X. *Adv. Mater.* **2013**, *25*, 1348.
- (358) Guo, Z.; Zhou, D.; Dong, X.; Qiu, Z.; Wang, Y.; Xia, Y. *Adv. Mater.* **2013**, *25*, 5668.
- (359) Zhao, Y.; Xu, L.; Mai, L.; Han, C.; An, Q.; Xu, X.; Liu, X.; Zhang, Q. *Proc. Natl. Acad. Sci. U.S.A.* **2012**, *109*, 19569.
- (360) Xu, J. J.; Xu, D.; Wang, Z. L.; Wang, H. G.; Zhang, L. L.; Zhang, X. B. *Angew. Chem., Int. Ed.* **2013**, *52*, 3887.
- (361) Lu, Q.; Zhao, Q.; Zhang, H.; Li, J.; Wang, X.; Wang, F. *ACS Macro Lett.* **2013**, *2*, 92.
- (362) Shi, C.; Feng, J.; Huang, L.; Liu, X.; Mai, L. *Int. J. Electrochem. Sci.* **2013**, *8*, 8924.
- (363) Zhang, G.; Zheng, J.; Liang, R.; Zhang, C.; Wang, B.; Au, M.; Hendrickson, M.; Plichta, E. *J. Electrochem. Soc.* **2011**, *158*, A822.
- (364) Yang, Y.; Zheng, G.; Cui, Y. *Chem. Soc. Rev.* **2013**, *42*, 3018.
- (365) Li, Z.; Yuan, L.; Yi, Z.; Liu, Y.; Xin, Y.; Zhang, Z.; Huang, Y. *Nanoscale* **2014**, *6*, 1653.
- (366) Wang, D.-W.; Zeng, Q.; Zhou, G.; Yin, L.; Li, F.; Cheng, H.-M.; Gentle, I. R.; Lu, G. Q. *M. J. Mater. Chem. A* **2013**, *1*, 9382.
- (367) Yin, Y. X.; Xin, S.; Guo, Y. G.; Wan, L. *J. Angew. Chem., Int. Ed.* **2013**, *52*, 13186.
- (368) Yao, H.; Zheng, G.; Li, W.; McDowell, M. T.; Seh, Z.; Liu, N.; Lu, Z.; Cui, Y. *Nano Lett.* **2013**, *13*, 3385.
- (369) Fu, Y.; Su, Y. S.; Manthiram, A. *Angew. Chem., Int. Ed.* **2013**, *125*, 7068.
- (370) Zhou, W.; Yu, Y.; Chen, H.; DiSalvo, F. J.; Abruña, H. c. D. *J. Am. Chem. Soc.* **2013**, *135*, 16736.
- (371) Seh, Z. W.; Li, W.; Cha, J. J.; Zheng, G.; Yang, Y.; McDowell, M. T.; Hsu, P.-C.; Cui, Y. *Nat. Commun.* **2013**, *4*, 1331.
- (372) Mikhaylik, Y. V.; Akridge, J. R. *J. Electrochem. Soc.* **2004**, *151*, A1969.
- (373) Zheng, G.; Yang, Y.; Cha, J. J.; Hong, S. S.; Cui, Y. *Nano Lett.* **2011**, *11*, 4462.
- (374) Xiao, L.; Cao, Y.; Xiao, J.; Schwenzer, B.; Engelhard, M. H.; Saraf, L. V.; Nie, Z.; Exarhos, G. J.; Liu, J. *Adv. Mater.* **2012**, *24*, 1176.
- (375) Chen, J.-J.; Zhang, Q.; Shi, Y.-N.; Qin, L.-L.; Cao, Y.; Zheng, M.-S.; Dong, Q.-F. *Phys. Chem. Chem. Phys.* **2012**, *14*, 5376.
- (376) Zheng, G.; Zhang, Q.; Cha, J. J.; Yang, Y.; Li, W.; Seh, Z. W.; Cui, Y. *Nano Lett.* **2013**, *13*, 1265.
- (377) Guo, J.; Xu, Y.; Wang, C. *Nano Lett.* **2011**, *11*, 4288.
- (378) Lu, S.; Cheng, Y.; Wu, X.; Liu, J. *Nano Lett.* **2013**, *13*, 2485.
- (379) Yan, J.; Wang, Q.; Wei, T.; Fan, Z. *Adv. Energy Mater.* **2014**, *4*, 1300816.
- (380) Liu, S.; Sun, S.; You, X.-Z. *Nanoscale* **2014**, *6*, 2037.
- (381) Bao, L.; Li, X. *Adv. Mater.* **2012**, *24*, 3246.
- (382) Zhu, H.; Wang, X.; Liu, X.; Yang, X. *Adv. Mater.* **2012**, *24*, 6524.
- (383) He, X.; Li, R.; Qiu, J.; Xie, K.; Ling, P.; Yu, M.; Zhang, X.; Zheng, M. *Carbon* **2012**, *50*, 4911.

- (384) Mao, S.; Wen, Z.; Kim, H.; Lu, G.; Hurley, P.; Chen, J. *ACS Nano* **2012**, *6*, 7505.
- (385) El-Kady, M. F.; Strong, V.; Dubin, S.; Kaner, R. B. *Science* **2012**, *335*, 1326.
- (386) Zhang, L. L.; Zhao, X.; Stoller, M. D.; Zhu, Y.; Ji, H.; Murali, S.; Wu, Y.; Perales, S.; Clevenger, B.; Ruoff, R. S. *Nano Lett.* **2012**, *12*, 1806.
- (387) Izadi-Najafabadi, A.; Yamada, T.; Futaba, D. N.; Yudasaka, M.; Takagi, H.; Hatori, H.; Iijima, S.; Hata, K. *ACS Nano* **2011**, *5*, 811.
- (388) Lu, W.; Qu, L.; Henry, K.; Dai, L. *J. Power Sources* **2009**, *189*, 1270.
- (389) Yoon, B.-J.; Jeong, S.-H.; Lee, K.-H.; Seok Kim, H.; Gyung Park, C.; Hun Han, J. *Chem. Phys. Lett.* **2004**, *388*, 170.
- (390) Sugimoto, W.; Makino, S.; Mukai, R.; Tatsumi, Y.; Fukuda, K.; Takasu, Y.; Yamauchi, Y. *J. Power Sources* **2012**, *204*, 244.
- (391) Wang, L.; Liu, X.; Wang, X.; Yang, X.; Lu, L. *J. Mater. Sci. Mater. Electron.* **2011**, *22*, 601.
- (392) Xue, T.; Wang, X.; Lee, J.-M. *J. Power Sources* **2012**, *201*, 382.
- (393) Jiang, J.; Liu, J.; Ding, R.; Zhu, J.; Li, Y.; Hu, A.; Li, X.; Huang, X. *ACS Appl. Mater. Interfaces* **2010**, *3*, 99.
- (394) Jiang, H.; Li, C.; Sun, T.; Ma, J. *Chem. Commun.* **2012**, *48*, 2606.
- (395) Xia, X.; Tu, J.; Zhang, Y.; Mai, Y.; Wang, X.; Gu, C.; Zhao, X. *J. Phys. Chem. C* **2011**, *115*, 22662.
- (396) Liu, J.; Jiang, J.; Cheng, C.; Li, H.; Zhang, J.; Gong, H.; Fan, H. *J. Adv. Mater.* **2011**, *23*, 2076.
- (397) Li, S.; Dong, Y.-F.; Wang, D.-D.; Chen, W.; Huang, L.; Shi, C.-W.; Mai, L.-Q. *Front. Phys.* **2014**, *9*, 303.
- (398) Liu, J.; Jiang, J.; Bosman, M.; Fan, H. *J. Mater. Chem.* **2012**, *22*, 2419.
- (399) Liu, R.; Duay, J.; Lee, S. B. *ACS Nano* **2010**, *4*, 4299.
- (400) Liu, R.; Duay, J.; Lane, T.; Lee, S. B. *Phys. Chem. Chem. Phys.* **2010**, *12*, 4309.
- (401) Jiang, H.; Ma, J.; Li, C. *J. Mater. Chem.* **2012**, *22*, 16939.
- (402) Mai, L.; Li, H.; Zhao, Y.; Xu, L.; Xu, X.; Luo, Y.; Zhang, Z.; Ke, W.; Niu, C.; Zhang, Q. *Sci. Rep.* **2013**, *3*, 1718.
- (403) Mai, L.-Q.; Minhas-Khan, A.; Tian, X.; Hercule, K. M.; Zhao, Y.-L.; Lin, X.; Xu, X. *Nat. Commun.* **2013**, *4*, 2923.
- (404) Fan, Z.; Yan, J.; Wei, T.; Zhi, L.; Ning, G.; Li, T.; Wei, F. *Adv. Funct. Mater.* **2011**, *21*, 2366.
- (405) Senthilkumar, S.; Selvan, R. K.; Melo, J. *J. Mater. Chem. A* **2013**, *1*, 12386.
- (406) Lukatskaya, M. R.; Mashtalir, O.; Ren, C. E.; Dall'Agnese, Y.; Rozier, P.; Taberna, P. L.; Naguib, M.; Simon, P.; Barsoum, M. W.; Gogotsi, Y. *Science* **2013**, *341*, 1502.
- (407) Ren, J.; Bai, W.; Guan, G.; Zhang, Y.; Peng, H. *Adv. Mater.* **2013**, *25*, 5965.
- (408) Chen, X.; Qiu, L.; Ren, J.; Guan, G.; Lin, H.; Zhang, Z.; Chen, P.; Wang, Y.; Peng, H. *Adv. Mater.* **2013**, *25*, 6436.
- (409) Yang, Z.; Deng, J.; Chen, X.; Ren, J.; Peng, H. *Angew. Chem., Int. Ed.* **2013**, *52*, 13453.
- (410) Sun, K.; Wei, T. S.; Ahn, B. Y.; Seo, J. Y.; Dillon, S. J.; Lewis, J. A. *Adv. Mater.* **2013**, *25*, 4539.
- (411) Pikul, J. H.; Zhang, H. G.; Cho, J.; Braun, P. V.; King, W. P. *Nat. Commun.* **2013**, *4*, 1732.
- (412) Shaijumon, M. M.; Perre, E.; Daffos, B.; Taberna, P. L.; Tarascon, J. M.; Simon, P. *Adv. Mater.* **2010**, *22*, 4978.
- (413) Notten, P. H.; Roozeboom, F.; Niessen, R. A.; Baggetto, L. *Adv. Mater.* **2007**, *19*, 4564.
- (414) Gerasopoulos, K.; Pomerantseva, E.; McCarthy, M.; Brown, A.; Wang, C.; Culver, J.; Ghodssi, R. *ACS Nano* **2012**, *6*, 6422.
- (415) Gowda, S. R.; Leela Mohana Reddy, A.; Zhan, X.; Ajayan, P. M. *Nano Lett.* **2011**, *11*, 3329.
- (416) Min, H.-S.; Park, B. Y.; Taherabadi, L.; Wang, C.; Yeh, Y.; Zaouk, R.; Madou, M. J.; Dunn, B. *J. Power Sources* **2008**, *178*, 795.
- (417) Beidaghi, M.; Gogotsi, Y. *Energy Environ. Sci.* **2014**, *7*, 867.
- (418) Wang, K.; Zou, W.; Quan, B.; Yu, A.; Wu, H.; Jiang, P.; Wei, Z. *Adv. Energy Mater.* **2011**, *1*, 1068.